THE AERODYNAMICS, FLIGHT MECHANICS AND PERFORMANCE PREDICTIONS FOR A MEDIUM RANGE CARGO AIRCRAFT

A THESIS SUBMITTED TO
THE GRADUATE SCHOOL OF NATURAL AND APPLIED SCIENCES
OF
THE MIDDLE EAST TECHNICAL UNIVERSITY

BY

CENGİZ KARAAĞAÇ

IN PARTIAL FULFILLMENT OF THE REQUIREMENTS FOR THE DEGREE OF

MASTER OF SCIENCE

IN

THE DEPARTMENT OF AERONAUTICAL ENGINEERING

NOVEMBER 1998

Approval of the Graduate School of Natural and Applied Sciences.

Prof. Dr. Tayfur ÖZTÜRK

Director

I certify that this thesis satisfies all the requirements as a thesis for the degree of Master of Science.

Prof. Dr. Nafiz ALEMDAROĞLU

Head of Department

This is to certify that we have read this thesis and that in our opinion it is fully adequate, in scope and quality, as a thesis for the degree of Master of Science.

Assoc. Prof. Dr. Mehmet Ş. KAVSAOĞLU	Prof. Dr. Nafiz ALEMDAROĞLU
Co- Supervisor	Supervisor

Examining Committee Members

Assoc. Prof. Dr. Yavuz YAMAN

Prof. Dr. Nafiz ALEMDAROĞLU

Assoc. Prof. Dr. Mehmet Ş. KAVSAOĞLU

Assoc. Prof. Dr. Sinan EYİ

Remzi BARLAS, M.S.

ABSTRACT

THE AERODYNAMICS, FLIGHT MECHANICS AND PERFORMANCE PREDICTIONS FOR A MEDIUM RANGE CARGO AIRCRAFT

KARAAĞAÇ, Cengiz

M. S., Department of Aeronautical Engineering

Supervisor: Prof. Dr. Nafiz ALEMDAROĞLU

Co-Supervisor: Assoc. Prof. Dr. Mehmet Ş. KAVSAOĞLU

November 1998, 143 pages

In this thesis, the first level aerodynamic calculations are performed for CASA CN-235 aircraft. Also based on the aerodynamic information obtained, performance and flight mechanics characteristics of this aircraft are performed.

First aerodynamic calculations are made. The results for the lift coefficient versus angle of attack curves, drag polar curves and pitching moment coefficient versus angle of attack curves are presented.

The calculations of static stability and control and dynamic stability and response characteristics are made. Results related to flying quality levels are listed. Dynamic responses of the aircraft for an input control surface deflection are presented.

The performance calculations are made. Finally the results of the present study are discussed and some conclusions are made.

Keywords: Aerodynamics, Flight Mechanics, Stability and Control, Performance, CASA CN-235 Aircraft.

ÖZ

ORTA MENZİL BİR KARGO UÇAĞININ AERODİNAMİK, UÇUŞ MEKANİĞİ VE PERFORMANS TAHMİNLERİ

KARAAĞAÇ, Cengiz

Yüksek Lisans, Havacılık Mühendisliği Bölümü

Tez Yöneticisi: Prof. Dr. Nafiz ALEMDAROĞLU

Ortak Tez Yöneticisi: Doç. Dr. Mehmet Ş. KAVSAOĞLU

Kasım 1998, 143 sayfa

Bu tezde, CASA CN-235 uçağının ilk aşama aerodinamik hesaplamaları yapılmıştır. Ayrıca elde edilen bu aerodinamik bilgilere dayanılarak, bu uçağın performans ve uçuş mekaniği özellikleri elde edilmiştir.

İlk olarak aerodinamik hesaplamalar yapılmıştır. Kaldırma katsayısı - hücum açısı eğrileri, sürükleme eğrileri ve yunuslama momenti - hücum açısı eğrileriyle ilgili sonuçlar listelenmiştir.

Statik kararlılık ve kontrol ve dinamik kararlılık ve tepki özellikleri elde edilmiştir. Uçuş kalite seviyeleriyle ilgili sonuçlar listelenmiştir. Kontrol yüzeylerine verilen bir kumandaya uçağın verdiği dinamik tepkisi gösterilmiştir.

Performans hesaplamaları yapılmıştır. Son olarak çalışmalara ait sonuçlar tartışılmış ve çeşitli kararlara varılmıştır.

Anahtar Kelimeler: Aerodinamik, Uçuş Mekaniği, Kararlılık ve Kontrol, Performans, CASA CN-235 Uçağı.

To my wife and daughter for their endless love, support and patience...

ACKNOWLEDGEMENT

I would like to express my sincere thanks and appreciation to my supervisor Prof. Dr. Nafiz ALEMDAROĞLU and co-supervisor Assoc. Prof. Dr. Mehmet Ş. KAVSAOĞLU for their support, suggestions and encouragement during the preparation of this thesis.

TABLE OF CONTENTS

LIST OF TABLES

LIST OF FIGURES

LIST OF SYMBOLS

REGULAR SYMBOLS

Symbol	Definition
A	Aspect ratio
A_h	Horizontal tail aspect ratio.
b	Width
b_h	Horizontal tail span.
B_v	Vertical tail span.
b_w	Wing span.
$\bar{c}$	Mean geometric chord
C_{bhp}	Specific fuel consumption
C_D	Aircraft drag coefficient
$C_{D_{can}}$	Drag coefficient due to canopy.
$C_{D_{cw}}$	Canopy/Windshield drag coefficient.
$C_{D_{emp}}$	Empennage drag coefficient.
C_{D_f}	Leading/Trailing edge flap drag coefficient.
$C_{D_{fus}}$	Fuselage drag coefficient.
$C_{D_{gear}}$	Landing gear drag coefficient.
$C_{D_{gear_{C_L=0}}}$	The zero-lift drag coefficient of the landing gear based on its own reference area.
$C_{D_{\text{int}}}$	Interference drag coefficient.
$C_{D_{i_h}}$	Total airplane drag change with stabilizer, α=0
$C_{D_{L_{emp}}}$	Empennage drag coefficient due to lift
$C_{D_{L_{fus}}}$	Fuselage drag coefficient due to lift.
$C_{D_{L_w}}$	Wing drag coefficient due to lift.
$C_{D_{misc}}$	Miscellaneous drag coefficient.
C_{D_n}	Nacelle drag coefficient.
$C_{D_{np}}$	Nacelle/Pylon drag coefficient.

C_{D_p}	Pylon drag coefficient.
C_{D_q}	Drag due to pitch rate derivative
C_{D_s}	Store(s) drag coefficient.
$C_{D_{trim}}$	Trim drag coefficient.
C_{D_u}	Drag coefficient due to speed
C_{D_w}	Wing drag coefficient.
$C_{D_{ws}}$	Drag coefficient due to windshield.
C_{D_0}	Total airplane drag coefficient for $\alpha=i_h=\delta_e=0$
$C_{D_{0_{emp}}}$	Empennage zero-lift drag coefficient
$C_{D_{0_{fus}}}$	Fuselage zero-lift drag coefficient.
$C_{D_{0_w}}$	Wing zero-lift drag coefficient.
C_{D_l}	Steady state drag coefficient
C_{D_α}	Total airplane drag change for with angle of attack at $i_h=\delta_e=0$
$C_{D_{\dot{\alpha}}}$	Drag due to rate of angle of attack derivative
$C_{D_{\delta_e}}$	Total airplane drag change with elevator, $\alpha=0$
$\bar{C}_h$	Horizontal tail mean chord.
C_L	Aircraft lift coefficient
$C_{L_{i_h}}$	Change in total airplane lift for unit stabilizer angle
$C_{L_{max}}$	Maximum lift coefficient
$C_{L_{max_w}}$	The wing maximum lift coefficient
C_{l_p}	The rolling moment due to roll rate derivative
C_{L_q}	Lift due to pitch rate derivative
C_{l_r}	The rolling moment due to yaw rate derivative
C_{L_u}	Lift coefficient due to speed
C_{L_w}	Wing lift coefficient
C_{L_0}	Total airplane lift coefficient for $\alpha=i_h=\delta_e=0$
$C_{L_{0_h}}$	Horizontal tail lift coefficient for zero angle of attack
$C_{L_{0_{wf}}}$	Wing-fuselage lift coefficient for zero angle of attack
C_{L_l}	Steady state lift coefficient
C_{L_α}	Total airplane lift curve slope
$C_{L_{\dot{\alpha}}}$	Lift due to rate of angle of attack derivative

$C_{l_{\alpha_w}}$	The average wing airfoil lift curve slope.
$\left(C_{L_{\alpha_w}}\right)_{\delta}$	The wing lift curve slope with flaps down
$C_{L_{\alpha_{wf}}}$	Wing-fuselage lift curve slope
$C_{L_{\alpha_h}}$	Horizontal tail lift curve slope
$C_{l_{\delta_a}}$	The rolling moment due to aileron derivative
$C_{L_{\delta_e}}$	Change in total airplane lift for unit elevator angle
$C_{l_{\delta_r}}$	The rolling moment due to rudder derivative
C_{l_β}	The rolling moment due to sideslip derivative
$C_{l_{\dot{\beta}}}$	The rolling moment due to rate of sideslip derivative
C_m	Aircraft pitching moment coefficient
$C_{m_{ac_{wf}}}$	Pitching moment coefficient of wing-fuselage at aerodynamic center
$C_{m_{i_h}}$	Change in total airplane pitching moment for unit stabilizer angle
C_{m_q}	Pitching moment due to pitch rate derivative
C_{mT_u}	Thrust moment due to speed derivative
$C_{m_{T1}}$	The steady state pitching moment coefficient due to thrust
C_{m_u}	Pitching moment coefficient due to speed
C_{m_0}	Total airplane pitching moment coefficient for $\alpha=i_h=\delta_e=0$
$C_{m_{0_f}}$	Fuselage pitching moment for zero angle of attack
$C_{m_{0_h}}$	Horizontal tail pitching moment for zero angle of attack
$C_{m_{0_r}}, C_{m_{0_t}}$	Root and tip airfoil pitching moment for zero angle of attack
$C_{m_{0_w}}$	Wing pitching moment for zero angle of attack
$C_{m_{0_{wf}}}$	Wing-fuselage pitching moment for zero angle of attack
C_{m_1}	Steady state pitching moment
C_{m_α}	Total airplane pitching moment coefficient versus angle of attack slope
$C_{m_{\dot{\alpha}}}$	Pitching moment due to rate of angle of attack

	derivative
$C_{m_{\alpha_{wf}}}$	Wing-fuselage pitching moment coefficient versus angle of attack slope
$C_{m_{\delta_e}}$	Change in total airplane pitching moment for unit elevator angle
C_{n_p}	The yawing moment due to roll rate derivative
C_{n_r}	The yawing moment due to yaw rate derivative
$C_{n_{T_\beta}}$	The yawing moment due to thrust in sideslip derivative
C_{n_β}	The yawing moment due to sideslip derivative
$C_{n_{\dot{\beta}}}$	The yawing moment due to rate of sideslip derivative
$C_{n_{\delta_a}}$	The yawing moment due to aileron derivative
$C_{n_{\delta_r}}$	The yawing moment due to rudder derivative
C_{r_h}	Horizontal tail chord length at root section.
C_{r_v}	Vertical tail chord length at root section.
C_{r_w}	Wing chord length at root section.
C_T	Thrust coefficient
C_{t_h}	Horizontal tail chord length at tip section.
C_{t_v}	Vertical tail chord length at tip section.
C_{t_w}	Wing chord length at tip section.
$C_{T_{xu}}$	Thrust due to speed derivative
$C_{T_{x1}}$	The steady state thrust coefficient component in the direction of the stability x-axis
$\bar{C}_v$	Vertical tail mean chord.
$\bar{C}_w$	Wing mean chord.
C_{y_r}	The side force due to yaw rate derivative
C_{y_β}	The side force due to sideslip derivative
$C_{y_{\delta_a}}$	The side force due to aileron derivative
$C_{y_{\delta_r}}$	The side force due to rudder derivative
d_f	Equivalent fuselage diameter.
D_p	Diameter of propeller
d_T	Distance of thrustline to center of gravity
e	Span efficiency factor.
E	Endurance

E_h	Oswald efficiency factor for the horizontal tail.
f_{A_x}	Perturbed aerodynamic force in x-axis
f_{A_y}	Perturbed aerodynamic force in y-axis
f_{A_z}	Perturbed aerodynamic force in z-axis
f_{T_x}	Perturbed thrust force in x-axis
f_{T_y}	Perturbed thrust force in x-axis
f_{T_z}	Perturbed thrust force in x-axis
g	Acceleration of gravity
h	Height
I_{xx}	Moments of inertia about X-axis
I_{xz}	Products of inertia in XZ system
I_{yy}	Moments of inertia about Y-axis
I_{zz}	Moments of inertia about X-axis
i_{cl_f}	Incidence angle of the i^{th} fuselage part
i_h	Incidence angle of the horizontal tail
i_w	Incidence angle of the wing
k'	Correction factor which accounts for nonlinearities at high elevator deflection angles.
K_a	The partial span aileron parameter.
K_b	The elevator span factor.
K_f	Fuselage correction factor.
K_s	Store interference factor.
K_{wf}	Wing-fuselage interference factor
k_{wh}	The wing on horizontal tail interference factor
L'	Thickness location parameter
l_A	Perturbed rolling moment due to aerodynamic forces
l_f	Fuselage length.
l_p	The moment arm of the propeller normal force to the reference point.
l_p	Horizontal distance between wing and vertical tail quarter chords.
L_v	Horizontal distance between vertical tail aerodynamic center and center of gravity.
M	Mass (airplane)
M	Airplane aerodynamic pitching moment
m_A	Perturbed pitching moment due to aerodynamic forces
m_T	Perturbed pitching moment due to thrust forces
M_1	Mach number in steady state
n	Load factor
n_A	Perturbed yawing moment due to aerodynamic forces
n_T	Perturbed yawing moment due to thrust forces
p	A factor which accounts for the variation of gear drag with lift.

p	Perturbed roll rate
q	Perturbed pitch rate
$\bar{q}$	Dynamic pressure
r	Perturbed yaw rate
R	Range
R_{LS}	Lifting surface correction factor
$R_{N\ antenna}$	Reynolds number of the antenna
$R_{N\ fus}$	Reynolds number on the fuselage at the antenna location
R_{wf}	Interference factor
R_x	Reynolds number
S	Wing area
S_{f_s}	Fuselage side area.
S_h	Horizontal tail area
S_{LG}	Landing ground roll
S_{gear}	Reference area.
S_{sp_i}	Flat plate area of each spoiler.
S_{TOG}	Takeoff ground roll
S_v	Vertical tail area
S_{wet}	Wetted area
T	Thrust force
T_R	Roll mode time constant
$T_{1/2}$	Time to half amplitude
T_2	Time to double amplitude
t/c	Thickness ratio
u	Perturbed forward velocity
U_1	Steady state airspeed
V	Perturbed side velocity
V_{LOF}	Liftoff speed
V_s	Stall speed
V_{S_L}	The stall speed for landing configuration.
$V_{S_{TO}}$	Stall speed at takeoff configuration.
W_{f_i}	Width of the i^{th} fuselage part
w_n	Undamped natural frequency
X	Distance
$\bar{x}_{ac_A}$	The location of the airplane aerodynamic center in fractions of the mean geometric center.
$\bar{x}_{ac_h}$	Position of horizontal tail aerodynamic center
$\bar{x}_{ac_{wf}}$	Location of aerodynamic center of wing-fuselage in terms of $\bar{c}$

$\bar{x}_{cg}$	Location of center of gravity in terms of $\bar{c}$
$\bar{x}_{ref}$	Position of reference point on wing mean geometric center
x_w	Distance of wing quarter chord mean geometric center to center of gravity.
z_f	Vertical height of fuselage at wing root chord.
z_p	Vertical distance between wing and vertical tail quarter chords.
Z_v	Vertical distance between vertical tail aerodynamic center and center of gravity.
z_w	Wing distance to fuselage centerline.

GREEK SYMBOLS

α	Angle of attack
$\dot{\alpha}$	Angle of attack rate
$\alpha_{C_{L_{max}}}$	Angle of attack for maximum lift coefficient coefficient
α_{0_L}	Zero lift angle of attack
β	Sideslip angle
$\dot{\beta}$	Sideslip angle rate
θ_1	Steady state pitching angle
δ	Boundary layer thickness
δ_a	Aileron deflection angle
δ_e	Elevator deflection angle
δ_r	Rudder deflection angle
η_h	Dynamic pressure ratio of the horizontal tail
η_p	Propeller efficiency
ε_{0_h}	Average downwash angle induced by the wing on the deflection
τ_e	Angle of attack effectiveness of the elevator
$\Lambda_{c/4}$	Wing quarter chord sweep angle
Γ	The wing geometric dihedral angle.
λ	Root of a characteristic equation
ξ	Damping ratio
ϕ	Perturbed bank (roll) angle
ψ	Perturbed heading angle
$\frac{d\varepsilon}{d\alpha}$	Rate of change in downwash with angle of attack

$\left(\frac{d\varepsilon}{d\alpha}\right)_{\delta}$	Rate of change in downwash with angle of attack with flaps down
$\frac{\partial C_D}{\partial C_L}$	Drag polar curve slope for steady state lift coefficient and Mach number.
$\frac{\partial C_D}{\partial M}$	The derivative of the airplane drag coefficient with respect to Mach number
$\Delta C_{D_{i_f}}$	The induced drag increment due to the.
$\Delta C_{D_{\text{int}_f}}$	The interference drag increment due to the flap.
$\Delta C_{D_{prof_f}}$	The flap profile drag increment.
$\Delta C_{D_{sp_i}}$	The drag coefficient increment of i^{th} element.
$\Delta C_{D_{trim_{prof}}}$	The profile drag coefficient increment due to the need for generating trim lift.
$\Delta C_{D_{trim_{lift}}}$	The induced drag coefficient increment due to the need for generating trim lift.
ΔC_l	Incremental airfoil lift coefficient due to flaps.
ΔC_{L_h}	Incremental tail lift coefficient to trim, based on
Δx_i	Length of the i^{th} fuselage part
$\Delta\alpha_{C_{L_{\max}}}$	Incremental aircraft angle of attack for maximum lift
$\Delta\varepsilon_f$	The increase in tail downwash angle due to wing flap

SUBCRIPTS

a	Aileron
A	Aerodynamic
ac	Aerodynamic center
can	Canopy
D	Dutch roll mode
e	Elevator
emp	Empennage
f	Flap
fus	Fuselage
h	Horizontal tail
i	i^{th} item, particle, component
int	Interference
l	Airfoil
M	(at a given) Mach number
max	Maximum

misc	Miscellaneous
n	Nacelle
np	Nacelle/pylon
p	Pylon
P	Phugoid mode
r	rudder
R	Rolling mode
s	Store
S	Spiral mode
sp	Spoiler
SP	Short period mode
T	Thrust or power effect
TL	Thrust line
TO	Takeoff
v	Vertical tail
w	Wing
wb	Wing-body
wf	wing-fuselage
ws	Windshield
0	Zero angle of attack
1	Steady state
δ	Deflection angle of flap, aileron, rudder or elevator

ACRONYMS

AAA	The software Advanced Aircraft Analysis
AOA	Angle of attack
cg, CG	Center of gravity
FAR	Federal Aviation Regulation
mgc	Mean geometric chord
SHP	Shaft horsepower

CHAPTER 1

1. INTRODUCTION

Designing an air vehicle was too simple at the end of the last century. Only important thing for them was to fly a few meters. But day by day necessities and requirements became more complicated. Their range and endurance increased, they could carry more payload or passenger.

During this century maybe more than 10,000 kinds of air vehicles were designed and constructed. After design and construction, many modifications were made to these aircraft. So designing an air vehicle is a continuous process.

The design process is too complicated. It has basically four main steps:

- Conceptual design with empirical methods.
- Preliminary design (usage of Computational Fluid Dynamics (CFD) codes, wind tunnel tests, etc.).
- Detail design.
- Prototype development, land and flight tests.

Either designing a new air vehicle or a modification requires these steps. They are connected each other and they have to be made with the sequence given above.

The designer must know the Performance and Flight Mechanics properties of the aircraft. These properties strongly depend upon the aerodynamic characteristics. Therefore analyses and tests to obtain aerodynamic, performance and flight mechanics characteristics have to be performed. Aerodynamic characteristics of an aircraft can be obtained by using methods of various levels.

The first level is by using empirical methods. It uses more basic methods with respect to other three levels. At the end of this step one can say that if this air vehicle can fly or can not. If it is made

for a modification, one can decide if it is proper or not. The values that are obtained in this level may have less accuracy when compared to the values obtained at other levels..

Second level is usage of the CFD codes. It requires more capable computers and gives more accurate information.

Next level is wind tunnel tests. A model of the air vehicle is put inside the wind tunnel test section. Very accurate values can be obtained at this level. After this level, one can say if a prototype can be manufactured or not.

Final level is flight tests. It gives real information about an air vehicle or modification. After this level, if results are positive, the serial manufacturing process of the air vehicle begins or the modifications are certified.

In this report, the first level aerodynamic calculations are performed for CASA CN-235 aircraft. Also based on the aerodynamic information obtained, performance and flight mechanics characteristics of this aircraft are predicted.

The analysis is divided into 6 parts. In Chapter 2, the description of the CASA CN-235 is presented. The values that are listed in this chapter are used as inputs in the following chapters.

In Chapter 3, aerodynamic calculations are performed. During calculation process a software that is called Advanced Aircraft Analysis (AAA) is mainly used. At the end of this chapter the results for the lift coefficient versus angle of attack curves, drag polar curves and pitching moment coefficient versus angle of attack curves are presented.

In Chapter 4, stability and control calculations are performed. Mainly the software AAA is used for calculations.

In Chapter 5, calculations of dynamic stability and response characteristics are made. The software Matlab as well as AAA is used for calculations. Results related to flying quality levels are listed. Finally dynamic responses of the aircraft for an input control surface deflection are presented.

In Chapter 6, the performance calculations are made.

In Chapter 7, the results of the present study are discussed and some conclusions are made.

CHAPTER 2

2. DESCRIPTION OF THE CASA CN-235

The following parameters that are used as inputs in the Software AAA[8] are taken from Jane's[3] (Appendix D) or calculated by AAA. Figure 2.1, 2.2 and 2.3 show three view of the CASA CN-235. In the following chapters, CASA CN-235 is called the test aircraft.

TYPE : Twin-turboprop commuter and utility transport.

WINGS : Cantilever high-wing monoplane. NACA 65_3218 wing section. Constant chord centre-section, without dihedral; 3° dihedral on tapered outer panels. Incidence 3°. Sweepback 3° 51' 56" at quarter chord on outer panels. Inboard flaps on centre section, outboard flap segments and ailerons on outer panels. Flaps are single slotted. Ailerons, of similar construction to flaps, are statically and dynamically balanced and have duplicated flight controls. Raked wingtips.

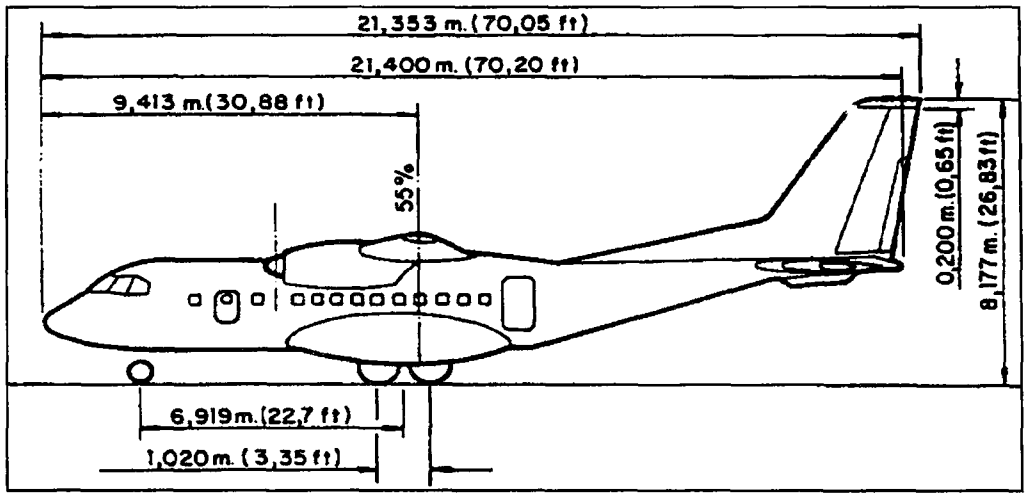

Figure 2.1 Side view of the CASA CN-235

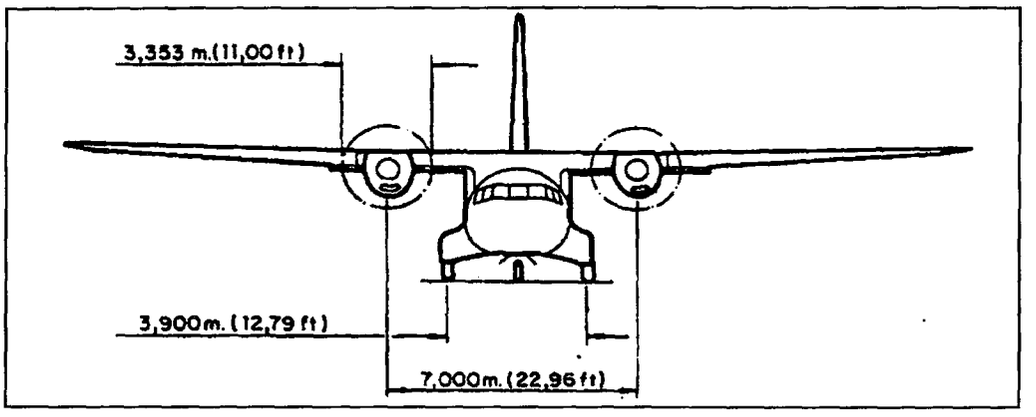

Figure 2.2 Front view of the CASA CN-235

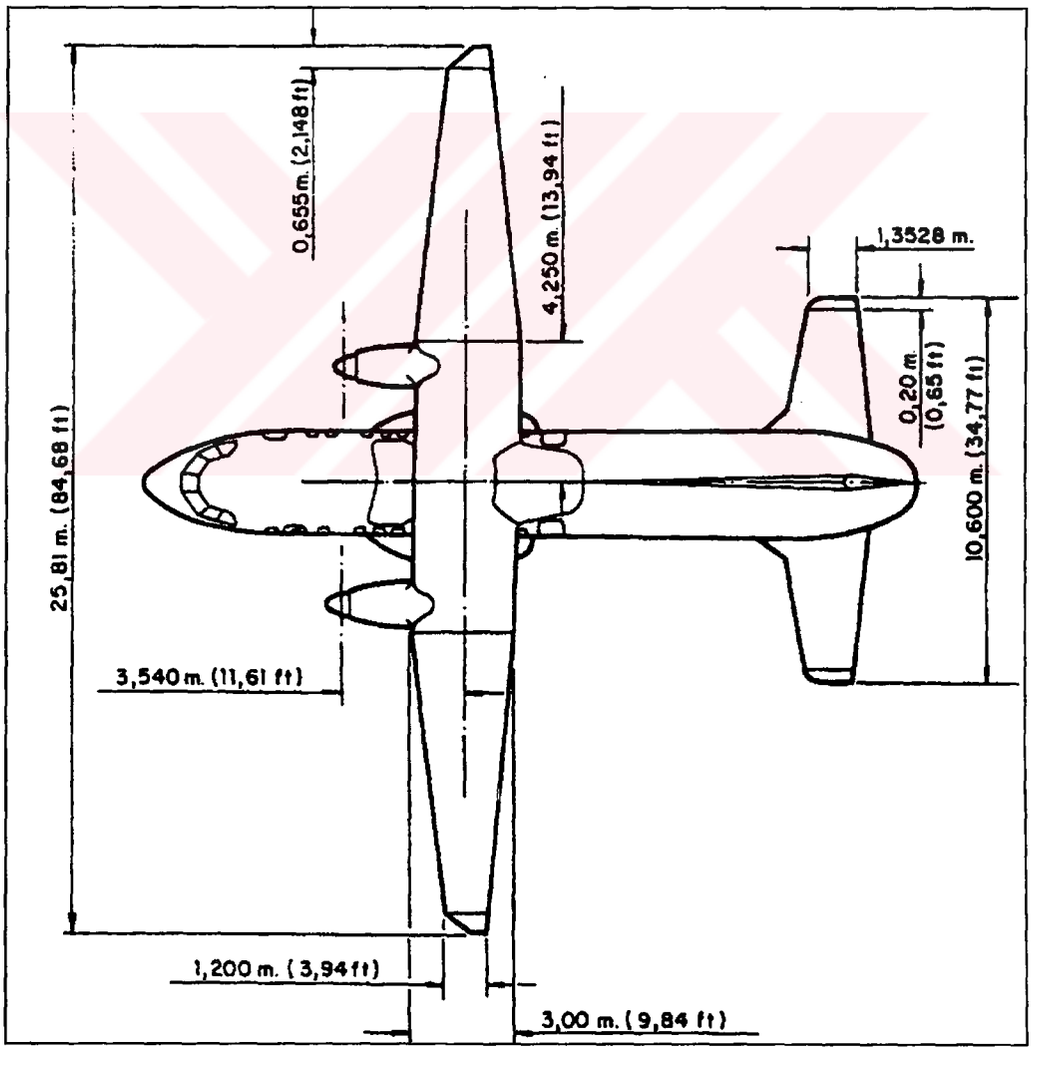

Figure 2.3 Top view of the CASA CN-235

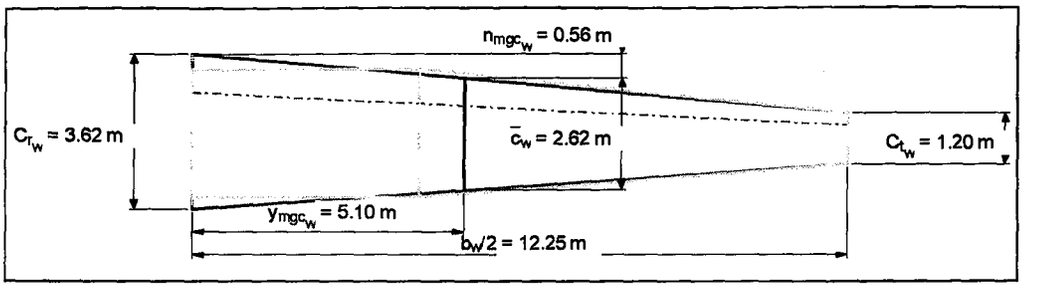

Figure 2.4 Wing

where:

C_{r_w} : Wing chord length at root section.

C_{t_w} : Wing chord length at tip section.

$\bar{C}_w$: Wing mean chord.

b_w : Wing span.

FUSELAGE : Flattened circular cross-section, upswept at rear.

HORIZONTAL TAIL : Non-swept fixed incidence. Statically and dynamically balanced elevators. NACA 64_1 012 airfoil.

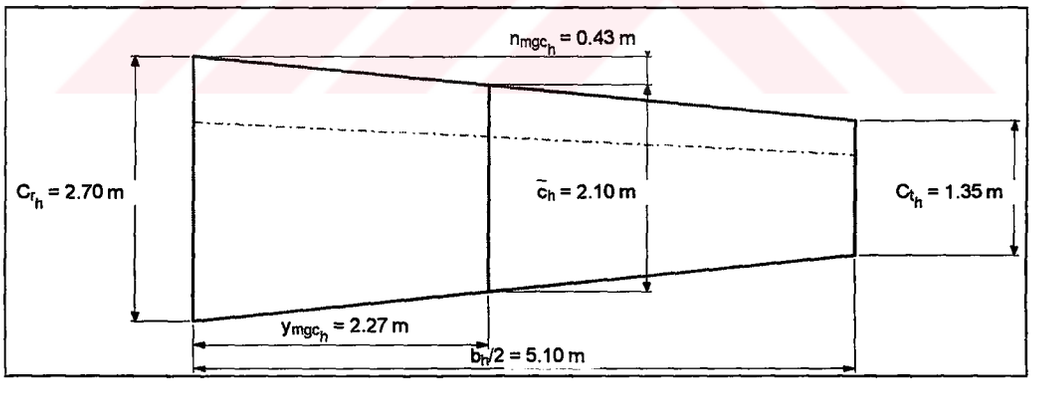

Figure 2.5 Horizontal tail

where:

C_{r_h} : Horizontal tail chord length at root section.

C_{t_h} : Horizontal tail chord length at tip section.

$\bar{C}h$: Horizontal tail mean chord.
b_h : Horizontal tail span.

VERTICAL TAIL : Sweptback fin and statically and dynamically balanced rudder. NACA 64_1 012 airfoil.

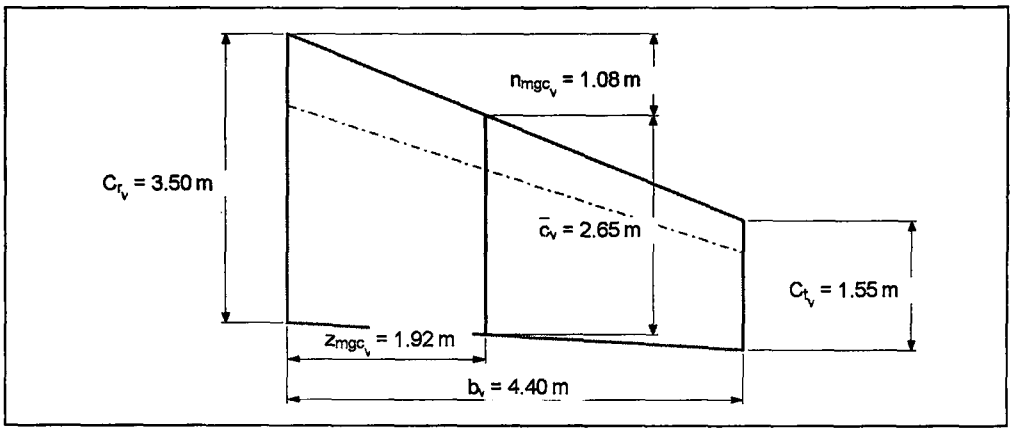

Figure 2.6 Vertical tail

where:

C_{r_v} : Vertical tail chord length at root section.
C_{t_v} : Vertical tail chord length at tip section.
$\bar{C}_v$: Vertical tail mean chord.
b_v : Vertical tail span.

LANDING GEAR : Retractable tricycle type. Wheel track is 3.9 m., wheel base is 6.919 m.

POWER PLANT : Two General Electric CT7-9C turboprops, each flat rated at 1305 kW (1750 shp) (S/L, to 41 °C) for take-off and 1394.5 kW (1870 shp) up to 31°C with automatic power reserve. Hamilton Standard 14-RF21 four blade constant speed propellers, with full feathering and reverse-pitch capability.

DIMENSIONS :

Length overall	: 21.353 m
Fuselage max depth	: 2.615 m
Propeller diameter	: 3.35 m

AREAS :

Wings, gross	: 59.1 m^2
Ailerons (total, including tabs)	: 3.07 m^2
Trailing edge flaps	: 10.87 m^2
Rudder, including tabs	: 3.32 m^2
Horizontal tail area	: 20.67 m^2
Elevators (total, including tabs)	: 6.17 m^2

WEIGHTS :

Max T-O weight	: 15100 kg
Max landing weight	: 15050 kg

ANTENNAS :

There are 10 antennas in 6 different types and a light on the aircraft (Table 2.1).

Table 2.1 Locations and numbers of the antennas and a light

NAME	NUMBER OF THE ANTENNAS	LOCATION ON THE CASA CN-235
IFF Antennas	2	Above and under the fuselage
DF Antenna	1	Under the fuselage
Beacon Antennas	2	Under the fuselage
ADF Antennas	1	Under the fuselage
DME Antennas	2	Above and under the fuselage
Altimeter Antennas	2	Under the fuselage
Light	1	Under the fuselage

CHAPTER 3

3. AERODYNAMIC CALCULATIONS

In this chapter, first the definitions and explanations of the aerodynamic forces and moments are presented. Then the calculations that are not done by the software AAA are performed. Finally results for the lift coefficient versus angle of attack curves, drag polar curves and pitching moment coefficient versus angle of attack curves are listed.

3.1 THEORY

In this chapter description of the theories used by AAA program for the calculation of Aerodynamic characteristics are presented . The theory part of this chapter is based on Reference 1, 2, and 11.

3.1.1 AERODYNAMIC FORCES AND MOMENTS

Aerodynamic forces and moments on the body are due to only two basic sources:

- Pressure distribution over the body surface
- Shear stress distribution over the body surface

The net effect of the pressure and shear stress distributions is a resultant aerodynamic force R and moment M on the body, as sketched in Figure 3.1. The aerodynamic force can be divided into two components, lift, L, is the component of R perpendicular to freestream, V_∞ and drag, D, is the component of R parallel to V_∞.

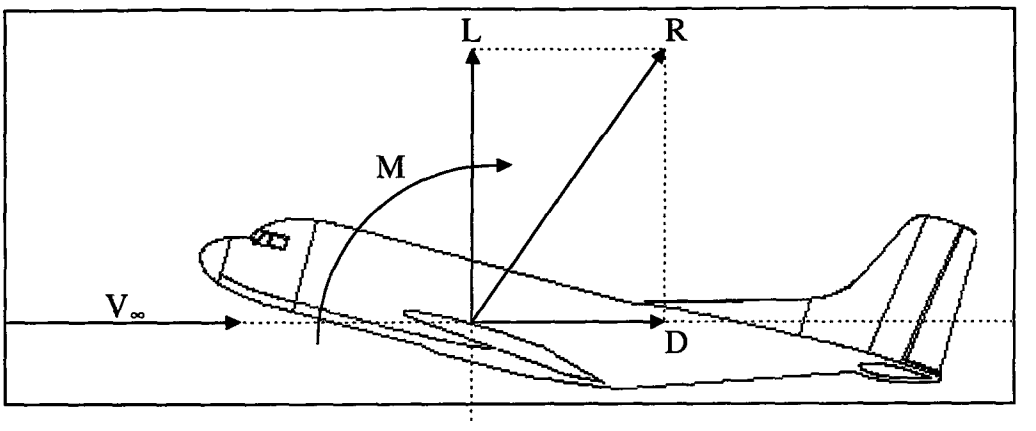

Figure 3.1 Aerodynamic forces and moment on the aircraft in the plane of symmetry.

3.1.2 LIFT

Total airplane lift is nondimensionalized as follows:

$$L = C_L \bar{q} S \tag{3.1}$$

where:

C_L : Aircraft lift coefficient

$\bar{q}$: Dynamic pressure

S : Wing area

The steady state airplane lift depends on the following parameters:

- Angle of attack
- Elevator and stabilizer angles
- Dynamic pressure
- Mach number

Dynamic pressure $\bar{q}$ is accounted for through in Equation 3.1. The functional dependence on the other parameters is usually expressed as:

$$C_L = C_{L_0} + C_{L_\alpha}\alpha + C_{L_{i_h}} i_h + C_{L_{\delta_e}} \delta_e \tag{3.2}$$

with:

$$C_{L_0} = C_{L_{0_{wf}}} + C_{L_{\alpha_h}} \eta_h \frac{S_h}{S}\left(i_h - \varepsilon_{0_h}\right) \tag{3.3}$$

$$C_{L_\alpha} = C_{L_{\alpha_{wf}}} + C_{L_{\alpha_h}} \eta_h \frac{S_h}{S}\left(1 - \frac{d\varepsilon}{d\alpha}\right) \tag{3.4}$$

$$C_{L_{i_h}} = C_{L_{\alpha_h}} \eta_h \frac{S_h}{S} \tag{3.5}$$

$$C_{L_{\delta_e}} = C_{L_{\alpha_h}} \eta_h \frac{S_h}{S} \tau_e \tag{3.6}$$

where:

C_{L_0} : total airplane lift coefficient for $\alpha=i_h=\delta_e=0$
α : angle of attack
C_{L_α} : total airplane lift curve slope
$C_{L_{i_h}}$: change in total airplane lift for unit stabilizer angle
i_h : incidence angle of the horizontal tail
$C_{L_{\delta_e}}$: change in total airplane lift for unit elevator angle
δ_e : elevator deflection angle
$C_{L_{0_{wf}}}$: wing-fuselage lift coefficient for zero angle of attack
$C_{L_{\alpha_h}}$: horizontal tail lift curve slope
η_h : dynamic pressure ratio of the horizontal tail
S_h : horizontal tail area
ε_{0_h} : average downwash angle induced by the wing on the horizontal tail when $\alpha=0$
$C_{L_{\alpha_{wf}}}$: wing-fuselage lift curve slope
$\frac{d\varepsilon}{d\alpha}$: rate of change in downwash with angle of attack
τ_e : angle of attack effectiveness of the elevator

Figure 3.2 shows the relationship between airplane lift and airplane angle of attack. It also shows the effects of the flaps.

The airplane zero-lift angle of attack:

$$\alpha_{o_L} = -\frac{C_{L_0}}{C_{L_\alpha}} \tag{3.7}$$

The airplane maximum lift coefficient:

$$C_{L_{max}} = C_{L_{max_w}} + \eta_h C_{L_{\alpha_h}} \frac{S_h}{S}\left[\alpha_{C_{L_{max}}}\left(1-\frac{d\varepsilon}{d\alpha}\right)-\varepsilon_{0_h}+i_h\right] \qquad (3.8)$$

where:

$C_{L_{max_w}}$: the wing maximum lift coefficient

$\alpha_{C_{L_{max}}}$: angle of attack for maximum lift coefficient of the wing

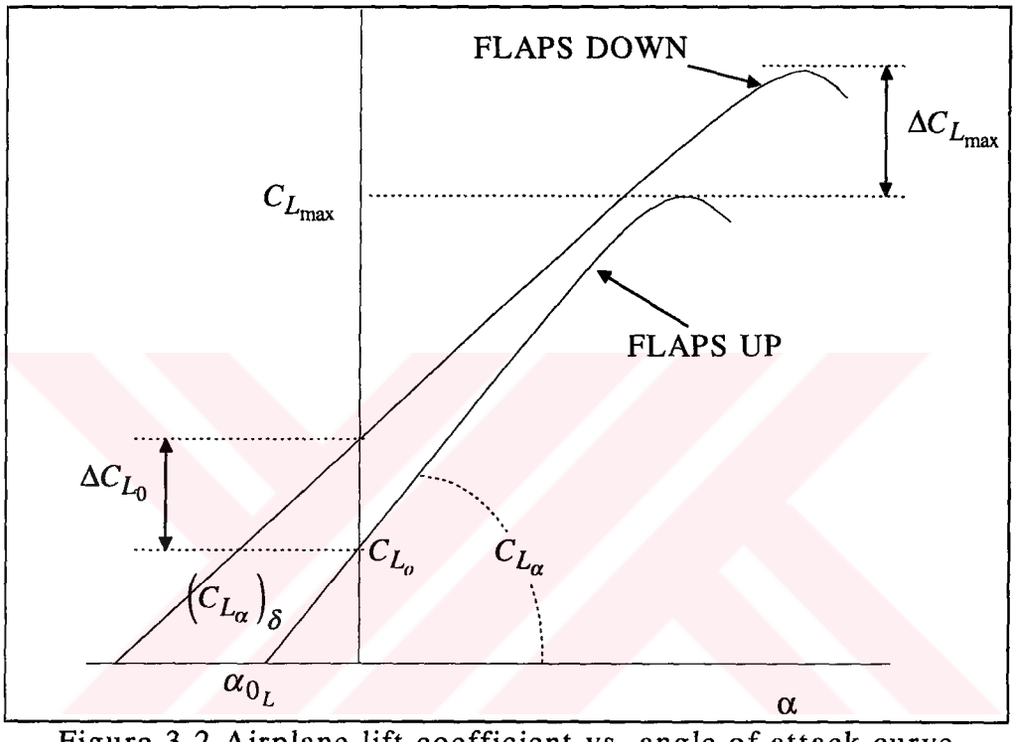

Figure 3.2 Airplane lift coefficient vs. angle of attack curve

The airplane lift increment due to flaps:

$$\Delta C_L = \Delta C_{L_w} + k_{wh}\frac{S_h}{S}\Delta C_{L_h} - C_{L_{\alpha_h}}\eta_h\frac{S_h}{S}\Delta\varepsilon_f \qquad (3.9)$$

where:

k_{wh} : the wing on horizontal tail interference factor

ΔC_{L_h} : incremental tail lift coefficient to trim, based on horizontal tail area

$\Delta\varepsilon_f$: the increase in tail downwash angle due to wing flap deflection

The airplane lift curve slope with the flaps down:

$$\left(C_{L_\alpha}\right)_\delta = K_{wf}\left(C_{L_{\alpha_w}}\right)_\delta + C_{L_{\alpha_h}}\eta_h\frac{S_h}{S}\left[1-\left(\frac{d\varepsilon}{d\alpha}\right)_\delta\right] \qquad (3.10)$$

where:

K_{wf} : wing-fuselage interference factor

$\left(C_{L_{\alpha_w}}\right)_\delta$: the wing lift curve slope with flaps down

$\left(\frac{d\varepsilon}{d\alpha}\right)_\delta$: rate of change in downwash with angle of attack with flaps down

The airplane maximum lift increment with the flaps:

$$\Delta C_{L_{max}} = \Delta C_{L_{max_w}} + C_{L_{\alpha_h}}\eta_h\frac{S_h}{S}\left[\alpha_{C_{L_{max}}}\left(1-\frac{d\varepsilon}{d\alpha}\right)+i_h-\Delta\varepsilon_f\right] \qquad (3.11)$$

3.1.3 DRAG

Total airplane drag is nondimensionalized as follows:

$$D = C_D\bar{q}S \qquad (3.12)$$

where:

C_D : aircraft drag coefficient

The steady state flight is defined as a flight condition for which all motion variables remain constant with the time relative to a body fixed axis system. The steady state airplane drag depends on the following parameters:

- Angle of attack
- Elevator and stabilizer angle
- Dynamic pressure
- Mach number and Reynolds number

Dynamic pressure $\bar{q}$ is accounted for through in Equation 3.12. The functional dependence on the other parameters is usually expressed as:

$$C_D = C_{D_0} + C_{D_\alpha}\alpha + C_{D_{i_h}}i_h + C_{D_{\delta_e}}\delta_e \qquad (3.13)$$

where:

C_{D_0} : total airplane drag coefficient for $\alpha=i_h=\delta_e=0$

C_{D_α} : total airplane drag change with angle of attack at $i_h=\delta_e=0$

$C_{D_{i_h}}$: total airplane drag change with stabilizer, $\alpha=\delta_e=0$

$C_{D_{\delta_e}}$: total airplane drag change with elevator, $\alpha=i_h=0$

Drag polar curve (Figure 3.3) shows the variation of drag with respect to lift. Because of the quadratic nature of the drag polar, the linear expansion reflected by Equation 3.13 must be viewed as a local linearization. For stability and control purposes the range of validity around some steady state angle of attack is usually sufficiently wide to allow Equation 3.13 to be used. It must be kept in mind however, that C_{D_0} and C_{D_α} are different for each steady state.

C_{L_1} and C_{D_1} are steady state lift and drag coefficients respectively.

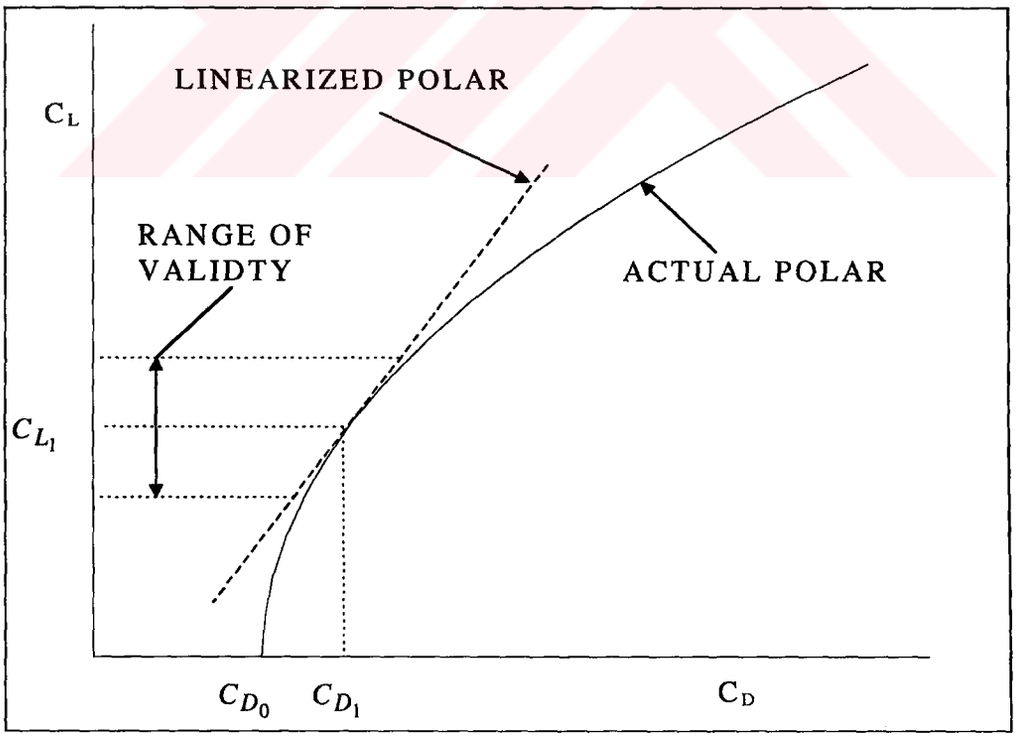

Figure 3.3 Drag polar curve

Total drag is the sum of zero-lift drag and induced drag. The total airplane drag coefficient can be calculated by using drag breakdown procedure method. It is broken down into the following components:

$$C_D = C_{D_w} + C_{D_{fus}} + C_{D_{emp}} + C_{D_{np}} + C_{D_f} + C_{D_{gear}} + C_{D_{cw}} + C_{D_s} + C_{D_{trim}} + C_{D_{\text{int}}} + C_{D_{misc}} \quad (3.14)$$

where :

C_{D_w} : Wing drag coefficient.

$C_{D_{fus}}$: Fuselage drag coefficient.

$C_{D_{emp}}$: Empennage drag coefficient.

$C_{D_{np}}$: Nacelle/Pylon drag coefficient.

C_{D_f} : Leading/Trailing edge flap drag coefficient.

$C_{D_{gear}}$: Landing gear drag coefficient.

$C_{D_{cw}}$: Canopy/Windshield drag coefficient.

C_{D_s} : Store(s) drag coefficient.

$C_{D_{trim}}$: Trim drag coefficient.

$C_{D_{\text{int}}}$: Interference drag coefficient.

$C_{D_{misc}}$: Miscellaneous drag coefficient.

3.1.3.1 WING DRAG COEFFICIENT

Wing drag is the sum of zero-lift drag and drag due to lift.

$$C_{D_w} = C_{D_{0_w}} + C_{D_{L_w}} \quad (3.15)$$

where :

$C_{D_{0_w}}$: Wing zero-lift drag coefficient.

$C_{D_{L_w}}$: Wing drag coefficient due to lift.

3.1.3.2 FUSELAGE DRAG COEFFICIENT

Fuselage drag is the sum of zero-lift drag and drag due to lift.

$$C_{D_{fus}} = C_{D_{0_{fus}}} + C_{D_{L_{fus}}} \quad (3.16)$$

where :

$C_{D_{0_{fus}}}$: Fuselage zero-lift drag coefficient.

$C_{D_{L_{fus}}}$: Fuselage drag coefficient due to lift.

3.1.3.3 EMPENNAGE DRAG COEFFICIENT

An airplane may have the following empennage surfaces:

- Horizontal tail surface(s)
- Canard surface(s)
- Vertical tail surface(s)

Empennage drag is the sum of zero-lift drag and drag due to lift of each empennage component.

.

$$C_{D_{emp}} = \sum_i \left[\left(C_{D_{0_{emp}}} \right)_i + \left(C_{D_{L_{emp}}} \right)_i \right] \tag{3.17}$$

where :

$\left(C_{D_{0_{emp}}} \right)_i$: Empennage zero-lift drag coefficient of the number i empennage surface.

$\left(C_{D_{L_{emp}}} \right)_i$: Empennage drag coefficient due to lift of the number i empennage surface.

3.1.3.4 NACELLE/PYLON DRAG COEFFICIENT

Nacelle/Pylon drag is the sum of zero-lift drag and drag due to lift of each nacelle and pylon component.

$$C_{D_{np}} = C_{D_n} + C_{D_P} \tag{3.18}$$

where :

C_{D_n} : Nacelle drag coefficient.

C_{D_p} : Pylon drag coefficient.

3.1.3.5 FLAP DRAG COEFFICIENT

Flap drag is the sum of the flap profile drag increment, the induced drag increment due to flaps, and the interference drag due to flap.

$$C_{D_f} = \Delta C_{D_{prof_f}} + \Delta C_{D_{i_f}} + \Delta C_{D_{\text{int}_f}} \tag{3.19}$$

where :

$\Delta C_{D_{prof_f}}$: The flap profile drag increment.

$\Delta C_{D_{i_f}}$: The induced drag increment due to the flap.

$\Delta C_{D_{\text{int}_f}}$: The interference drag increment due to the flap.

3.1.3.6 LANDING GEAR DRAG COEFFICIENT

Landing gear drag is calculated using the following equation.

$$C_{D_{gear}} = \sum_i \left\{ \left[\left(C_{D_{gear_{C_L=0}}} \right)_i + p_i C_L \right] \frac{(S_{gear})_i}{S} \right\} \tag{3.20}$$

where :

$\left(C_{D_{gear_{C_L=0}}} \right)_i$: The zero-lift drag coefficient of the landing gear based on its own reference area.

S_{gear} : Reference area of the gear.

p : A factor which accounts for the variation of gear drag with lift.

3.1.3.7 CANOPY/WINDSHIELD DRAG COEFFICIENT

The drag amount which is caused by canopy and windshield.

$$C_{D_{cw}} = C_{D_{can}} + C_{D_{ws}} \tag{3.21}$$

where :

$C_{D_{can}}$: Drag coefficient due to canopy.

$C_{D_{ws}}$: Drag coefficient due to windshield.

3.1.3.8 STORE DRAG COEFFICIENT

The drag amount which is caused by store(s).

$$C_{D_s} = \sum_i \left[(K_s)_i \left(C_{D_s} \right)_i \right] \tag{3.22}$$

where :

$(K_s)_i$: Store interference factor.

$(C_{D_s})_i$: Drag coefficient of the isolated store.

3.1.3.9 TRIM DRAG COEFFICIENT

Trim drag is caused by lift generated on a horizontal tail and/or a canard as a result of the requirement to moment trim an airplane. It is the sum of the trim drag due to lift generated on the trimming surface and profile drag generated on the trimming surface due to a control surface.

$$C_{D_{trim}} = \Delta C_{D_{trim_{lift}}} + \Delta C_{D_{trim_{prof}}} \tag{3.23}$$

where :

$\Delta C_{D_{trim_{lift}}}$: The induced drag coefficient increment due to the need for generating trim lift.

$\Delta C_{D_{trim_{prof}}}$: The profile drag coefficient increment due to the need for generating trim lift.

3.1.3.10 INTERFERENCE DRAG COEFFICIENT

Interference drag is the type of drag caused by the flowfield interaction two components. Its effect is that the total drag of two or more airplane components, when integrated in configuration, is always larger than the sum of the individual component drags.

3.1.3.11 MISCELLANEOUS DRAG

Miscellaneous drag is result of the spoilers/speed brakes, surface roughness, and other causes.

3.1.3.11.1 Drag Due To Spoilers / Speed Brakes

Spoilers are commonly used on jet transports to augment roll control at low speed, and can also be used to reduce lift and add drag during the landing phase. Speed brakes are used to decrease velocity by increasing drag.

$$\Delta C_{D_{sp}} = \sum_i \left[\Delta C_{D_{sp_i}} \frac{S_{sp_i}}{S} \right] \tag{3.24}$$

where :

$\Delta C_{D_{sp_i}}$: The drag coefficient increment of i^{th} element.

S_{sp_i} : Flat plate area of each spoiler.

3.1.3.11.2 Drag Due To Surface Roughness

If a surface is rough, additional drag is created. It depends on the amount of the surface roughness.

3.1.3.11.3 Drag Due To Other Causes

Other causes for drag may be items such as : struts, antennas, surface gaps, extra drag caused by inlet air spillage and by exhaust nozzle integration.

3.1.3.11.3.1 Drag of the antennas which shape is like a flat plate of finite width

The variation of C_D with the plate width to height ratio (b/h) is shown in Figure 9.10 of Reference 5 (Appendix C). For b/h = 1.0, the drag coefficient is a minimum at C_D = 1.18.

$$S_i = bh \tag{3.25}$$

where:

b : width

h : height

Aspect ratio of the antenna:

$$A = \frac{b}{h} \tag{3.26}$$

Drag contribution of the i^{th} antenna to aircraft drag:

$$\Delta C_{D_i} = C_{D_i} \frac{S_i}{S} \tag{3.27}$$

where:

C_{D_i} : Drag coefficient of i^{th} antenna or element

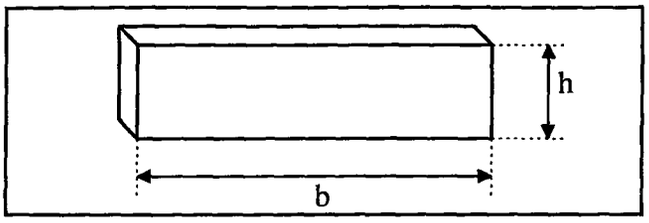

Figure 3.4 Antenna which shape is like a flat plate of finite end.

3.1.3.11.3.2 Drag of the antennas which shape is like a circular cylinder

The drag coefficient for flow over a circular cylinder is shown in Figure 9.13 of Reference 5 (Appendix C).

3.1.4 PITCHING MOMENT

Total airplane aerodynamic pitching moment is nondimensionalized as follows:

$$M = C_m \bar{q} S \bar{c} \tag{3.28}$$

where:

C_m : aircraft pitching moment coefficient

$\bar{c}$: mean aerodynamic chord

The steady state airplane pitching moment depends on the following parameters:

- Angle of attack
- Elevator and stabilizer angles
- Dynamic pressure
- Mach number

The functional dependence on these parameters is usually expressed as:

$$C_m = C_{m_0} + C_{m_\alpha}\alpha + C_{m i_h} i_h + C_{m_{\delta_e}} \delta_e \tag{3.29}$$

where:

C_{m_0} : total airplane pitching moment coefficient for $\alpha=i_h=\delta_e=0$

C_{m_α} : total airplane pitching moment coefficient versus angle of attack slope

$C_{m_{i_h}}$: change in total airplane pitching moment for unit stabilizer angle

$C_{m_{\delta_e}}$: change in total airplane pitching moment for unit elevator angle

with:

$$C_{m_0} = C_{m_{ac_{wf}}} + C_{L_{0_{wf}}}\left(-\bar{x}_{ac_{wf}} + \bar{x}_{cg}\right) + \\ -C_{L_{\alpha_h}}\eta_h\frac{S_h}{S}\left(\bar{x}_{ac_h} - \bar{x}_{cg}\right)\left(i_h - \varepsilon_0\right) \tag{3.30}$$

$$C_{m_\alpha} = C_{m_{\alpha_{wf}}}\left(\bar{x}_{cg} - \bar{x}_{ac_{wf}}\right) \\ -C_{L_{\alpha_h}}\eta_h\frac{S_h}{S}\left(\bar{x}_{ac_h} - \bar{x}_{cg}\right)\left(1 - \frac{d\varepsilon}{d\alpha}\right) \tag{3.31}$$

$$C_{m_{i_h}} = -C_{L_{\alpha_h}}\eta_h\frac{S_h}{S}\left(\bar{x}_{ac_h} - \bar{x}_{cg}\right) \tag{3.32}$$

$$C_{m_{\delta_e}} = -C_{L_{\alpha_h}}\eta_h\frac{S_h}{S}\left(\bar{x}_{ac_h} - \bar{x}_{cg}\right)\tau_e \tag{3.33}$$

where:

$C_{m_{ac_{wf}}}$: pitching moment coefficient of wing-fuselage at aerodynamic center

$\bar{x}_{ac_{wf}}$: location of aerodynamic center of wing-fuselage in terms of $\bar{c}$

$\bar{x}_{cg}$: location of center of gravity in terms of $\bar{c}$

$C_{m_{\alpha_{wf}}}$: wing-fuselage pitching moment coefficient versus angle of attack slope

Figure 3.5 shows pitching moment versus angle of attack variation for different elevator deflection. The slopes of the lines in Figure 3.5 are total airplane pitching moment coefficient versus angle of

attack slopes for different elevator deflections. Crossing points of these lines on angle of attack axis are trim points.

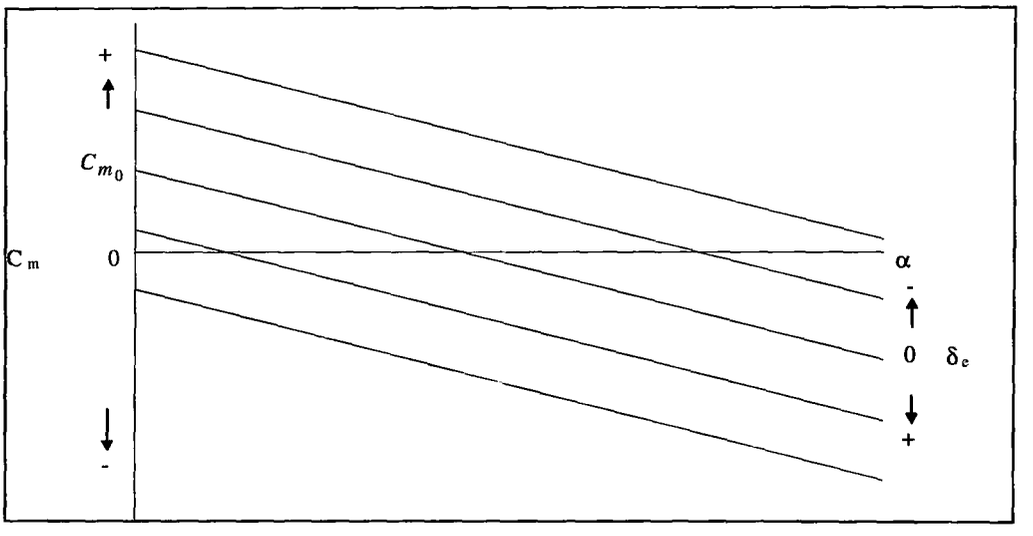

Figure 3.5 Pitching moment versus angle of attack curve

3.2 AERODYNAMIC CALCULATIONS FOR THE TEST AIRCRAFT

The software AAA was used for most of the calculations. This software is based on the method of Dr. Jan Roskam[1]. The aerodynamics part of this theory is described in Chapter 3.1. The miscellaneous drag force of antennas are calculated by using theoretical or empirical information from various sources. This information will be described in this chapter when appropriate.

The values taken from Jane's and CASA MAINTATENANCE MANUAL as inputs were used to calculate aerodynamic parameters. But some parameters which can not be found in any source are calculated in following sections. CASA CN-235 was examined for three flight conditions, cruise, takeoff, and landing.

3.2.1 STALL SPEED AT SEA LEVEL

δ_f is flap deflection angle.

Cruise (δ_f=0 degree)

Weight of the aircraft is assumed 145000 N. $C_{L_{max}}$=1.501 is calculated by AAA. ρ is air density and S is wing area.

$$V_s = \sqrt{\frac{2W}{\rho C_{L_{max}} S}} = \sqrt{\frac{2(145000)}{(1.225)(1.501)(59.1)}} = 51.60 m/s$$

Takeoff (δ_f=10 degree)

W=148131 N is taken from Jane's. $C_{L_{max}}$=1.688 is calculated by AAA.

$$V_s = \sqrt{\frac{2W}{\rho C_{L_{max}} S}} = \sqrt{\frac{2(148131)}{(1.225)(1.688)(59.1)}} = 49.24 m/s$$

Landing (δ_f=23 degree)

W=147640.5 N is taken from Jane's. $C_{L_{max}}$=1.905 is calculated by AAA.

$$V_s = \sqrt{\frac{2W}{\rho C_{L_{max}} S}} = \sqrt{\frac{2(147640.5)}{(1.225)(1.905)(59.1)}} = 46.27 m/s$$

3.2.2 VELOCITIES OF THE FLIGHT CONDITIONS

Cruise

V = 452 km/h = 125.56 m/s is taken from Jane's. Altitude is 15000 feet.

$$\bar{q} = \frac{\rho V^2}{2} = \frac{(0.7708)(125.56)^2}{2} = 6075.77 \frac{N}{m^2}$$

Takeoff

Altitude is sea level.

V = (1.1)V_s = (1.1)(49.24) = 54.16 m/s = 195 km/h

where:

V_s : Stall speed

$$\bar{q} = \frac{\rho V^2}{2} = \frac{(1.225)(54.16)^2}{2} = 1797.08 \frac{N}{m^2}$$

Landing

Altitude is sea level.

V = (1.2)V_s = (1.1)(46.27) = 55.52 m/s = 200 km/h

$$\bar{q} = \frac{\rho V^2}{2} = \frac{(1.225)(55.52)^2}{2} = 1890.42 \frac{N}{m^2}$$

3.2.3 STEADY STATE LIFT COEFFICIENT (C_{L_1})

Cruise

$$C_{L_1} = \frac{nW}{\bar{q}S} = \frac{(1)(145000)}{(6075.77)(59.1)} = 0.4038$$

where:

n : load factor

Takeoff

$$C_{L_1} = \frac{nW}{\bar{q}S} = \frac{(1)(148131)}{(1797.08)(59.1)} = 1.3947$$

Landing

$$C_{L_1} = \frac{nW}{\bar{q}S} = \frac{(1)(147640.5)}{(1890.42)(59.1)} = 1.3215$$

3.2.4 CALCULATION OF TRANSITION POINTS OF THE AIRFOILS

A computer program[7] for the incompressible aerodynamic analysis of airfoils was used to calculate the transition points. These calculation were made for the airfoils of the wing, horizontal tail, and vertical tail for different flight conditions and they were used as inputs in AAA.

Table 3.1 Transition points.

Component	Transition point for cruise ($\%\bar{c}$)	Transition point for takeoff ($\%\bar{c}$)	Transition point for landing ($\%\bar{c}$)
Wing	38.50	34.38	35.96
Horizontal Tail	37.60	36.75	45.25
Vertical Tail	42.19	36.91	39.61

3.2.5 ANGLE OF ATTACK (AOA)

Cruise

By using AAA software, the following parameters were calculated for cruise.

$$C_{L_0} = 0.3587$$

$$C_{L_\alpha} = 0.1068 \text{ deg}^{-1}$$

$$\alpha = \frac{\left[C_{L_1} - C_{L_0}\right]}{C_{L_\alpha}} = \frac{[0.4038 - 0.3587]}{0.1068} = 0.42 \text{deg}$$

Takeoff

$$C_{L_0} = 0.5221$$

$$C_{L_\alpha} = 0.0796 \text{ deg}^{-1}$$

$$\alpha = \frac{\left[C_{L_1} - C_{L_0}\right]}{C_{L_\alpha}} = \frac{[1.3947 - 0.5221]}{0.0796} = 10.96 \text{deg}$$

Landing

$$C_{L_0} = 0.7117$$

$$C_{L_\alpha} = 0.0796 \text{ deg}^{-1}$$

$$\alpha = \frac{\left[C_{L_1} - C_{L_0}\right]}{C_{L_\alpha}} = \frac{[1.3215 - 0.7117]}{0.0796} = 7.66 \text{deg}$$

3.2.6 CALCULATION OF MISCELLANEOUS DRAG COEFFICIENT

Miscellaneous drag for CASA CN-235 consists of only the drags of the antennas and a light. First the drag force of the component

is obtained (Equation 3.34), then this is recalculated in terms of contribution to aircraft total drag (Equation 3.35).

$$D_i = C'_{D_i} q S_i \tag{3.34}$$

$$\Delta C_{D_i} = \frac{D_i}{qS} = \frac{C'_{D_i} q S_i}{qS} = \frac{C'_{D_i} S_i}{S} \tag{3.35}$$

where :

D_i : Drag force i^{th} component

C'_{D_i} : Drag coefficient of i^{th} component

ΔC_{D_i} : Drag coefficient contribution of i^{th} component

S_i : Reference area of the i^{th} component

Miscellaneous drag is calculated for 4 different C_L values for each flight condition.

Cruise (15000 feet)

Table 3.2 Lift coefficients for cruise

C_L	Velocity (m/s)	Mach Number
0.4038	125.55	0.39
0.8	89.19	0.28
1.2	72.83	0.23
1.501	65.19	0.20

Takeoff & Landing (Sea Level)

Same C_L values for takeoff and landing give nearly the same velocities and same Reynolds numbers. Therefore calculations for takeoff and landing are made together.

Table 3.3 Lift coefficients for takeoff and landing

C_L	Velocity (m/s)	Mach Number
0.7	76.37	0.22
1.0	63.9	0.19
1.3	56.04	0.16
1.6	50.51	0.15

While calculating drags of components, boundary layer effect is added. All of the antennas and a light are on the center section above or under the center fuselage. For calculation of boundary layer thickness, the fuselage is assumed as a flat plate, and Prandtl Analysis for turbulent boundary layer over a flat plate[9] is used. Equation 3.36 was taken from Reference 9.

$$\frac{\delta}{x} = \frac{0.375}{\sqrt[5]{R_x}} \tag{3.36}$$

where:

δ : boundary layer thickness
x : distance
R_x : Reynolds number

If some part of a component is inside a boundary layer the drag of this part is lesser than the case it was placed in a flow external to boundary layers. The reason for this effect is the reduction of dynamic pressure inside a boundary layer. This depends on Mach number of the free stream velocity. Using Figure 19 from Reference 10 (Appendix C), the drag in the boundary layer for Mach numbers around 0.3 is 65% of the normal value. After adding the boundary layer effects, Equation 3.35 becomes Equation 3.37.

$$\Delta C_{D_i} = \frac{(0.65)C_{D_i}^{'} S_{i_{inner}}}{S} + \frac{C_{D_i}^{'} S_{i_{outer}}}{S} \tag{3.37}$$

where:

$S_{i_{inner}}$: The reference area of the i^{th} component inside the boundary layer.
$S_{i_{outer}}$: The reference area of the i^{th} component outside the boundary layer.

There are 10 antennas in 6 different types and a light on the aircraft.

3.2.6.1 IFF antennas

There are two IFF antennas (Figure 3.6) on the CASA CN-235, one of them is above the fuselage, 4.25 m away from the nose of the aircraft and the other one is under the fuselage, 3.7 m away from the nose.

$$\Delta C_{D_i} = R_{wf} R_{LS} C_{f_i} \left[1 + L^{'} \frac{t}{c} + 100 \left(\frac{t}{c} \right)^4 \right] \frac{S_{wet_i}}{S}$$

where:

R_{wf} : interference factor

S_{wet_i} : wetted area

R_{LS} : lifting surface correction factor

L' : thickness location parameter

t/c : thickness ratio

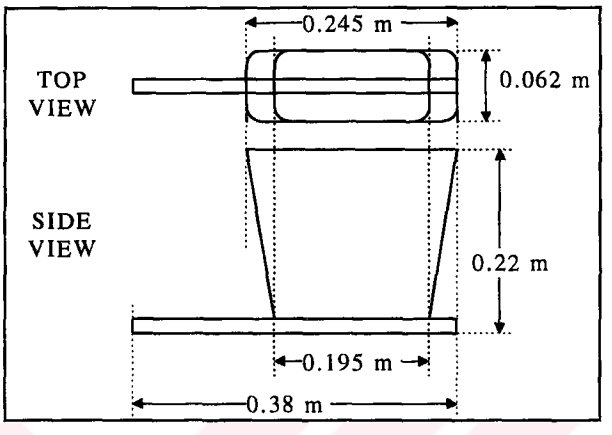

Figure 3.6 IFF Antenna

R_{wf} from Figure 4.1 of Reference 1.

R_{LS} from Figure 4.2 of Reference 1.

C_{f_i} from Figure 4.3 of Reference 1.

L' = 1.2 from Figure 4.4 of Reference 1

$S_{wet_i} = 0.12408 m^2$

$\frac{t}{c} = 0.282$

Table 3.4 Drag calculation of IFF Antenna

	Mach	R_{LS}	upper antenna			lower antenna			$R_{N,antenna}$ ($*10^6$)	C_f	ΔC_{D_i} (10^{-3})
			$R_{N,fus}$ ($*10^8$	R_{wf}	δ	$R_{N,fus}$ ($*10^8$	R_{wf}	δ			
Cruise	0.39	1.10	25.1	0.97	0.053	21.8	0.97	0.047	1.30	0.0042	0.034
	0.28	1.09	17.8	0.94	0.057	15.5	0.94	0.051	0.92	0.0045	0.035
	0.23	1.07	14.5	0.92	0.059	12.7	0.92	0.053	0.75	0.0047	0.035
	0.20	1.07	13.0	0.92	0.060	11.3	0.92	0.054	0.67	0.0047	0.035
T/O & landing	0.22	1.07	22.2	0.92	0.054	19.3	0.92	0.048	1.15	0.0041	0.031
	0.19	1.07	18.6	0.92	0.056	16.1	0.92	0.050	0.96	0.0044	0.033
	0.16	1.07	16.3	0.92	0.058	14.2	0.92	0.052	0.84	0.0045	0.033
	0.15	1.07	14.7	0.92	0.059	12.8	0.92	0.053	0.76	0.0047	0.035

where:

$R_{N\ fus}$: Reynolds number on the fuselage at the antenna location

$R_{N\ antenna}$: Reynolds number of the antenna

3.2.6.2 DF antenna

It is under the fuselage and 10.95 m away from the nose. Figure 9.13 of Reference 5 was used.

$S_i = 0.0583\ m^2$

Table 3.5 Drag calculation of DF antenna

	C_L	δ (m)	ΔC_{D_i} (10^{-3})
Cruise	0.4038	0.113	0.224
	0.8	0.121	0.224
	1.2	0.126	0.224
	1.501	0.128	0.224
T/O & Landing	0.7	0.115	0.224
	1.0	0.120	0.224
	1.3	0.123	0.224
	1.6	0.125	0.224

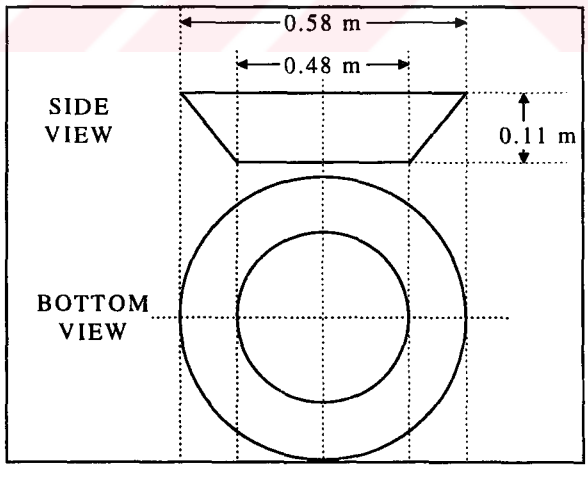

Figure 3.7 DF Antenna

3.2.6.3 Beacon antennas

There are two Beacon antennas (Figure 3.8) under the fuselage. They are 9.30 m away from the nose.

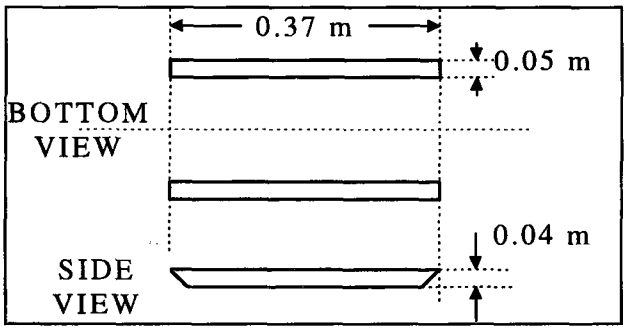

Figure 3.8 Beacon Antenna

$S_i = 0.002\ m^2$

$C'_{D_i} = 1.18$, using Fig. 9.10 of Reference 5

Table 3.6 Drag calculation of Beacon antennas

	C_L	δ (m)	ΔC_{D_i} (10^{-3})
Cruise	0.4038	0.099	0.052
	0.8	0.106	0.052
	1.2	0.110	0.052
	1.501	0.113	0.052
T/O & Landing	0.7	0.101	0.052
	1.0	0.105	0.052
	1.3	0.108	0.052
	1.6	0.110	0.052

3.2.6.4 ADF Antenna

It is under the fuselage and 6.90 m away from the nose(Figure3.9).

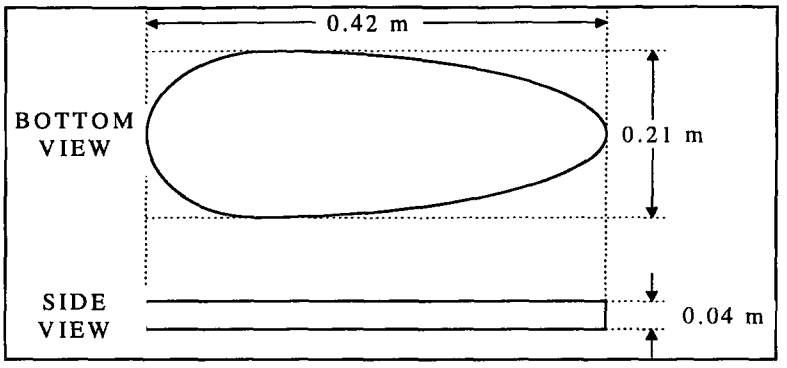

Figure 3.9 ADF Antenna

L' = 1.2 from Figure 4.4 of Reference 1

$S_{wet_i} = 0.06m^2$

$\frac{t}{c} = 0.5$

Table 3.7 Drag calculation of ADF Antenna

	Mach	$R_{N,fus}$ ($*10^8$)	$R_{N,antenna}$ ($*10^6$)	R_{wf}	R_{LS}	C_f	δ	ΔC_{D_i} (10^{-3})
Cruise	0.39	1.23	2.47	0.98	1.10	0.0037	0.078	0.021
	0.28	0.87	1.76	0.94	1.08	0.0040	0.083	0.021
	0.23	0.71	1.43	0.92	1.07	0.0041	0.087	0.021
	0.20	0.64	1.28	0.91	1.07	0.0042	0.089	0.021
T/O & landing	0.22	1.09	2.19	0.92	1.07	0.0039	0.080	0.021
	0.19	0.91	1.84	0.91	1.07	0.0040	0.083	0.021
	0.16	0.80	1.61	0.89	1.07	0.0041	0.085	0.021
	0.15	0.72	1.45	0.88	1.07	0.0042	0.087	0.021

3.2.6.5 DME antennas

There are two antennas (Figure 3.10), one of them is above the fuselage, 4.65 m away from the nose, and the other one is under the fuselage, 5.40 m away from the nose. Figure 9.13 of Reference 5 was used.

$S_i = 0.00309\ m^2$

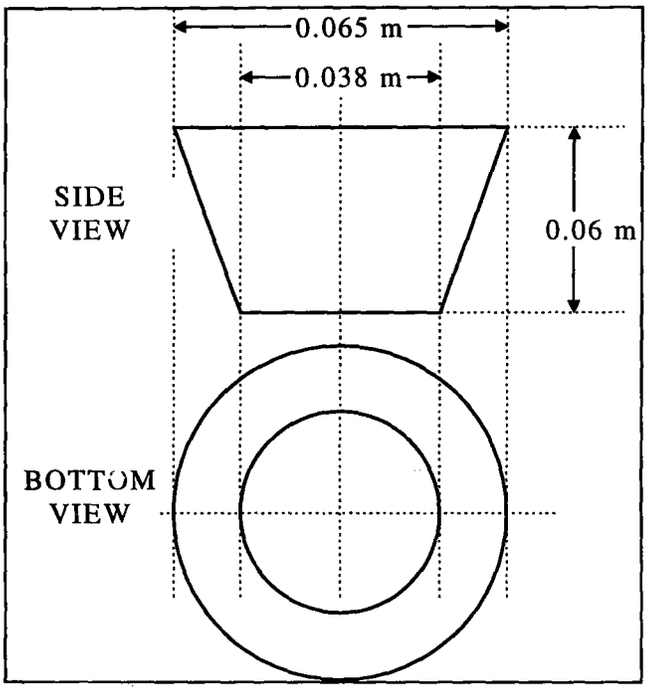

Figure 3.10 DME Antenna

Table 3.8 Drag calculation of DME Antenna

	C_L	upper antenna			lower antenna			Total
		δ (m)	C'_{D_i}	ΔC_{D_i} (10^{-3})	δ (m)	C'_{D_i}	ΔC_{D_i} (10^{-3})	ΔC_{D_i} (10^{-3})
Cruise	0.4038	0.057	0.94	0.032	0.064	0.94	0.031	0.063
	0.8	0.061	1.08	0.037	0.068	1.08	0.037	0.074
	1.2	0.063	1.14	0.039	0.071	1.14	0.039	0.078
	1.501	0.065	1.17	0.039	0.073	1.17	0.039	0.078
T/O & landing	0.7	0.058	0.99	0.034	0.066	0.99	0.033	0.067
	1.0	0.060	1.02	0.035	0.068	1.02	0.035	0.070
	1.3	0.062	1.10	0.037	0.070	1.10	0.037	0.074
	1.6	0.063	1.13	0.039	0.071	1.13	0.039	0.078

3.2.6.6 Altimeter antennas

There are two altimeter antennas (Figure 3.11) under the fuselage. First one is 5.35 m away from the nose, second one is 6.35 m away from the tip. Figure 9.13 of Reference 5 was used.

$S_i = 0.00704\ m^2$

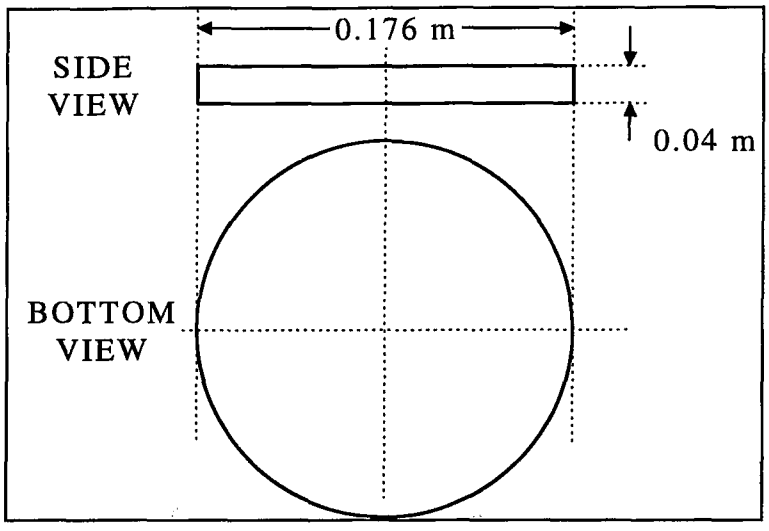

Figure 3.11 Altimeter antenna

Table 3.9 Drag calculation of Altimeter antenna

	C_L	front antenna			back antenna			Total
		δ (m)	C'_{D_i}	ΔC_{D_i} (10^{-3})	δ (m)	C'_{D_i}	ΔC_{D_i} (10^{-3})	ΔC_{D_i} (10^{-3})
Cruise	0.4038	0.063	0.350	0.027	0.073	0.350	0.027	0.055
	0.8	0.068	0.325	0.025	0.078	0.325	0.025	0.051
	1.2	0.071	0.310	0.024	0.081	0.310	0.024	0.048
	1.501	0.072	0.305	0.023	0.083	0.305	0.023	0.047
T/O & landing	0.7	0.065	0.340	0.027	0.075	0.340	0.027	0.053
	1.0	0.067	0.327	0.025	0.077	0.327	0.025	0.051
	1.3	0.069	0.317	0.025	0.079	0.317	0.025	0.049
	1.6	0.071	0.310	0.024	0.081	0.310	0.024	0.048

3.2.6.7 Light

The light (Figure 3.12) is under the fuselage and 3.85 m away from the nose. It is divided into two parts for calculation the drag coefficient. Figure 9.13 of Reference 5 was used.

$S_a = 0.0065\ m^2$
$S_b = 0.00455\ m^2$

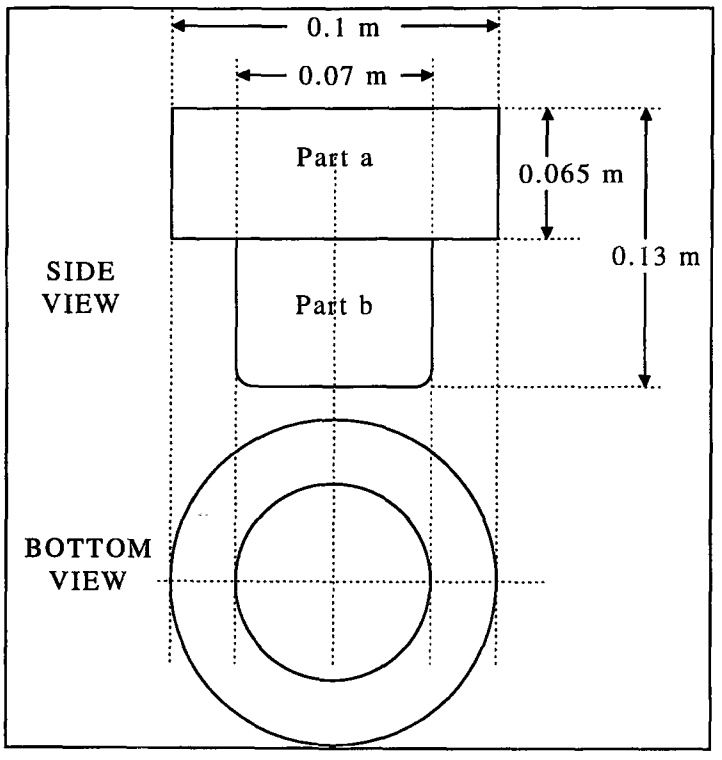

Figure 3.12 Light

Table 3.10 Drag calculation of Light

	C_L	δ (m)	part a		part b		Total
			C'_{D_i}	ΔC_{D_i} (10^{-3})	C'_{D_i}	ΔC_{D_i} (10^{-3})	ΔC_{D_i} (10^{-3})
Cruise	0.4038	0.049	0.31	0.025	0.55	0.042	0.067
	0.8	0.052	0.50	0.040	0.96	0.074	0.114
	1.2	0.054	0.85	0.066	1.04	0.080	0.148
	1.501	0.056	0.94	0.072	1.09	0.084	0.156
T/O & Landing	0.7	0.050	0.30	0.023	0.78	0.060	0.083
	1.0	0.052	0.40	0.032	0.94	0.072	0.104
	1.3	0.053	0.70	0.055	1.00	0.077	0.132
	1.6	0.054	0.84	0.065	1.04	0.080	0.145

3.2.6.8 RESULTS RELATED MISCELLANEOUS DRAG

Table 3.11 shows the miscellaneous drag for the aircraft.

Table 3.11 Miscellaneous drag.

	CRUISE				T/O & LANDING			
C_L	0,404	0,8	1,2	1,501	0,7	1	1,3	1,6
PART	ΔC_{D_i} (*10^{-3})				ΔC_{D_i} (*10^{-3})			
IFF antennas	0.034	0.035	0.035	0.035	0.031	0.033	0.033	0.035
DF antenna	0,224	0,224	0,224	0,224	0,224	0,224	0,224	0,224
Beacon antennas	0,052	0,052	0,052	0,052	0,052	0,052	0,052	0,052
ADF antenna	0,021	0,021	0,021	0,021	0,021	0,021	0,021	0,021
DME antennas	0,063	0,074	0,078	0,078	0,067	0,070	0,074	0,078
Altimeter antennas	0,055	0,051	0,048	0,047	0,053	0,051	0,049	0,048
Light	0,067	0,114	0,146	0,156	0,083	0,104	0,132	0,145
TOTAL $C_{D,misc}$	0.516	0.571	0.604	0.613	0.531	0.555	0.585	0.603

Miscellaneous drag changes with lift coefficient. If we take the curve fit of these values, following equations are obtained. These are used as inputs of the AAA software.

For cruise:

$$C_{D_{misc}} = -7.26*10^{-5}\, C_L^2 + 2.27*10^{-4} C_L + 0.000436$$

For takeoff and landing:

$$C_{D_{misc}} = -1.67*10^{-5}\, C_L^2 + 1.20*10^{-4} C_L + 0.000454$$

3.2.7 CALCULATION OF AOA FOR MAXIMUM LIFT COEFFICIENT ($\alpha_{C_{L_{max}}}$)

α_{0_L}, C_{L_α}, and $C_{L_{max}}$ are calculated by AAA.

Cruise

α_{0_L} = -3.36 deg

C_{L_α} = 0.1068 deg^{-1}

$C_{L_{max}}$ = 1.501

$\Delta\alpha_{C_{L_{max}}}$ = 1.75 deg, using Fig. 12.10 from Reference 2.

where:

$\Delta\alpha_{C_{L_{max}}}$: incremental aircraft angle of attack for maximum lift coefficient

$$\alpha_{C_{L_{max}}} = \frac{C_{L_{max}}}{C_{L_\alpha}} + \alpha_{0_L} + \Delta\alpha_{C_{L_{max}}} = \frac{1.501}{0.1068} + (-3.36) + 1.75 = 12.44\,\text{deg}$$

Takeoff

α_{0_L} = -6.56 deg

C_{L_α} = 0.0796 deg^{-1}

$C_{L_{max}}$ = 1.688

$\Delta\alpha_{C_{L_{max}}}$ = 1.75 deg, using Fig. 12.10 from Reference 2.

$$\alpha_{C_{L_{max}}} = \frac{C_{L_{max}}}{C_{L_\alpha}} + \alpha_{0_L} + \Delta\alpha_{C_{L_{max}}} = \frac{1.688}{0.0796} + (-6.56) + 1.75 = 16.40\,\text{deg}$$

Landing

α_{0_L} = -8.94 deg

C_{L_α} = 0.0796 deg^{-1}

$C_{L_{max}}$ = 1.905

$\Delta\alpha_{C_{L_{max}}}$ = 1.75 deg, using Fig. 12.10 from Reference 2.

$$\alpha_{C_{L_{max}}} = \frac{C_{L_{max}}}{C_{L_\alpha}} + \alpha_{0_L} + \Delta\alpha_{C_{L_{max}}} = \frac{1.905}{0.0796} + (-8.94) + 1.75 = 16.74\,\text{deg}$$

3.2.8 CALCULATION OF ZERO LIFT PITCHING MOMENT COEFFICIENT (C_{m_0})

Stability and dynamic calculations are made for two different center of gravity (cg) locations. These cg limits are taken from CASA Maintenance Manual (Reference 6). First one is at %16 of the mean chord, and the other one is at %30 of mean chord. During flight, cg location must be maintained between these two cg limits.

3.2.8.1 C_{m_0} FOR $\bar{x}_{cg}$ IS AT 0.16 $\bar{c}$

Cruise

$C_{m_{0_r}} = C_{m_{0_t}} = -0.03$ from airfoil data

A = 10.16

$\Lambda_{c/4}$ = 3.4 deg

where:

$C_{m_{0_r}}, C_{m_{0_t}}$: root and tip airfoil pitching moment for zero angle of attack

$\Lambda_{c/4}$: wing quarter chord sweep angle

$$C_{m_{0_w}} = \frac{A\cos^2 \Lambda_{c/4}}{A + 2\cos\Lambda_{c/4}} \frac{C_{m_{0_r}} + C_{m_{0_t}}}{2} = -0.02498$$

k_2-k_1 = 0.9 using Fig. 8.111 from Reference 1.

$\alpha_{0_{L_w}} = -1.38$deg

S = 59.1 m^2

$\bar{c}$ = 2.62 m

i_w = 3 deg

where:

$C_{m_{0_w}}$: wing pitching moment for zero angle of attack

i_w : incidence angle of the wing

The fuselage is divided into 9 parts. Table 3.12 shows parameters of each part.

Table 3.12 Fuselage parameters

Part	W_{f_i} (m)	Δx_i (m)	i_{cl_f} (deg)
1	1.0	1.031	-13
2	2.24	0.966	-13
3	2.61	1.208	0
4	2.9	4.495	0
5	2.9	3.0	0
6	2.9	0.448	0
7	2.9	7.432	-10.32
8	2.8	1.32	-10.32
9	2.6	1	0

where:

W_{f_i} : width of the ith fuselage part

Δx_i : length of the ith fuselage part

i_{cl_f} : incidence angle of the ith fuselage part

$$C_{m_{0_f}} = \frac{k_2 - k_1}{(36.5)S\bar{c}}\left\{\sum_i \left[W_{f_i}^2\left(i_w + \varepsilon_{0_{L_w}} + i_{cl_f}\right)\Delta x_i\right]\right\} = -0.001579$$

where:

$C_{m_{0_f}}$: fuselage pitching moment for zero angle of attack

$$\frac{C_{m_{0_M}}}{C_{m_{0_{M=0}}}} = 1.025 \text{ using Fig. 8.99 from Reference 1.}$$

$$C_{m_{0_{wf}}} = \left[C_{m_{0_w}} + C_{m_{0_f}}\right]\frac{C_{m_{0_M}}}{C_{m_{0_{M=0}}}} = -0.0272$$

where:

$C_{m_{0_{wf}}}$: wing-fuselage pitching moment for zero angle of attack

$C_{L_{\alpha_h}} = 0.0753 \text{ deg}^{-1}$

$\eta_h = 1$

$S_h = 20.67 \text{ m}^2$

$i_h = 0$

ε_{0_h} = 1.32 deg

$$C_{L_{0_h}} = C_{L_{\alpha_h}} \eta_h \frac{S_h}{S}\left(i_h - \varepsilon_{0_h}\right) = -0.03475$$

where:

$C_{L_{0_h}}$: horizontal tail lift coefficient for zero angle of attack

$\bar{x}_{ac_h}$ = 7.10

$\bar{x}_{ref}$ = $\bar{x}_{cg}$ =3.19

where:

$\bar{x}_{ac_h}$: position of horizontal tail aerodynamic center

$\bar{x}_{ref}$: position of reference point on wing mean geometric center

$$C_{m_{0_h}} = -\left(\bar{x}_{ac_h} - \bar{x}_{ref}\right) C_{L_{0_h}} = 0.1355$$

where:

$C_{m_{0_h}}$: horizontal tail pitching moment for zero angle of attack

$$C_{m_0} = C_{m_{0_{wf}}} + C_{m_{0_h}} = 0.1083$$

Takeoff

$C_{m_{0_w}}$ = -0.02498

$C_{m_{0_f}}$ = -0.001579

$\frac{C_{m_{0_M}}}{C_{m_{0_{M=0}}}}$ = 1.0 using Fig. 8.99 from Reference 1.

$$C_{m_{0_{wf}}} = \left[C_{m_{0_w}} + C_{m_{0_f}}\right] \frac{C_{m_{0_M}}}{C_{m_{0_{M=0}}}} = -0.0266$$

$C_{L_{\alpha_h}}$ = 0.0753 deg^{-1}

η_h = 1

$S_h = 20.67\ m^2$
$i_h = 0$
$\varepsilon_{0_h} = 3.49$ deg

$$C_{L_{0_h}} = C_{L_{\alpha_h}} \eta_h \frac{S_h}{S}\left(i_h - \varepsilon_{0_h}\right) = -0.0919$$

$\bar{x}_{ac_h} = 7.10$

$\bar{x}_{ref} = 3.19$

$$C_{m_{0_h}} = -\left(\bar{x}_{ac_h} - \bar{x}_{ref}\right) C_{L_{0_h}} = 0.3584$$
$$C_{m_0} = C_{m_{0_{wf}}} + C_{m_{0_h}} = 0.3318$$

Landing

$C_{m_{0_w}} = -0.02498$
$C_{m_{0_f}} = -0.001579$
$\frac{C_{m_{0_M}}}{C_{m_{0_{M=0}}}} = 1.0$ using Fig. 8.99 from Reference 1.

$$C_{m_{0_{wf}}} = \left[C_{m_{0_w}} + C_{m_{0_f}}\right] \frac{C_{m_{0_M}}}{C_{m_{0_{M=0}}}} = -0.0266$$

$C_{L_{\alpha_h}} = 0.0753\ deg^{-1}$
$\eta_h = 1$
$S_h = 20.67\ m^2$
$i_h = 0$
$\varepsilon_{0_h} = 5.61$ deg

$$C_{L_{0_h}} = C_{L_{\alpha_h}} \eta_h \frac{S_h}{S}\left(i_h - \varepsilon_{0_h}\right) = -0.1477$$

$\bar{x}_{ac_h} = 7.10$

$\bar{x}_{ref} = 3.19$

$$C_{m_{0_h}} = -\left(\bar{x}_{ac_h} - \bar{x}_{ref}\right) C_{L_{0_h}} = 0.5760$$

$$C_{m_0} = C_{m_{0_{wf}}} + C_{m_{0_h}} = 0.5495$$

3.2.8.2 C_{m_0} FOR $\bar{x}_{cg}$ IS AT 0.30 $\bar{c}$

Cruise

$C_{m_{0_{wf}}}$ = -0.0272

$C_{L_{0_h}}$ = -0.03475

$\bar{x}_{ac_h}$ = 7.10

$\bar{x}_{ref}$ = 3.34

$$C_{m_{0_h}} = -\left(\bar{x}_{ac_h} - \bar{x}_{ref}\right) C_{L_{0_h}} = 0.1307$$

$$C_{m_0} = C_{m_{0_{wf}}} + C_{m_{0_h}} = 0.1035$$

Takeoff

$C_{m_{0_{wf}}}$ = -0.0266

$C_{L_{0_h}}$ = -0.0919

$\bar{x}_{ac_h}$ = 7.10

$\bar{x}_{ref}$ = 3.34

$$C_{m_{0_h}} = -\left(\bar{x}_{ac_h} - \bar{x}_{ref}\right) C_{L_{0_h}} = 0.3455$$

$$C_{m_0} = C_{m_{0_{wf}}} + C_{m_{0_h}} = 0.3189$$

Landing

$C_{m_{0_{wf}}}$ = -0.0266

$C_{L_{0_h}}$ = -0.1477

$\bar{x}_{ac_h} = 7.10$

$\bar{x}_{ref} = 3.34$

$$C_{m_{0_h}} = -\left(\bar{x}_{ac_h} - \bar{x}_{ref}\right) C_{L_{0_h}} = 0.5554$$

$$C_{m_0} = C_{m_{0_{wf}}} + C_{m_{0_h}} = 0.5288$$

3.2.9 CALCULATION OF ELEVATOR DEFLECTION ANGLE (δ_e) FOR STEADY STATE

For steady state flight condition, all the forces acts on the aircraft must be balanced and there must not be any moment which affects the aircraft. For small pitch angles, lift equals to weight and thrust equals to drag. Finding δ_e needs an iteration process.

3.2.9.1 δ_e FOR $\bar{x}_{cg}$ IS AT 0.16 $\bar{c}$

Cruise

For steady state, C_m = 0. Using Equation 3.29 with the thrust effect, Equation 3.38 is obtained.

$$C_m = C_{m_0} + C_{m_\alpha}\alpha + C_{m_{\delta_e}}\delta_e + C_T\frac{d_T}{\bar{c}} \qquad (3.38)$$

where:

C_T : Thrust coefficient
d_T : distance of thrustline to center of gravity

$C_T = C_{D_1} = 0.0276$ (steady state drag coefficient without trim drag)

$C_{m_0} = 0.1083$
$d_t = -1.437$ m
$\alpha = 0.42$ deg

$C_{m\alpha}$ and $C_{m\delta_e}$ are calculated by AAA.

$C_{m\alpha} = -0.0451$ deg^{-1}
$C_{m\delta_e} = -0.0394$ deg^{-1}

$\Rightarrow \delta_e = 1.89$ deg

Now the steady state drag coefficient must be updated with first calculated elevator deflection using Equation 3.13:

$$C_{D_\alpha} = 0.00327 \text{ deg}^{-1}$$
$$C_{D_{\delta_e}} = 0.000301 \text{ deg}^{-1}$$
$$C_{D_0} = 0.0262$$

$$C_T = C_{D_1} = C_{D_0} + C_{D_\alpha}\alpha + C_{D_{\delta_e}}\delta_e = 0.0282$$

Repeat the calculation of the elevator deflection for new C_T:

$\Rightarrow \delta_e = 1.88$ deg

$$C_T = C_{D_1} = C_{D_0} + C_{D_\alpha}\alpha + C_{D_{\delta_e}}\delta_e = 0.0282$$

Steady state drag coefficient is same as the previous one. Therefore iteration process ended.

Takeoff

During takeoff maximum power is used.

bhp = 1750 : horse power
$\eta_p = 0.85$: propeller efficiency

$$T = \frac{550 bhp \eta_p}{V} = \frac{550(2)(1750)(0.85)}{(54.164)(3.2808)}(4.4482) = 40957.95 \text{ N}$$

where:
T : thrust force

$$C_T = \frac{T}{qS} = 0.3855$$

$\Rightarrow \delta_e = -10.08$ deg

Landing

During landing thrust can be assumed nearly zero.

$C_T = 0$

$\Rightarrow \delta_e = 4.48$ deg

3.2.9.2 δ_e FOR $\bar{x}_{cg}$ IS AT 0.30$\bar{c}$

The same methods used in previous parts are used for the following calculations.

Cruise

$\Rightarrow \delta_e = 2.00$ deg

Takeoff

$\Rightarrow \delta_e = -7.62$ deg

Landing

$\Rightarrow \delta_e = 5.66$ deg

3.3 RESULTS

3.3.1 RESULTS RELATED TO C_L vs. AOA CURVES

After calculation process by using AAA and other methods, results related to C_L vs. AOA curves are listed in Table 3.13. Figure 3.20 shows C_L-α curves for three flight conditions. Center of gravity position does not affect C_L-α curves.

Table 3.13 Parameters for C_L-α curves

Parameter	Cruise	Takeoff	Landing
Zero lift angle of attack, α_{0_L} (degree)	-3.36	-6.56	-8.94
Zero angle of attack lift coefficient, C_{L_0}	0.3587	0.5221	0.7117
Steady state lift coefficient, C_{L_1}	0.4038	1.3947	1.3215
Steady state angle of attack, α_1 (degree)	0.42	10.96	7.66
Maximum lift coefficient, $C_{L_{max}}$	1.501	1.688	1.905
Angle of attack for maximum lift coefficient, $\alpha_{CL_{max}}$ (degree)	12.44	16.40	16.74
Lift curve slope, C_{L_α} (rad^{-1})	6.1199	4.5598	4.5620

Effects of using single slotted flaps :

- Zero lift angle of attack angle is decreased.
- Aircraft lift curve slope is decreased.
- Aircraft maximum lift coefficient is increased

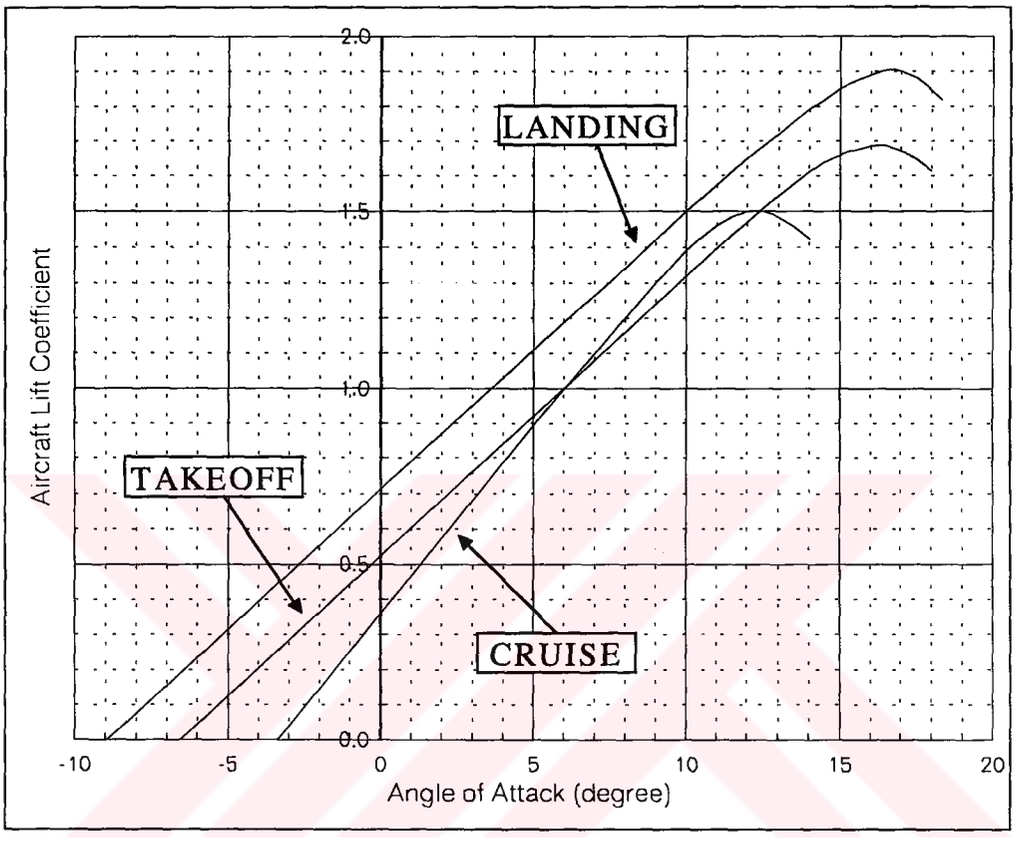

Figure 3.13 Lift coefficient vs. angle of attack curves

3.3.2 RESULTS RELATED TO DRAG POLAR CURVES

Results related to drag of components are listed in Table 3.14. Table 3.15 lists other drag related parameters. Figure 3.14 shows drag polar curves of the aircraft for three flight conditions.

For cruise condition, zero lift drag coefficient and minimum drag coefficient have the same value, $C_{D_0} = C_{D_{min}} = 0.0220$. Because flap deflection angle is zero for cruise.

But for the other two flight conditions, zero lift drag coefficient and minimum drag coefficient don't have the same values. Because the flap deflection angles are different from zero. For takeoff, zero lift drag coefficient is 0.0410 and minimum drag coefficient is 0.0406. For landing, zero lift drag coefficient is 0.0473 and minimum drag coefficient is 0.0452. As a result, after using flap deflection, minimum drag coefficient is obtained for a lift coefficient value different from zero lift.

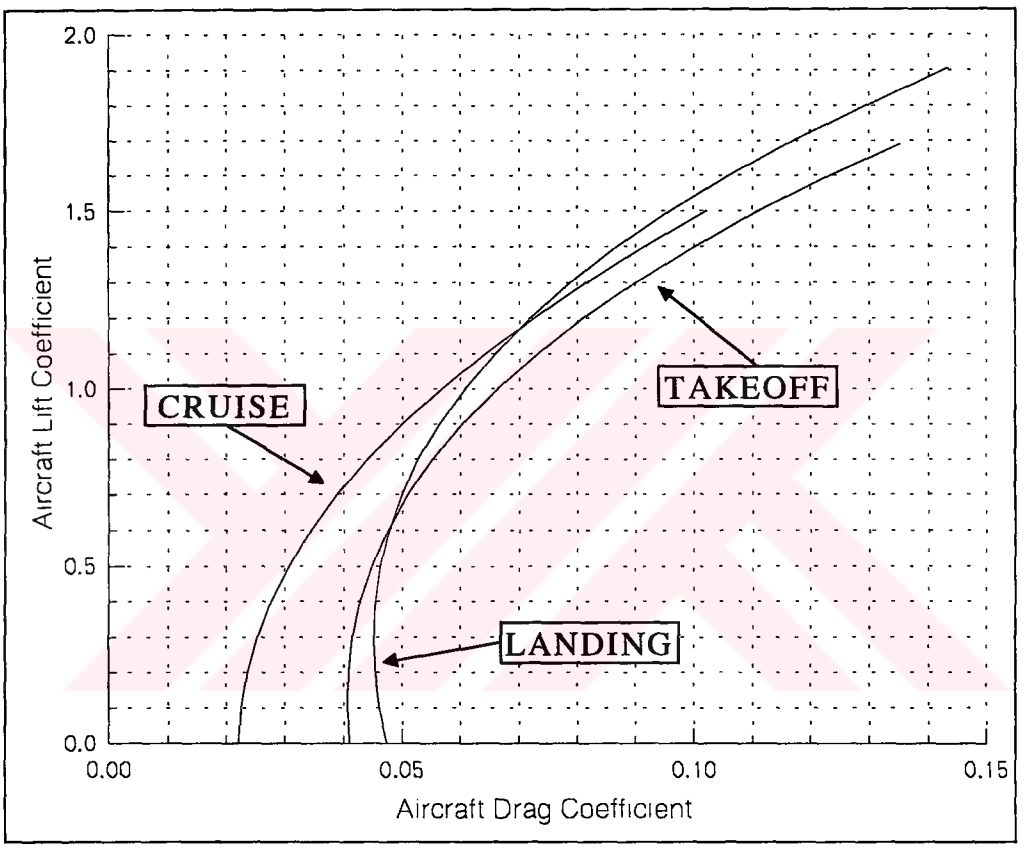

Figure 3.14 Drag polar curves of the aircraft.

Table 3.14 Parameters for drag polar curves

Parameter	Cruise	Takeoff	Landing
Zero lift drag coefficient for steady state, C_{D_0}	0.0223	0.0370	0.0445
Steady state drag coefficient, C_{D_1}	0.0278	0.0973	0.0805
Drag curve slope for steady state, C_{D_α} (rad^{-1})	0.1872	0.4816	0.4565
total airplane drag change with elevator, $C_{D_{\delta_e}}$ (rad^{-1})	0.0177	0.0625	0.0592

Table 3.15 Drag of components for cruise, takeoff, and landing

	Cruise	T/O	landing
Wing zero-lift drag coefficient, $C_{D_{0_w}}$	0.0051	0.0051	0.0051
Wing drag coefficient due to lift, $C_{D_{L_w}}$	0.0056	0.0545	0.0337
Horizontal tail zero-lift drag coefficient, $C_{D_{0_h}}$	0.0020	0.0020	0.0021
Horizontal tail drag coefficient due to lift, $C_{D_{L_h}}$	0.0000	0.0008	0.0007
Vertical tail zero-lift drag coefficient, $C_{D_{0_v}}$	0.0009	0.0010	0.0010
Fuselage zero-lift drag coefficient, $C_{D_{0_{fus}}}$	0.0055	0.0054	0.0054
Fuselage drag coefficient due to lift, $C_{D_{L_{fus}}}$	0.0000	0.0050	0.0017
Nacelle drag coefficient, C_{D_n}	0.0054	0.0056	0.0056
Flap drag coefficient, C_{D_f}	0.0000	0.0020	0.0102
Retractable gear drag coefficient, $C_{D_{retract}}$	0.0000	0.0104	0.0101
Windshield drag coefficient, $C_{D_{ws}}$	0.0016	0.0016	0.0016
Trim drag coefficient, $C_{D_{trim}}$	0.0010	0.0053	0.0025
Miscellaneous drag, $C_{D_{misc}}$	0.0005	0.0006	0.0006

3.3.3 RESULTS RELATED TO PITCHING MOMENT VERSUS AOA CURVES

Calculations for pitching moment were made for two center of gravity locations. Table 3.16 lists the parameters related to pitching moment versus angle of attack curves. Figures 3.15, 3.16 and 3.17 show pitching moment versus angle of attack curves for two different center of gravity locations.

Zero lift pitching moment coefficients, C_{m_0}, for three flight condition have different values for same cg location. All of input parameters except horizontal tail downwash angle for zero wing body angle of attack, ε_{0_h}, are same. Thus ε_{0_h} creates the difference in C_{m_0} for same cg location.

There is also difference between the C_{m_0} values for two cg locations for same flight condition. This is because of the change in cg location.

Total airplane pitching moment coefficient vs. AOA slope, C_{m_α}, is the function of airplane lift curve lift slope, C_{L_α}, the cg location and the aerodynamic center of the aircraft. The difference in three flight conditions for same cg location is the result of C_{L_α}. But the difference in C_{m_α} for same flight condition is because of the change in cg location.

Using different elevator deflection angle does not change the total airplane pitching moment coefficient vs. AOA slope. But pitch moment for same angle of attack changes. It decreases if elevator deflection angle increases and it increases if elevator deflection angle decreases. For instance for cruise condition at one degree angle of attack, pitching moment coefficient is 0.05 for zero elevator deflection, but it is -0.03 for 2 degree elevator deflection.

As seen from Figures 3.15, 3.16 and 3.17, if cg location goes backward, total airplane pitching moment coefficient vs. AOA slope becomes less negative. For steady state, the pitching moment of the aircraft must be zero. Because of this, different elevator deflections are used for same angle of attack. For example the steady state angle of attack for cruise is 0.42 degree and the elevator deflection angle at front cg is 1.88 degree and 2.00 degree at aft cg.

Table 3.16 Parameters related to C_m-α curves

Parameters	$x_{cg} = 0.16\bar{c}$			$x_{cg} = 0.30\bar{c}$		
	cruise	takeoff	landing	cruise	takeoff	landing
Zero lift pitching moment coefficient, C_{m_0}	0.1083	0.3318	0.5495	0.1035	0.3186	0.5288
total airplane pitching moment coefficient vs. AOA slope, C_{m_α} (rad^{-1})	-2.5839	-2.7579	-2.7580	-1.7274	-2.1128	-2.1126
change in total airplane pitching for unit elevator angle, $C_{m_{\delta_e}}$ (rad^{-1})	-2.2558	-2.3142	-2.3136	-2.1749	-2.2304	-2.2299

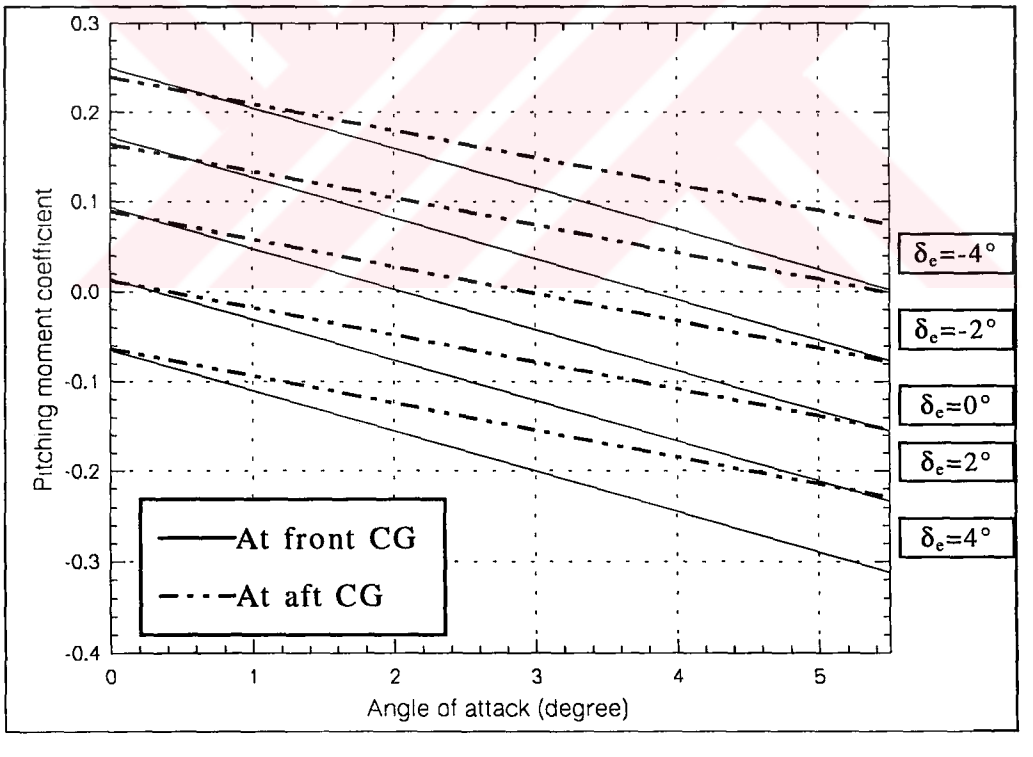

Figure 3.15 C_m-α curves for cruise

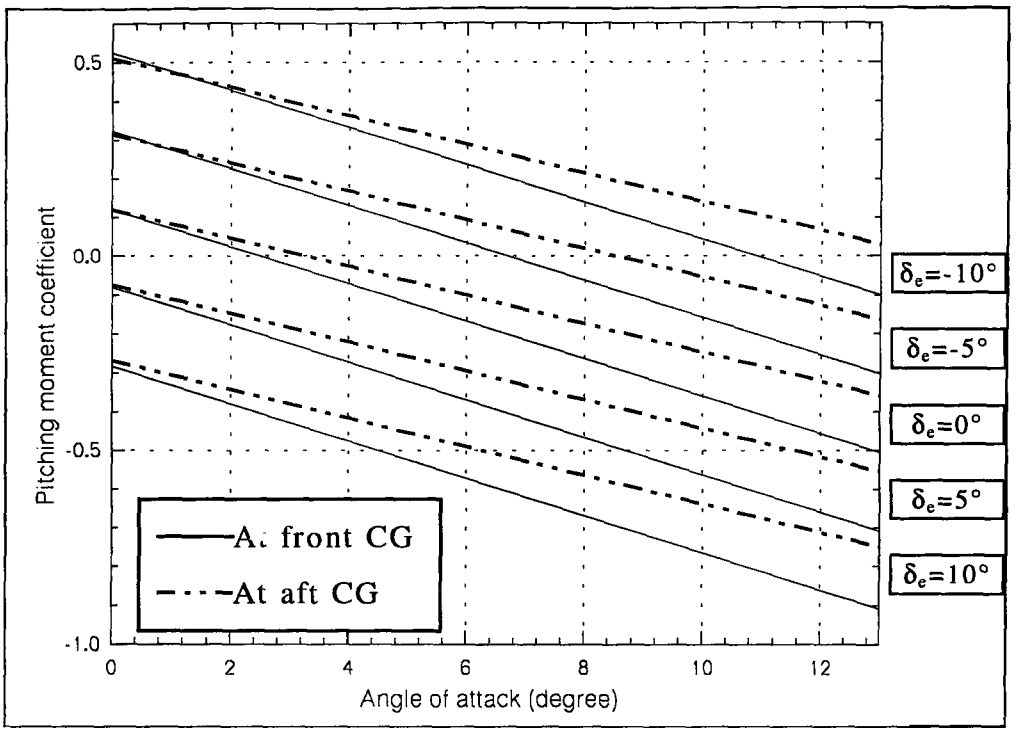

Figure 3.16 C_m-α curves for takeoff.

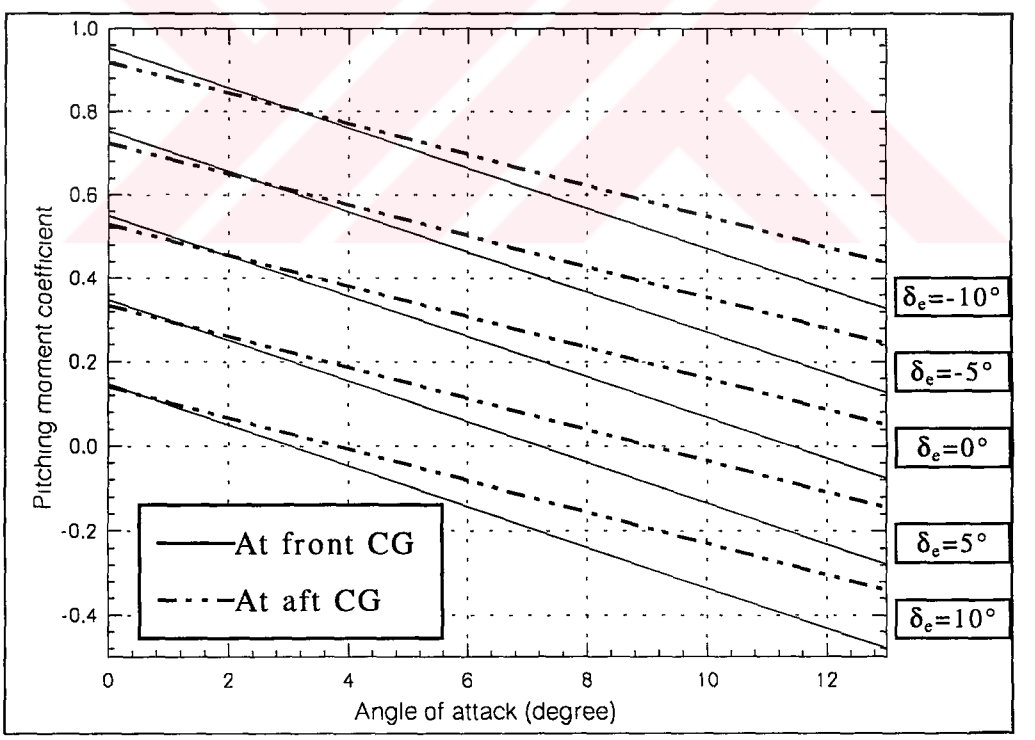

Figure 3.17 C_m-α curves for landing

CHAPTER 4

4. STATIC STABILITY AND CONTROL CALCULATIONS

In this chapter, stability and control calculations are made. Mainly the software AAA are used for calculations.

4.1 THEORY *OF STATIC STABILITY AND CONTROL CALCULATIONS*

The theory that is used in this chapter is based on Reference 1, 11 and 12. The purpose of this chapter is to present methods for the calculation of stability and control derivatives. These derivatives are required as input to the determination of static and dynamic stability and control behavior (handling qualities) of airplane.

Tables 4.1 and 4.2 presents the mathematical model used in representing longitudinal aerodynamic and thrust forces and moments. Tables 4.3 and 4.4 are for lateral-directional aerodynamic and thrust forces and moments. The meanings of the various terms used in these tables are explained in Chapters 4.1.1, 4.1.2 and 4.1.3. The meaning of other terms:

f_{A_x} : perturbed aerodynamic force in x-axis

f_{A_y} : perturbed aerodynamic force in y-axis

f_{A_z} : perturbed aerodynamic force in z-axis

m_A : perturbed pitching moment due to aerodynamic forces

l_A : perturbed rolling moment due to aerodynamic forces

n_A : perturbed yawing moment due to aerodynamic forces

f_{T_x} : perturbed thrust force in x-axis

f_{T_y} : perturbed thrust force in x-axis

f_{T_z} : perturbed thrust force in x-axis

m_T : perturbed pitching moment due to thrust forces

l_T : perturbed rolling moment due to thrust forces

n_T : perturbed yawing moment due to thrust forces
U_1 : steady state airspeed
u : perturbed forward velocity
$\dot{\alpha}$: angle of attack rate
q : perturbed pitch rate
β : sideslip angle
$\dot{\beta}$: sideslip angle rate
p : perturbed roll rate
r : perturbed yaw rate
δ_a : aileron deflection angle
δ_r : rudder deflection angle

Table 4.1 Longitudinal aerodynamic forces and moments

$$\begin{bmatrix} \frac{f_{A_x}}{\bar{q}S} \\ \frac{f_{A_z}}{\bar{q}S} \\ \frac{m_A}{\bar{q}S} \end{bmatrix} = \begin{bmatrix} -\left(C_{D_u}+2C_{D_1}\right) & \left(C_{D_\alpha}+C_{L_1}\right) & C_{D_{\dot{\alpha}}} & C_{D_q} & -C_{D_{\delta_e}} \\ -\left(C_{L_u}+2C_{L_1}\right) & \left(-C_{L_\alpha}-C_{D_1}\right) & C_{L_{\dot{\alpha}}} & C_{L_q} & -C_{L_{\delta_e}} \\ \left(C_{m_u}+2C_{m_1}\right) & C_{m_\alpha} & C_{m_{\dot{\alpha}}} & C_{m_q} & C_{m_{\delta_e}} \end{bmatrix} \begin{bmatrix} \frac{u}{U_1} \\ \alpha \\ \frac{\dot{\alpha}\bar{c}}{2U_1} \\ \frac{\bar{q}c}{2U_1} \\ \delta_e \end{bmatrix}$$

Table 4.2 Longitudinal thrust forces and moments

$$\begin{bmatrix} \frac{f_{T_x}}{\bar{q}S} \\ \frac{f_{T_z}}{\bar{q}S} \\ \frac{m_T}{\bar{q}S\bar{c}} \end{bmatrix} = \left[\begin{array}{c|c} \left(C_{T_{xu}} + 2C_{T_{x1}}\right) & 0 \\ \hline 0 & 0 \\ \hline \left(C_{m_{T_u}} + 2C_{m_{T_1}}\right) & C_{m_{T_e}} \end{array}\right] \begin{bmatrix} \frac{u}{U_1} \\ \alpha \end{bmatrix}$$

Table 4.3 Lateral-Directional aerodynamic forces and moments

$$\begin{bmatrix} \frac{f_{A_y}}{\bar{q}S} \\ \frac{l_A}{\bar{q}Sb} \\ \frac{n_A}{\bar{q}Sb} \end{bmatrix} = \begin{bmatrix} C_{y_\beta} & C_{y_{\dot{\beta}}} & C_{y_p} & C_{y_r} & C_{y_{\delta_a}} & C_{y_{\delta_r}} \\ C_{n_\beta} & C_{n_{\dot{\beta}}} & C_{n_p} & C_{n_r} & C_{n_{\delta_a}} & C_{y_{\delta_r}} \\ C_{n_\beta} & C_{n_{\dot{\beta}}} & C_{n_p} & C_{n_r} & C_{n_{\delta_a}} & C_{n_{\delta_r}} \end{bmatrix} \begin{bmatrix} \beta \\ \frac{\dot{\beta}b}{2U_1} \\ \frac{pb}{2U_1} \\ \frac{rb}{2U_1} \\ \delta_a \\ \delta_r \end{bmatrix}$$

Table 4.4 Lateral-Directional thrust forces and moments

$$\begin{bmatrix} \dfrac{f_{T_y}}{\bar{q}S} \\ \dfrac{l_T}{\bar{q}Sb} \\ \dfrac{n_T}{\bar{q}S\bar{c}} \end{bmatrix} = \begin{bmatrix} 0 \\ 0 \\ C_{n_{T_\beta}} \end{bmatrix}$$

4.1.1 STEADY STATE COEFFICIENTS

In Tables 4.1 to 4.4 there appear following steady state coefficients:

- C_{L_1} is the steady state lift coefficient. It is found in Chapter 3.2.3.
- C_{D_1} is the steady state drag coefficient. It is calculated in Chapter 3.3.
- C_{m_1} is the steady state pitching moment coefficient.
- $C_{T_{x1}}$ is the steady state thrust coefficient component in the direction of the stability x-axis.

$$C_{T_{x1}} = C_{D_1} + C_{L_1} \sin\theta_1 \tag{4.1}$$

where:

θ_1 : steady state pitching angle

- $C_{m_{T_1}}$ is the steady state pitching moment coefficient due to thrust.

$$C_{m_{T_1}} = -\left(C_{m_0} + C_{m_\alpha}\alpha_1 + C_{mi_h} i_{h_1} + C_{m_{\delta_e}} \delta_{e_1}\right) \tag{4.2}$$

4.1.2 STABILITY DERIVATIVES

4.1.2.1 SPEED DERIVATIVES

4.1.2.1.1 Aerodynamic Speed Derivatives

The stability derivatives C_{D_u}, C_{L_u}, and C_{m_u} are the changes in drag, lift, and pitching moment coefficients, respectively, with the speed. These changes at low speeds are really Reynolds number effects and can usually be considered to be zero.

Drag due to speed derivative, C_{D_u}

$$C_{D_u} = M_1 \frac{\partial C_D}{\partial M} \tag{4.3}$$

where:

M_1 : mach number in steady state

$\frac{\partial C_D}{\partial M}$: the derivative of the airplane drag coefficient with respect to Mach number

Lift due to speed derivative, C_{L_u}

Subsonic: $$C_{L_u} = \frac{M_1^2 (\cos \Lambda_{c/4})^2 C_{L_1}}{1 - M_1^2 (\cos \Lambda_{c/4})^2} \tag{4.4}$$

Pitching moment due to speed derivative, C_{m_u}

$$C_{m_u} = -C_{L_1} \frac{\partial \bar{x}_{ac_A}}{\partial M} \tag{4.5}$$

4.1.2.1.2 Thrust Versus Speed Derivatives

Thrust due to speed derivative, $C_{T_{xu}}$

For propeller driven with variable pitch (constant speed) airplanes:

$$C_{T_{x_u}} = -3C_{T_{x_1}} \tag{4.6}$$

Thrust moment due to speed derivative, C_{mT_u}

$$C_{m_{T_u}} = C_{T_{x_u}} \frac{d_t}{\bar{c}} \tag{4.7}$$

4.1.2.2 ANGLE OF ATTACK DERIVATIVES

4.1.2.2.1 Aerodynamic angle of attack derivatives

Drag due to angle of attack derivative, C_{D_α}

It is the change in drag coefficient with varying angle of attack. Above the angle of attack for minimum drag the drag coefficient increases as the angle of attack increases; thus it is positive in sign. It usually has little effect on the short period mode and has only a small effect on the phugoid mode in that a decrease in C_{D_α} usually increases stability.

$$C_{D_\alpha} = \frac{\partial C_D}{\partial C_L} C_{L_\alpha} \tag{4.8}$$

where.

$\frac{\partial C_D}{\partial C_L}$: drag polar curve slope for steady state lift coefficient and Mach number.

For airplanes with parabolic drag polars it is often more convenient to use:

$$C_{D_\alpha} = \frac{2C_{L_1}}{\pi A e} C_{L_\alpha} \tag{4.9}$$

where:

e : span efficiency factor.

Lift due to angle of attack derivative, C_{L_α}

It is the change in lift coefficient with angle of attack and commonly known as the lift curve slope. This derivative is always positive for angles of attack below the stall.

$$C_{L_\alpha} = C_{L_{\alpha_{wf}}} + C_{L_{\alpha_h}} \eta_h \frac{S_h}{S} \left(1 - \frac{d\varepsilon}{d\alpha}\right) \tag{4.10}$$

Pitching moment due to angle of attack derivative, C_{m_α}

It is perhaps the most important derivative related to longitudinal stability and control, since it primarily establishes the natural frequency of the short period mode and is a major factor in determining the response of the airframe to elevator motion and gusts. Usually, a large negative value of C_{m_α} is desired (-0.5 to -1.0 for light airplanes), but if it is too large, the required elevator effectiveness may become unreasonably high.

$$C_{m_\alpha} = \frac{\partial C_m}{\partial C_L} C_{L_\alpha} \tag{4.11}$$

where:

$$\frac{\partial C_m}{\partial C_L} = \bar{x}_{ref} - \bar{x}_{ac_A} \tag{4.12}$$

$\bar{x}_{ac_A}$: the location of the airplane aerodynamic center in fractions of the mean geometric center.

4.1.2.2.2 Thrust versus angle of attack derivative, C_{mT_α}

$$C_{m_{T\alpha}} = \left[\Delta \left(\frac{\partial C_m}{\partial C_L} \right)_T \right] C_{L_\alpha} \tag{4.13}$$

with:

$$\Delta \left(\frac{\partial C_m}{\partial C_L} \right)_T = \left(\frac{\partial C_m}{\partial C_L} \right)_{TL} + \left(\frac{\partial C_m}{\partial C_L} \right)_N \tag{4.14}$$

where:

$\left(\frac{\partial C_m}{\partial C_L} \right)_{TL}$: the effect of thrustline offset on longitudinal stability.

$\left(\frac{\partial C_m}{\partial C_L} \right)_N$: the effect of propeller or inlet normal force on longitudinal stability.

4.1.2.3 RATE OF ANGLE OF ATTACK DERIVATIVES

Drag due to rate of angle of attack derivative, $C_{D_{\dot{\alpha}}}$

It is the change in drag coefficient with the rate of change of angle of attack. It arises from the aerodynamic lag effect and various dead-weight aeroelastic effects. It is normally negligible.

$$C_{D_{\dot{\alpha}}} = 0 \tag{4.15}$$

Lift due to rate of angle of attack derivative, $C_{L_{\dot{\alpha}}}$

It is the change in lift coefficient with the rate of change of angle of attack. This derivative arises from a type of plunging motion along the z-axis, during which the angle of pitch remains zero. For low speed flight, the derivative results primarily from the aerodynamic time lag effect at the horizontal tail, and its sign is positive.

$$C_{L_{\dot{\alpha}}} = 2C_{L_{\alpha_h}} \eta_h \frac{S_h}{S} \left(\bar{x}_{ac_h} - \bar{x}_{cg} \right) \frac{d\varepsilon}{d\alpha} \tag{4.16}$$

Pitching moment due to rate of angle of attack derivative, $C_{m_{\dot{\alpha}}}$

It is the change in pitching moment coefficient with the rate of change of angle of attack. It is quite important in longitudinal dynamics, since it is involved in the damping of the short period mode. A negative value increases short period damping; thus negative values are desirable. This derivative is actually caused by a lag effect of the downwash at the horizontal tail of the aircraft.

$$C_{m_{\dot{\alpha}}} = -2C_{L_{\alpha_h}} \eta_h \frac{S_h}{S} \left(\bar{x}_{ac_h} - \bar{x}_{cg} \right)^2 \frac{d\varepsilon}{d\alpha} \tag{4.17}$$

4.1.2.4 ANGLE OF SIDESLIP DERIVATIVES

4.1.2.4.1 Aerodynamic Angle Of Sideslip Derivatives

The side force due to sideslip derivative, C_{y_β}

It is the change in side force caused by a variation in sideslip angle. When the airframe has a positive sideslip, β, the relative wind strikes the wing, fuselage, and vertical tail obliquely from the

The wing contribution:

$$C_{y\beta_w} = -0.00573(|\Gamma|) \tag{4.19}$$

where:

Γ : the wing geometric dihedral angle.

The fuselage contribution:

$$C_{y\beta_f} = -2K_i \frac{S_0}{S} \tag{4.20}$$

where:

K_i : defined in Figure 10.8 of Reference 1.

S_0 : the cross sectional area of the fuselage at station x_0, where the flow ceases to be potential.

The vertical tail contribution for single vertical tails:

$$C_{y\beta_v} = -k_v C_{L_{\alpha_v}} \left(1+\frac{d\sigma}{d\beta}\right)\eta_v \frac{S_v}{S} \tag{4.21}$$

where:

k_v : defined in Figure 10.12 of Reference 1.

$$\left(1+\frac{d\sigma}{d\beta}\right)\eta_v = 0.724 + 3.06\frac{\frac{S_v}{S}}{1+\cos\Lambda_{c/4}} + 0.4\frac{z_w}{z_f} + 0.009A \tag{4.22}$$

where:

z_w : wing distance to fuselage centerline.

z_f : vertical height of fuselage at wing root chord.

S_v : vertical tail area

The rolling moment due to sideslip derivative, C_{l_β}

It is the change in rolling moment caused by a variation in sideslip angle, and referred to as the effective dihedral derivative. In popular usage, a positive dihedral effect means a negative value. For most conventional configurations, the value is negative; however, this value can easily be adjusted by changing the moment of built-in wing dihedral.

$$C_{l_\beta} = C_{l_{\beta_w}} + C_{l_{\beta_h}} + C_{l_{\beta_v}} \tag{4.23}$$

The wing contribution:

$$C_{l_{\beta_w}} = 57.3\left\{\begin{array}{l} C_{L_{wf}}\left[\left(\frac{C_{l_\beta}}{C_L}\right)_{\Lambda_{c/2}} K_{M_\Lambda} K_f + \left(\frac{C_{l_\beta}}{C_L}\right)_A\right] + \\ +\Gamma\left[\left(\frac{C_{l_\beta}}{\Gamma}\right) K_{M_\Gamma} + \left(\frac{\Delta C_{l_\beta}}{\Gamma}\right)\right] + \left(\Delta C_{l_\beta}\right)_{z_w} + \\ +\varepsilon_t \tan\Lambda_{c/4} \dfrac{\Delta C_{l_\beta}}{\varepsilon_t \tan\Lambda_{c/4}} \end{array}\right\} \tag{4.24}$$

where:

$\left(\frac{C_{l_\beta}}{C_L}\right)_{\Lambda_{c/2}}$: wing sweep contribution.

K_{M_Λ} : the compressibility correction.

K_f : fuselage correction factor.

$\left(\frac{C_{l_\beta}}{C_L}\right)_A$: the aspect ratio contribution.

$\left(\frac{C_{l_\beta}}{\Gamma}\right)$: the wing dihedral effect.

K_{M_Γ} : the compressibility correction to dihedral.

$\left(\frac{\Delta C_{l_\beta}}{\Gamma}\right)$: the fuselage induced effect on the wing height.

$\frac{\Delta C_{l_\beta}}{\varepsilon_t \tan \Lambda_{c/4}}$: wing twist correction.

$$\left(\Delta C_{l_\beta}\right)_{z_w} = 0.042\sqrt{A}\,\frac{z_w}{b}\,\frac{d_f}{b} \tag{4.25}$$

where:

d_f : equivalent fuselage diameter.

The horizontal tail contribution:

$$C_{l_{\beta_h}} = C_{l_{\beta_{hf}}}\,\frac{S_h}{S}\,\frac{b_h}{b} \tag{4.26}$$

where:

$C_{l_{\beta_{hf}}}$: the horizontal tail dihedral effect as computed from Equation 3.24 with appropriate substitution of tail-fuselage for wing fuselage parameters.

The vertical tail contribution for single vertical tails:

$$C_{l_{\beta_v}} = C_{y_{\beta_v}}\,\frac{z_v \cos\alpha - l_v \sin\alpha}{b} \tag{4.27}$$

The yawing moment due to sideslip derivative, C_{n_β}

It is the change in yawing moment caused by a variation in sideslip angle and is also called static directional derivative or weathercock. The vertical tail, fuselage, and wing contribute to C_{n_β}, with the vertical tail the dominant factor. For positive sideslip, the vertical tail causes a positive yawing moment; thus it usually positive, even though the fuselage contribution is normally negative. The wing contribution is usually positive, but quite small compared to that of the vertical tail and fuselage.

$$C_{n_\beta} = C_{n_{\beta_w}} + C_{n_{\beta_f}} + C_{n_{\beta_v}} \tag{4.28}$$

The wing contribution is important only at high angle of attack. For preliminary design purposes:

$$C_{n_{\beta_w}} = 0 \tag{4.29}$$

The fuselage contribution:

$$C_{n\beta_f} = -57.3 K_N K_{R_1} \frac{S_{f_s}}{S} \frac{l_f}{b} \tag{4.30}$$

where:

K_N : an empirical factor determined from Figure 10.28 of Reference 1.

K_{R_1} : a factor dependent on Reynold's Number.

S_{f_s} : fuselage side area.

l_f : fuselage length.

The vertical tail contribution for single vertical tails:

$$C_{n\beta_v} = -C_{y\beta_v} \frac{l_v \cos\alpha + z_v \sin\alpha}{b} \tag{4.31}$$

4.1.2.4.2 Thrust Versus Sideslip Derivatives

The yawing moment due to thrust in sideslip derivative, $C_{n_{T\beta}}$

$$C_{n_{T\beta}} = \sum_{i=1}^{n} \left[\frac{\left(\frac{dC_N}{d\alpha}\right)_{p_i} (0.79) D_{p_i}^2 l_{p_i}}{Sb} \right] \tag{4.32}$$

where:

$\left(\frac{dC_N}{d\alpha}\right)_{p_i}$: the change in propeller normal force coefficient with angle of attack.

D_{p_i} : diameter of propeller i.

l_{p_i} : the moment arm of the propeller normal force to the reference point.

4.1.2.5 RATE OF ANGLE OF SIDESLIP DERIVATIVES

The side force due to rate of sideslip derivative, $C_{y_{\dot{\beta}}}$

$$C_{y_{\dot{\beta}}} = 2C_{l_{\alpha_v}} \frac{d\sigma}{d\beta} \frac{S_v}{S} \frac{l_p \cos\alpha_f - z_p \sin\alpha_f}{b} \tag{4.33}$$

$$\frac{d\sigma}{d\beta} = \sigma_{\beta_\alpha} \alpha_f + \sigma_{\beta_\Gamma} \frac{\Gamma}{57.3} - \sigma_{\beta_{\varepsilon_t}} \varepsilon_t + \sigma_{\beta_{wf}} \tag{4.34}$$

where:

σ_{β_α} : the sidewash contribution due to angle of attack.

α_f : the angle of attack of the fuselage.

σ_{β_Γ} : the sidewash contribution due to wing dihedral.

$\sigma_{\beta_{\varepsilon_t}}$: the sidewash contribution due to wing twist.

$\sigma_{\beta_{wf}}$: the sidewash effect due to fuselage.

z_p : vertical distance between wing and vertical tail quarter chords.

l_p : horizontal distance between wing and vertical tail quarter chords.

The rolling moment due to rate of sideslip derivative, $C_{l_{\dot{\beta}}}$

$$C_{l_{\dot{\beta}}} = C_{y_{\dot{\beta}}} \frac{z_p \cos\alpha_f - l_p \sin\alpha_f}{b} \tag{4.35}$$

The yawing moment due to rate of sideslip derivative, $C_{n_{\dot{\beta}}}$

$$C_{n_{\dot{\beta}}} = C_{y_{\dot{\beta}}} \frac{l_p \cos\alpha_f + z_p \sin\alpha_f}{b} \tag{4.36}$$

4.1.2.6 ROLL RATE DERIVATIVES

The side force due to roll rate derivative, C_{y_p}

It is the change in side force resulting from rolling velocity, with the vertical tail the main contributor, even though, for some

configurations, the wing may make a significant contribution. Its sign may be either positive or negative. It is relatively insignificant and commonly neglected.

$$C_{y_p} = 2C_{y_{\beta_v}} \frac{z_v \cos\alpha - l_v \sin\alpha}{b} \tag{4.37}$$

where:

z_v : vertical distance between vertical tail aerodynamic center and center of gravity.

l_v : horizontal distance between vertical tail aerodynamic center and center of gravity.

The rolling moment due to roll rate derivative, C_{l_p}

It is the change in rolling moment coefficient resulting from rolling velocity. For a positive roll, it is the result, primarily, of an increase in lift on the down moving wing and a decrease in lift on the up moving wing, thus creating a moment which opposes the motion of the roll; thus its sign is negative. It is the principal determinant of the damping-in-roll characteristics of the aircraft.

$$C_{l_p} = C_{l_{p_w}} + C_{l_{p_h}} + C_{l_{p_v}} \tag{4.38}$$

The wing contribution:

$$C_{l_{p_w}} = \left(\frac{\beta C_{l_p}}{k}\right)_{C_L=0} \left(\frac{k}{\beta}\right) \frac{\left(C_{L_{\alpha_w}}\right)_{C_L}}{\left(C_{L_{\alpha_w}}\right)_{C_L=0}} \frac{\left(C_{l_p}\right)_{\Gamma}}{\left(C_{l_p}\right)_{\Gamma=0}} + \left(\Delta C_{l_p}\right)_{drag} \tag{4.39}$$

Note: the parameter β in Equation 3.39 is not sideslip. In this case:

$$\beta = \sqrt{1 - M^2} \tag{4.40}$$

where:

$\left(\frac{\beta C_{l_p}}{k}\right)_{C_L=0}$: the roll damping parameter at zero lift.

$\left(C_{L_{\alpha_w}}\right)_{C_L}$: the wing lift curve slope at any lift coefficient.

$\left(C_{L_{\alpha_w}}\right)_{C_L=0}$: the wing lift curve slope at zero lift.

$\dfrac{\left(C_{l_p}\right)_\Gamma}{\left(C_{l_p}\right)_{\Gamma=0}}$: the dihedral effect parameter.

$\left(\Delta C_{l_p}\right)_{drag}$: the wing drag contribution to roll damping.

The horizontal tail contribution:

$$C_{l_{ph}} = 0.5\left(C_{l_p}\right)_h \frac{S_h}{S}\left(\frac{b_h}{b}\right)^2 \tag{4.41}$$

where:

$\left(C_{l_p}\right)_h$: the roll damping derivative of the horizontal tail based on its own reference geometry. It is obtained from Equation 3.39 with appropriate substitution of horizontal tail parameters for wing parameters.

The vertical tail contribution for single vertical tails:

$$C_{l_{pv}} = 2\left(\frac{z_v}{b}\right)^2 C_{y_{\beta_v}} \tag{4.42}$$

The yawing moment due to roll rate derivative, C_{n_p}

It is the change in yawing moment coefficient resulting from rolling velocity, with the wing and vertical tail the main contributors. For a positive roll, the produced yawing moment is a result of the unsymmetrical lift distribution causing increased drag on the left wing and decreased drag on the right wing and is negative. The vertical contribution may be either positive or negative, depending on tail geometry, angle of attack, and sidewash from the wing. Dutch Roll damping is influenced by C_{n_p} in that the larger its negative value, the less Dutch Roll damping. Therefore a positive value is desired.

$$C_{n_p} = C_{n_{p_w}} + C_{n_{p_v}} \tag{4.43}$$

The wing contribution:

$$C_{n_{p_w}} = -\left(\frac{C_{n_p}}{C_L}\right)_{C_L=0} C_L + \frac{C_{n_p}}{\varepsilon_t}\varepsilon_t + \frac{\Delta C_{n_p}}{\alpha_{\delta_f}\delta_f}\alpha_{\delta_f}\delta_f \tag{4.44}$$

with:

$$\left(\frac{C_{n_p}}{C_L}\right)_{C_L=0} = \frac{A+4\cos\Lambda_{c/4}}{AB+4\cos\Lambda_{c/4}} * \\ * \frac{AB+\frac{1}{2}(AB+4\cos\Lambda_{c/4})\tan^2\Lambda_{c/4}}{A+\frac{1}{2}(A+4\cos\Lambda_{c/4})\tan^2\Lambda_{c/4}} \left(\frac{C_{n_p}}{C_L}\right)_{\substack{C_L=0 \\ M=0}} \tag{4.45}$$

with:

$$B = \sqrt{1-M^2\cos^2\Lambda_{c/4}} \tag{4.46}$$

$$\left(\frac{C_{n_p}}{C_L}\right)_{\substack{C_L=0 \\ M=0}} = -\frac{1}{6}\frac{A+6(A+4\cos\Lambda_{c/4})(\frac{\bar{x}}{\bar{c}}\frac{\tan\Lambda_{c/4}}{A}+\frac{\tan^2\Lambda_{c/4}}{12}}{A+4\cos\Lambda_{c/4}} \tag{4.47}$$

$$\alpha_{\delta_f} = \frac{\Delta C_l}{C_{l_\alpha}}\delta_f \tag{4.48}$$

where:

$\frac{C_{n_p}}{\varepsilon_t}$: the wing twist contribution.

$\frac{\Delta C_{n_p}}{\alpha_{\delta_f}\delta_f}$: the contribution due to symmetrical flap deflection.

ΔC_l : incremental airfoil lift coefficient due to flaps.

The vertical tail contribution:

$$C_{n_{p_v}} = -\frac{2}{b^2}(l_v \cos\alpha + z_v \sin\alpha)(z_v \cos\alpha - l_v \sin\alpha - z_v)C_{y_{\beta_v}} \tag{4.49}$$

4.1.2.7 PITCH RATE DERIVATIVES

Drag due to pitch rate derivative, C_{D_q}

It is the change in airplane drag with varying pitching velocity while the angle of attack of the airplane as a whole remains constant. It has contributions from both the wing and the fuselage but both contributions are very small. It is negligible for almost all airplanes.

$$C_{D_q} = 0 \tag{4.50}$$

Lift due to pitch rate derivative, C_{L_q}

It represents the change in airplane lift with varying pitching velocity while the angle of attack of the airplane as a whole remains constant. Contributions are made by both the wing and horizontal tail, but the tail is far the more important. The general consensus is that it plays only a minor part in estimating the longitudinal response of the aircraft.

$$C_{L_q} = C_{L_{q_w}} + C_{L_{q_h}} \tag{4.51}$$

The wing contribution:

$$C_{L_{q_w}} = \frac{A + 2\cos\Lambda_{c/4}}{AB + 2\cos\Lambda_{c/}}\left(C_{L_{q_w}}\right)_{M=0} \tag{4.52}$$

with:

$$\left(C_{L_{q_w}}\right)_{M=0} = \left(0.5 + 2\frac{x_w}{\bar{c}}\right)C_{l_{\alpha_w}} \tag{4.53}$$

where:

x_w : distance of wing quarter chord mean geometric center to center of gravity.

$C_{l_{\alpha_w}}$: the average wing airfoil lift curve slope.

Horizontal tail contribution:

$$C_{L_{qh}} = 2C_{L_{\alpha_h}} \eta_h \left(\bar{x}_{ac_h} - \bar{x}_{cg} \right) \frac{S_h}{S} \tag{4.54}$$

Pitching moment due to pitch rate derivative, C_{m_q}

It is the change in airplane pitching moment with varying pitching velocity while the angle of attack of the airplane as a whole remains constant. The derivative is sometimes referred to as the pitch damping derivative and is usually negative.

$$C_{m_q} = C_{m_{q_w}} + C_{m_{q_h}} \tag{4.55}$$

The wing contribution:

$$C_{m_{q_w}} = \frac{\frac{A^3 + 2\tan^2 \Lambda_{c/4}}{AB + 6\cos\Lambda_{c/}} + \frac{3}{B}}{\frac{A^3 + 2\tan^2 \Lambda_{c/4}}{A + 6\cos\Lambda_{c/}} + 3} \left(C_{m_{q_w}} \right)_{M=0} \tag{4.56}$$

$$\left(C_{m_{q_w}} \right)_{M=0} = -K_w C_{l_{\alpha_w}} \cos\Lambda_{c/4} \left[\frac{A\left(2\left(\frac{x_w}{\bar{c}} \right)^2 + 0.5\frac{x_w}{\bar{c}} \right)}{A + 2\cos\Lambda_{c/4}} + \frac{A^3 \tan^2 \Lambda_{c/4}}{24\left(A + 6\cos\Lambda_{c/4} \right)} + \frac{1}{8} \right] \tag{4.57}$$

Horizontal tail contribution:

$$C_{m_{q_h}} = -2C_{L_{\alpha_h}} \eta_h \left(\bar{x}_{ac_h} - \bar{x}_{cg} \right)^2 \frac{S_h}{S} \tag{4.58}$$

4.1.2.8 YAW RATE DERIVATIVES

The side force due to yaw rate derivative, C_{y_r}

It is the change in side force resulting from a change in yawing velocity. As the airframe undergoes a positive yaw, an effective positive side force develops on the vertical tail, which is the

dominant contributor to C_{y_r}. Since this force is normally small, it usually has a small positive value.

$$C_{y_r} = -2C_{y_{\beta_v}} \frac{l_v \cos\alpha + z_v \sin\alpha}{b} \tag{4.59}$$

The rolling moment due to yaw rate derivative, C_{l_r}

It is the change in rolling moment resulting from a change in yawing velocity. The wing provides the major contribution, with the vertical tail having a major effect. When there is a positive yaw rate, the left wing moves faster than the right wing, producing more lift on the left wing and, consequently, a positive rolling moment. Although it has little effect on Dutch Roll damping, it is quite important to the spiral mode. For spiral stability, it is desirable that C_{l_r} be as small a positive number as possible.

$$C_{l_r} = C_{l_{r_w}} + C_{l_{r_v}} \tag{4.60}$$

The wing contribution:

$$C_{l_{r_w}} = C_{L_w}\left(\frac{C_{l_r}}{C_L}\right)_{\substack{C_L=0 \\ M}} + \frac{\Delta C_{l_r}}{\Gamma}\Gamma + \frac{\Delta C_{l_r}}{\varepsilon_t}\varepsilon_t + \frac{\Delta C_{l_r}}{\alpha_{\delta_f}\delta_f}\alpha_{\delta_f}\delta_f \tag{4.61}$$

$$\left(\frac{C_{l_p}}{C_L}\right)_{\substack{C_L=0 \\ M}} = \frac{1 + \dfrac{A(1-B^2)}{2B(AB+2\cos\Lambda_{c/4})} + \dfrac{AB+2\cos\Lambda_{c/4}}{AB+4\cos\Lambda_{c/4}}\dfrac{\tan^2\Lambda_{c/4}}{8}}{1 + \dfrac{A+2\cos\Lambda_{c/4}}{A+4\cos\Lambda_{c/4}}\dfrac{\tan^2\Lambda_{c/4}}{8}}\left(\frac{C_{l_r}}{C_L}\right)_{\substack{C_L=0 \\ M=0}} \tag{4.62}$$

$$\frac{\Delta C_{l_r}}{\Gamma} = 0.083\frac{\pi . A \sin\Lambda_{c/4}}{A + 4\cos\Lambda_{c/4}} \tag{4.63}$$

where:

C_{L_w} : wing lift coefficient

$\left(\dfrac{C_{l_r}}{C_L}\right)_{\substack{C_L=0 \\ M=0}}$: the slope of the low speed rolling moment due to yaw rate at zero lift.

$\frac{\Delta C_{l_r}}{\varepsilon_t}$: the increment in C_{l_r} due to twist.

$\frac{\Delta C_{l_r}}{\alpha_{\delta_f}\delta_f}$: the effect of symmetric flap deflection on the rolling moment due to roll rate.

The vertical tail contribution for single vertical tails:

$$C_{l_{r_v}} = -\frac{2}{b^2}(l_v \cos\alpha + z_v \sin\alpha)(z_v \cos\alpha - l_v \sin\alpha)C_{y_{\beta_v}} \qquad (4.64)$$

The yawing moment due to yaw rate derivative, C_{n_r}

It is the change in yawing moment resulting from a change in yawing velocity and also known as the yaw damping derivative. The derivative C_{n_r} is the main contributor to the damping of the Dutch Roll mode and also plays a significant role in determining spiral stability, making it vital to lateral stability. For best effects in each of these modes, large negative values of C_{n_r} are desired.

$$C_{n_r} = C_{n_{r_w}} + C_{n_{r_v}} \qquad (4.65)$$

The wing contribution:

$$C_{n_{r_w}} = \frac{C_{n_r}}{C_L^2} C_{L_w}^2 + \frac{C_{n_r}}{C_{D_0}} C_{D_{0_w}} \qquad (4.66)$$

where:

$\frac{C_{n_r}}{C_L^2}$: found from Figure 10.44 of Reference 1.

$\frac{C_{n_r}}{C_{D_0}}$: found from Figure 10.45 of Reference 1.

The vertical tail contribution:

$$C_{n_{r_v}} = \frac{2}{b^2}(l_v \cos\alpha + z_v \sin\alpha)^2 C_{y_{\beta_v}} \qquad (4.67)$$

4.1.3 CONTROL DERIVATIVES

4.1.3.1 ELEVATOR CONTROL DERIVATIVES

Although many airplanes carry approximately full span elevators on the horizontal stabilize, exceptions do occur. For that reason the elevator should be thought of as a partial span, plain flap.

The drag due to elevator derivative, $C_{D_{\delta_e}}$

It is the change in drag coefficient due a to change in elevator angle. For an elevator of reasonable size, the total airplane drag does not change appreciably with elevator deflection. For this reason it is often neglected.

$$C_{D_{\delta_e}} = \alpha_{\delta_e} C_{D_{i_h}} \tag{4.68}$$

with:

$$\alpha_{\delta_e} = K_b \frac{C_{l_\delta}}{\left(C_{l_\delta}\right)_{theory}} \left(C_{l_\delta}\right)_{theory} \frac{k'}{C_{l_{\alpha_h}}} \frac{(\alpha_\delta)_{C_L}}{(\alpha_\delta)_{C_l}} \tag{4.69}$$

$$C_{D_{i_h}} = 2\frac{C_{L_h}}{\pi . A_h e_h} C_{L_{\alpha_h}} \eta_h \tag{4.70}$$

where:

K_b : the elevator span factor.

$\frac{C_{l_\delta}}{\left(C_{l_\delta}\right)_{theory}}$: found from Figure 8.15 of Reference 1.

$\left(C_{l_\delta}\right)_{theory}$: found from Figure 8.14 of Reference 1.

k' : correction factor which accounts for nonlinearities at high elevator deflection angles.

$\frac{(\alpha_\delta)_{C_L}}{(\alpha_\delta)_{C_l}}$: found from Figure 8.53 of Reference 1.

A_h : the horizontal tail aspect ratio.

e_h : Oswald efficiency factor for the horizontal tail.

The lift due to elevator derivative, $C_{L_{\delta_e}}$

It is the change in lift coefficient due to elevator deflection. Since downward deflection of the elevator is defined as positive, producing a positive lift, it is positive in sign.

$$C_{L_{\delta_e}} = \alpha_{\delta_e} C_{L_{i_h}} \tag{4.71}$$

with:

$$C_{L_{i_h}} = C_{L_{\alpha_h}} \eta_h \frac{S_h}{S} \tag{4.72}$$

The pitching moment due to elevator derivative, $C_{m_{\delta_e}}$

It is the change in pitching moment coefficient due to elevator deflection, usually referred to as elevator power or elevator effectiveness. Since a positive elevator deflection is defined as down, a positive elevator deflection gives a negative pitching moment contribution, making the sign negative.

$$C_{m_{\delta_e}} = \alpha_{\delta_e} C_{m_{i_h}} \tag{4.73}$$

with:

$$C_{m_{i_h}} = -C_{L_{\alpha_h}} \eta_h \left(\bar{x}_{ac_h} - \bar{x}_{cg} \right) \frac{S_h}{S} \tag{4.74}$$

4.1.3.2 AILERON CONTROL DERIVATIVES

The side force due to aileron derivative, $C_{y_{\delta_a}}$

It is the change in side force coefficient with variation in aileron deflection. It is negligible for most conventional aileron arrangements.

$$C_{y_{\delta_a}} = 0 \tag{4.75}$$

The rolling moment due to aileron derivative, $C_{l_{\delta_a}}$

It is the change in rolling moment coefficient with variation in aileron deflection and known as the aileron effectiveness or aileron power. Since left aileron down is defined as positive, a positive deflection produces a rolling moment to the right, which is also

positive, making it positive. It is calculated with the method in Reference 1.

The yawing moment due to aileron derivative, $C_{n_{\delta_a}}$

It is the change in yawing moment coefficient with variation in aileron deflection, results from the difference between drag on the up and down ailerons. Since a positive deflection is with the aileron on the left wing down, it is usually negative. A negative value for $C_{n_{\delta_a}}$ is known as adverse yaw coefficient due to ailerons because it is the result of initial yawing of the airframe in a direction opposite that desired for a turn. Thus, the desired value of $C_{n_{\delta_a}}$ is either zero or a very small positive value.

$$C_{n_{\delta_a}} = K_a C_{L_w} C_{l_{\delta_a}} \tag{4.76}$$

where:

K_a : the partial span aileron parameter.

4.1.3.3 RUDDER CONTROL DERIVATIVES

The side force due to rudder derivative, $C_{y_{\delta_r}}$

It is the change in side force with variation in rudder deflection. For a positive rudder deflection, or rudder toward the left wing, a positive side force results; hence, it is positive.

$$C_{y_{\delta_r}} = C_{L_{\alpha_v}} k' K_b \frac{(\alpha_\delta)_{C_L}}{(\alpha_\delta)_{C_l}} (\alpha_\delta)_{C_l} \frac{S_v}{S} \tag{4.77}$$

The rolling moment due to rudder derivative, $C_{l_{\delta_r}}$

It is the change in rolling moment coefficient with variation in rudder deflection. Because the rudder is normally located above the x-axis, a positive rudder deflection (rudder to the left) causes a positive rolling moment, making $C_{l_{\delta_r}}$ positive.

$$C_{l_{\delta_r}} = C_{y_{\delta_r}} \frac{z_v \cos\alpha - l_v \sin\alpha}{b} \tag{4.78}$$

The yawing moment due to rudder derivative, $C_{n_{\delta_r}}$

It is the change in yawing moment coefficient with variation in rudder deflection. Also known as the rudder power, this derivative is negative, since a positive rudder deflection toward the left wing creates a negative yawing moment.

$$C_{n_{\delta_r}} = -C_{y_{\delta_r}} \frac{l_v \cos\alpha + z_v \sin\alpha}{b} \qquad (4.79)$$

4.2 STATIC STABILITY AND CONTROL CALCULATIONS FOR THE TEST AIRCRAFT

The software AAA was used for most of the calculations. This software is based on the method of Dr. Jan Roskam[1]. The stability and control part of this theory is described in Chapter 4.1. The results that are obtained with using AAA are presented in Chapter 4.3. The calculation of thrust related derivatives are made in this chapter. Then these calculated values are used as inputs of AAA.

4.2.1 CALCULATION OF THRUST RELATED DERIVATIVES

4.2.1.1 THE STEADY STATE THRUST COEFFICIENT COMPONENT IN THE DIRECTION OF THE STABILITY X-AXIS

The input data used in the calculations were obtained in previous chapters or taken from different references.

$C_{T_{x1}}$ For $\bar{x}_{cg}$ Is At $0.16\bar{c}$

$C_{D_1} = 0.0278$

$C_{L_1} = 0.4038$

$\theta_1 = 0.42$ degree

$$C_{T_{x1}} = C_{D_1} + C_{L_1} \sin\theta_1 = 0.0308$$

$C_{T_{x1}}$ For $\bar{x}_{cg}$ Is At $0.30\bar{c}$

$C_{D_1} = 0.0278$

$C_{L_1} = 0.4038$

$\theta_1 = 0.42$ degree

$C_{T_{x1}} = C_{D_1} + C_{L_1} \sin\theta_1 = 0.0308$

4.2.1.2 THRUST DUE TO SPEED DERIVATIVE

$C_{T_{xu}}$ For $\bar{x}_{cg}$ Is At 0.16 $\bar{c}$

$C_{T_{x1}} = 0.0308$

$C_{T_{x_u}} = -3C_{T_{x1}} = -0.0923$

$C_{T_{xu}}$ For $\bar{x}_{cg}$ Is At 0.30 $\bar{c}$

$C_{T_{x1}} = 0.0308$

$C_{T_{x_u}} = -3C_{T_{x1}} = -0.0923$

4.2.1.3 THRUST MOMENT DUE TO SPEED DERIVATIVE

C_{mT_u} For $\bar{x}_{cg}$ Is At 0.16 $\bar{c}$

$C_{T_{xu}} = -0.0923$

$d_t = -1.437$ m

$\bar{c} = 2.62$ m

$$C_{m_{T_u}} = C_{T_{x_u}} \frac{d_t}{\bar{x}} = 0.0506$$

C_{mT_u} For $\bar{x}_{cg}$ Is At 0.30 $\bar{c}$

$C_{T_{xu}} = -0.0923$

$d_t = -1.437$ m

$\bar{c} = 2.62$ m

$$C_{m_{T_u}} = C_{T_{x_u}} \frac{d_t}{\bar{x}} = 0.0506$$

4.2.1.4 THE STEADY STATE PITCHING MOMENT COEFFICIENT DUE TO THRUST

$C_{m_{T_1}}$ **For** $\bar{x}_{cg}$ **Is At 0.16** $\bar{c}$

C_{m_0} = 0.1083
C_{m_α} = -2.5857 rad^{-1}
α_1 = 0.42 degree
$C_{m_{\delta_e}}$ = -2.2558 rad^{-1}
δ_{e_1} = 1.88 degree

$$C_{m_{T_1}} = -\left(C_{m_0} + C_{m_\alpha}\alpha_1 + C_{m_{\delta_e}}\delta_{e_1}\right) = -0.0153$$

$C_{m_{T_1}}$ **For** $\bar{x}_{cg}$ **Is At 0.30** $\bar{c}$

C_{m_0} = 0.1035
C_{m_α} = -1.7274 rad^{-1}
α_1 = 0.42 degree
$C_{m_{\delta_e}}$ = -2.1749 rad^{-1}
δ_{e_1} = 2.0 degree

$$C_{m_{T_1}} = -\left(C_{m_0} + C_{m_\alpha}\alpha_1 + C_{m_{\delta_e}}\delta_{e_1}\right) = -0.0148$$

4.2.1.5 THRUST VERSUS ANGLE OF ATTACK DERIVATIVE

C_{mT_α} **For** $\bar{x}_{cg}$ **Is At 0.16** $\bar{c}$

$\frac{\partial C_{n_p}}{\partial \alpha}$ = 0.192
$\frac{\partial \varepsilon_p}{\partial \alpha}$ = 2.25 from Figure 8.115 of Reference 1.
n = 2 , number of engines.

$$S_p = \frac{\pi}{4}d_p^2 = \frac{\pi}{4}(3.35)^2 = 8.814 \text{ m}^2$$
$$x_p = x_{cg} - x_{apex_{naclle}} = 8.37 - 5.40 = 2.97 \text{ m}$$

$$C_{mT_\alpha} = n\frac{x_p}{\bar{c}}\frac{S_p}{S}\frac{\partial.C_{n_p}}{\partial.\alpha}\left(1+\frac{\partial.\varepsilon_p}{\partial.\alpha}\right) = 0.2110$$

C_{mT_α} For $\bar{x}_{cg}$ Is At 0.30 $\bar{c}$

$$x_p = x_{cg} - x_{apex_{naclle}} = 8.736 - 5.40 = 3.336 \text{ m}$$

$$C_{mT_\alpha} = n\frac{x_p}{\bar{c}}\frac{S_p}{S}\frac{\partial.C_{n_p}}{\partial.\alpha}\left(1+\frac{\partial.\varepsilon_p}{\partial.\alpha}\right) = 0.2370$$

4.2.1.6 THE YAWING MOMENT DUE TO THRUST IN SIDESLIP DERIVATIVE

$C_{n_{T_\beta}}$ For $\bar{x}_{cg}$ Is At 0.16 $\bar{c}$

$$x_p = x_{cg} - x_{apex_{naclle}} = 8.37 - 5.40 = 2.97 \text{ m}$$

$$C_{nT_\beta} = n\frac{\partial.C_{n_p}}{\partial.\alpha}\frac{S_p}{S}\frac{x_p}{b} = -0.0069$$

$C_{n_{T_\beta}}$ For $\bar{x}_{cg}$ Is At 0.30 $\bar{c}$

$$x_p = x_{cg} - x_{apex_{naclle}} = 8.736 - 5.40 = 3.336 \text{ m}$$

$$C_{nT_\beta} = n\frac{\partial.C_{n_p}}{\partial.\alpha}\frac{S_p}{S}\frac{x_p}{b} = -0.0078$$

4.3 SUMMARY OF RESULTS RELATED TO STATIC STABILITY AND CONTROL

Result related to stability and control derivatives are listed in Tables 4.5 and 4.6.

The drag, lift, and pitching moment coefficients with the speed, C_{D_u}, C_{L_u}, and C_{m_u} can usually be considered to be zero. In this case they are not zero but they are too small.

The change in drag coefficient with varying angle of attack, C_{D_α} has little effect on the short period mode and has only a small effect on the phugoid mode. Above the angle of attack for minimum drag the drag coefficient increases as the angle of attack increases; thus its sign must be positive. In this case it is positive.

The change in lift curve slope, C_{L_α} has always a positive value for angles of attack below the stall. It is positive in this case.

The change in pitching moment coefficient with angle of attack, C_{m_α} is perhaps the most important derivative related to longitudinal stability and control, since it primarily establishes the natural frequency of the short period mode and is a major factor in determining the response of the airframe to elevator motion and gusts. Usually, a large negative value of C_{m_α} is desired, but if it is too large, the required elevator effectiveness may become unreasonably high. It has a negative sign in this case.

The change in drag coefficient with the rate of change of angle of attack, $C_{D_{\dot{\alpha}}}$ is normally negligible. It is zero in this case.

The change in lift coefficient with the rate of change of angle of attack, $C_{L_{\dot{\alpha}}}$ must have a positive sign. It has a positive sign in our case.

The change in pitching moment coefficient with the rate of change of angle of attack, $C_{m_{\dot{\alpha}}}$ is quite important in longitudinal dynamics, since it is involved in the damping of the short period mode. A negative value increases short period damping; thus negative values are desirable. Its sign is negative.

The change in airplane drag with varying pitching velocity while the angle of attack of the airplane as a whole remains constant, C_{D_q} is negligible for almost all airplanes. It is also zero for this case.

The change in airplane lift with varying pitching velocity while the angle of attack of the airplane as a whole remains constant, C_{L_q} plays only a minor part in estimating the longitudinal response of the aircraft.

The change in airplane pitching moment with varying pitching velocity while the angle of attack of the airplane as a whole remains constant, C_{m_q} is sometimes referred to as the pitch damping derivative and is usually negative. Its sign is negative.

The change in side force caused by a variation in sideslip angle, C_{y_β} contributes to the damping of the Dutch Roll mode, large negative values are desirable. It has a negative sign.

The change in rolling moment caused by a variation in sideslip angle, C_{l_β} has negative sign; however, this value can easily be adjusted by changing the moment of built-in wing dihedral. It is negative.

The change in yawing moment caused by a variation in sideslip angle, C_{n_β} is also called static directional derivative or weathercock. The vertical tail, fuselage, and wing contribute to it, with the vertical tail the dominant factor. For positive sideslip, the vertical tail causes a positive yawing moment. Its sign is positive.

The change in side force resulting from rolling velocity, C_{y_p} may have either positive or negative sign. It is relatively insignificant and commonly neglected. Its sign is negative and it is too small in this case.

The change in rolling moment coefficient resulting from rolling velocity, C_{l_p} has negative sign. It is the principal determinant of the damping-in-roll characteristics of the aircraft. It has a negative sign.

The change in yawing moment coefficient resulting from rolling velocity, C_{n_p} has a negative sign. Dutch Roll damping is influenced by C_{n_p} in that the larger its negative value, the less Dutch Roll damping. Therefore a positive value is desired. In this case its sign is negative.

The change in side force resulting from a change in yawing velocity, C_{y_r} is normally small, it usually has a small positive value. It has a positive value in this case.

The change in rolling moment resulting from a change in yawing velocity, C_{l_r} has little effect on Dutch Roll damping, but it is quite important to the spiral mode. For spiral stability, it is desirable that C_{l_r} be as small a positive number as possible. It has a small positive value in this case.

The change in yawing moment resulting from a change in yawing velocity, C_{n_r} and also known as the yaw damping derivative is the main contributor to the damping of the Dutch Roll mode and also plays a significant role in determining spiral stability, making it vital to lateral stability. For best effects in each of these modes, large negative values of C_{n_r} are desired. Its sign is negative.

The change in drag coefficient due a to change in elevator angle, $C_{D_{\delta_e}}$ does not change airplane drag coefficient too much. For this reason it is often neglected. In this case it has a small value.

The change in lift coefficient due to elevator deflection, $C_{L_{\delta_e}}$ is positive in sign. It has a positive sign in this case.

The change in pitching moment coefficient due to elevator deflection, $C_{m_{\delta_e}}$ usually referred to as elevator power or elevator effectiveness has a negative sign. Its sign is positive.

The change in side force coefficient with variation in aileron deflection, $C_{y_{\delta_a}}$ is negligible for most conventional aileron arrangements. It is zero in this case.

The change in rolling moment coefficient with variation in aileron deflection, $C_{n_{\delta_a}}$ and known as the aileron effectiveness or aileron power has a positive value. Its sign is positive.

The change in yawing moment coefficient with variation in aileron deflection, $C_{n_{\delta_a}}$ results from the difference between drag on the up and down ailerons. Since a positive deflection is with the aileron on the left wing down, it is usually negative. A negative value for $C_{n_{\delta_a}}$ is known as adverse yaw coefficient due to ailerons because it is the result of initial yawing of the airframe in a direction opposite that desired for a turn. Thus, the desired value

of $C_{n_{\delta_a}}$ is either zero or a very small positive value. But it is also negative in this case.

The change in side force with variation in rudder deflection, $C_{y_{\delta_r}}$ is positive. It is also positive in this case.

The change in rolling moment coefficient with variation in rudder deflection, $C_{l_{\delta_r}}$ is normally positive. Its sign is positive.

The change in yawing moment coefficient with variation in rudder deflection, $C_{n_{\delta_r}}$, also known as the rudder power, is negative. It has a negative value.

Table 4.5 Results related to static stability and control derivatives.

	$0.16\bar{c}$	$0.30\bar{c}$	Usual sign of the derivative
C_{D_u}	-0.0012	-0.0012	
C_{L_u}	0.0720	0.0720	
C_{m_u}	0.0266	0.0266	
C_{D_α}	0.1872	0.1872	+
C_{L_α}	6.1199	6.1199	+
C_{m_α}	-2.5839	-1.7274	-
$C_{D_{\dot{\alpha}}}$	0.0000	0.0000	
$C_{L_{\dot{\alpha}}}$	4.6337	4.4677	+
$C_{m_{\dot{\alpha}}}$	-18.1050	-16.8113	-
C_{D_q}	0.0000	0.0000	
C_{L_q}	15.5338	13.5515	
C_{m_q}	-47.0907	-43.4753	-
C_{y_β}	-1.3933	-1.3933	-
C_{l_β}	-0.1117	-0.1123	-
C_{n_β}	0.0380	0.0263	+

Table 4.6 Results related to static stability and control derivatives.

	$0.16\,\bar{c}$	$0.30\,\bar{c}$	Usual sign of the derivative
$C_{y_{\dot{\beta}}}$	-0.0465	-0.0465	
$C_{l_{\dot{\beta}}}$	-0.0037	-0.0037	
$C_{n_{\dot{\beta}}}$	-0.0199	-0.0199	
C_{y_p}	-0.0516	-0.0517	-,+
C_{l_p}	-0.4000	-0.4000	-
C_{n_p}	-0.0477	-0.0458	-
C_{y_r}	0.3246	0.3134	+
C_{l_r}	0.1208	0.1166	+
C_{n_r}	-0.1452	-0.1355	-
$C_{D\delta_e}$	0.0177	0.0177	
$C_{L\delta_e}$	0.5773	0.5773	+
$C_{m\delta_e}$	-2.2557	-2.1749	-
$C_{y\delta_a}$	0.0000	0.0000	
$C_{l\delta_a}$	0.1448	0.1448	+
$C_{n\delta_a}$	-0.0077	-0.0074	-
$C_{y\delta_r}$	0.2688	0.2688	+
$C_{l\delta_r}$	0.0185	0.0185	+
$C_{n\delta_r}$	-0.1174	-0.1134	-
$C_{T_{x1}}$	0.0308	0.0308	
$C_{T_{xu}}$	-0.0923	-0.0923	
C_{mT_u}	0.0506	0.0506	
$C_{m_{T1}}$	-0.0153	-0.0148	
$C_{n_{T\beta}}$	-0.0069	-0.0078	
C_{mT_α}	0.2110	0.2370	

CHAPTER 5

5. CALCULATIONS OF DYNAMIC STABILITY AND RESPONSE CHARECTERISTICS

The purpose of this chapter is to examine the dynamic stability and response characteristics of the airplane. Analysis is made for cruise condition with zero flap deflection and landing gears in up position. Theory part of this chapter is based on the Reference 11.

5.1 THEORY *OF DYNAMIC STABILITY AND RESPONSE CHARECTERISTICS*

Dynamic stability is defined as the tendency of the amplitudes of the perturbed motion of an airplane to decrease to zero or to values corresponding to a new steady state at some time after the disturbance has stopped. For example, when the airplane is disturbed in pitch from a steady state flight condition and the resulting perturbed motion is damped out after some time, while the new steady state is not significantly different from the original one, the airplane called dynamically stable.

Airplane response is defined as the change with time of motion variables relative to some steady state flight condition as a result of an externally generated disturbance. Externally generated disturbances could be changes in angle of attack or sideslip due to atmospheric variations such as gust. Internally generated disturbances could be control surface deflections.

Experience has shown that in many cases, the dynamic behavior of airplanes can be satisfactorily represented by assuming that perturbations away from steady state flight are small. In that case the equations of motion can be approximated by a set of equations with constant coefficients. These equations are called small perturbation equations. Combining small perturbation equations with the perturbed force and moment expressions yields the equations presented in Table 5.1 and 5.2.

Table 5.1 Longitudinal Small Perturbation Equations

$$m\dot{u} = -mg\theta\cos\theta_1 + \bar{q}_1 S\begin{bmatrix} -\left(C_{D_u} + 2C_{D_1}\right)\frac{u}{U_1} + \\ +\left(C_{T_{x_u}} + 2C_{T_{x_1}}\right)\frac{u}{U_1} - \\ -\left(C_{D_\alpha} - C_{L_1}\right)\alpha - C_{D_{\delta_e}}\delta_e \end{bmatrix} \tag{5.1}$$

$$m\left(w - \dot{U}_1 q\right) = -mg\theta\sin\theta_1 + \bar{q}_1 S\begin{bmatrix} -\left(C_{L_u} + 2C_{L_1}\right)\frac{u}{U_1} - \\ -\left(C_{L_\alpha} + C_{D_1}\right)\alpha - C_{L_{\dot{\alpha}}}\frac{\dot{\alpha}\bar{c}}{2U_1} - \\ -C_{L_q}\frac{q\bar{c}}{2U_1} - C_{L_{\delta_e}}\delta_e \end{bmatrix} \tag{5.2}$$

$$I_{yy}\dot{q} = \bar{q}_1 S\bar{c}\begin{bmatrix} \left(C_{m_u} + 2C_{m_1}\right)\frac{u}{U_1} + \left(C_{m_{T_u}} + 2C_{m_{T_1}}\right)\frac{u}{U_1} + C_{m_\alpha}\alpha + \\ +C_{m_{T_\alpha}}\alpha + C_{m_{\dot{\alpha}}}\frac{\dot{\alpha}\bar{c}}{2U_1} + C_{m_q}\frac{q\bar{c}}{2U_1} + C_{m_{\delta_e}}\delta_e \end{bmatrix} \tag{5.3}$$

Table 5.2 Lateral-Directional Small Perturbation Equations

$$m\left(v + \dot{U}_1 r\right) = mg\phi\cos\theta_1 + \bar{q}_1 S\begin{bmatrix} C_{y_\beta}\beta + C_{y_p}\frac{pb}{2U_1} + C_{y_r}\frac{rb}{2U_1} + \\ +C_{y_{\delta_a}}\delta_a + C_{y_{\delta_r}}\delta_r \end{bmatrix} \tag{5.4}$$

$$I_{xx}\dot{p} - I_{xz}\dot{r} = \bar{q}_1 Sb\begin{bmatrix} C_{l_\beta}\beta + C_{l_p}\frac{pb}{2U_1} + C_{l_r}\frac{rb}{2U_1} + \\ +C_{l_{\delta_a}}\delta_a + C_{l_{\delta_r}}\delta_r \end{bmatrix} \tag{5.5}$$

$$I_{zz}\dot{r} - I_{xz}\dot{p} = \bar{q}_1 Sb\begin{bmatrix} C_{n_\beta}\beta + C_{n_{T_\beta}}\beta + C_{n_p}\frac{pb}{2U_1} + \\ +C_{n_r}\frac{rb}{2U_1} + C_{n_{\delta_a}}\delta_a + C_{n_{\delta_r}}\delta_r \end{bmatrix} \tag{5.6}$$

where:

m	: mass (airplane)
g	: acceleration of gravity
v	: perturbed side velocity
I_{xx}	: moments of inertia about X-axis
I_{yy}	: moments of inertia about Y-axis
I_{zz}	: moments of inertia about X-axis

It is seen from Equations 5.1-5.6 that the small perturbation equations have been split into three longitudinal and three lateral-directional differential equations of motion. These two sets are independent each other. Therefore, the dynamic stability characteristics of the airplane are discussed into two groups, longitudinal and lateral directional perturbations.

5.1.1 LONGITUDINAL DYNAMIC STABILITY AND RESPONSE

5.1.1.1 EQUATIONS OF MOTION AND TRANSFER FUNCTIONS

For better visibility into the physical characteristics represented by Equations 5.1-5.3 it is customary to divide both sides of Equations 5.1-5.3 by m or I_{yy}, whatever applicable. It is also convenient to assign new symbols to the resulting expressions for aerodynamic and thrust forces and moments. These new symbols are called 'dimensional stability derivatives' and their definitions are given in Table 5.3.

Table 5.3a Longitudinal Dimensional Stability Derivatives

$X_u = -\frac{\bar{q}_1 S\left(C_{D_u} + 2C_{D_1}\right)}{mU_1}$	$Z_{\delta_e} = -\frac{\bar{q}_1 S C_{L_{\delta_e}}}{m}$
$X_{T_u} = \frac{\bar{q}_1 S\left(C_{T_{x_u}} + 2C_{T_{x1}}\right)}{mU_1}$	$M_u = \frac{\bar{q}_1 S \bar{c}\left(C_{m_u} + 2C_{m_1}\right)}{I_{yy}U_1}$
$X_\alpha = -\frac{\bar{q}_1 S\left(C_{D_\alpha} - 2C_{L_1}\right)}{m}$	$M_{T_u} = \frac{\bar{q}_1 S \bar{c}\left(C_{mT_u} + 2C_{mT_1}\right)}{I_{yy}U_1}$
$X_{\delta_e} = -\frac{\bar{q}_1 S C_{D_{\delta_e}}}{m}$	$M_\alpha = \frac{\bar{q}_1 S \bar{c} C_{m_\alpha}}{I_{yy}}$

Table 5.3b Longitudinal Dimensional Stability Derivatives

$$Z_u = -\frac{\bar{q}_1 S\left(C_{L_u} + 2C_{L_1}\right)}{mU_1} \qquad M_{T_\alpha} = \frac{\bar{q}_1 S \bar{c} C_{m_{T_\alpha}}}{I_{yy}}$$

$$Z_\alpha = -\frac{\bar{q}_1 S\left(C_{L_\alpha} + 2C_{D_1}\right)}{m} \qquad M_{\dot{\alpha}} = \frac{\bar{q}_1 S \bar{c}^2 C_{m_{\dot{\alpha}}}}{2I_{yy}U_1}$$

$$Z_{\dot{\alpha}} = -\frac{\bar{q}_1 S C_{L_{\dot{\alpha}}} \bar{c}}{2mU_1} \qquad M_q = \frac{\bar{q}_1 S \bar{c}^2 C_{m_q}}{2I_{yy}U_1}$$

$$Z_q = -\frac{\bar{q}_1 S C_{L_q} \bar{c}}{2mU_1} \qquad M_{\delta_e} = \frac{\bar{q}_1 S \bar{c} C_{m_{\delta_e}}}{I_{yy}}$$

The resulting Equations 5.7-5.9 are shown in Table 5.4. They have the virtue of being algebraically simple as they contain nothing but accelerations, linear or angular. To solve Equations 5.7-5.9 the one-sided Laplace Transform for zero initial conditions is applied and the result rearranged to form Equations 5.10-5.12. Then these equations rewrote in the matrix format (Equation 5.13).

Observe that the column matrix of variables has been written in terms of the ratio of the Laplace Transform of the particular motion variable to the Laplace Transform of the elevator input. These ratios $\frac{u(s)}{\delta_e(s)}$, $\frac{\alpha(s)}{\delta_e(s)}$, and $\frac{\theta(s)}{\delta_e(s)}$ are called the longitudinal airplane transfer functions. It is possible to solve Equations 5.13 for these transfer functions by standard methods of linear algebra. The resulting explicit formulas for $\frac{u(s)}{\delta_e(s)}$, $\frac{\alpha(s)}{\delta_e(s)}$, and $\frac{\theta(s)}{\delta_e(s)}$ are shown in Equations 5.14, 5.17, and 5.19.

Table 5.4 Development of the longitudinal small perturbation equations of motion in dimensional derivatives and matrix format.

$$\dot{u} = -g\theta\cos\theta_1 + X_u + X_{T_u} + X_\alpha\alpha + X_{\delta_e}\delta_e \tag{5.7}$$

$$\dot{w} - U_1 q = -g\theta\sin\theta_1 + Z_u + Z_\alpha\alpha + Z_{\dot{\alpha}}\dot{\alpha} + Z_q q + Z_{\delta_e}\delta_e \tag{5.8}$$

$$\dot{q} = M_u u + M_{T_u} u + M_\alpha\alpha + M_{T_\alpha}\alpha + M_{\dot{\alpha}}\dot{\alpha} + M_q q + M_{\delta_e}\delta_e \tag{5.9}$$

$$\left(s - X_u - X_{T_u}\right)u(s) \quad - X_\alpha\alpha(s) \quad + g\cos\theta_1\theta(s) \quad = X_{\delta_e}\delta_e(s) \tag{5.10}$$

$$-Z_u u(s) \quad + \left[s\left(U_1 - Z_{\dot{\alpha}}\right) - Z_\alpha\right]\alpha(s) \quad + \left[-\left(Z_q + U_1\right)s + g\sin\theta_1\right]\theta(s) \quad = Z_{\delta_e}\delta_e(s) \tag{5.11}$$

$$-\left(M_u + M_{T_u}\right)u(s) \quad - \left(M_{\dot{\alpha}}s + M_\alpha + M_{T_\alpha}\right)\alpha(s) \quad + \left(s^2 - M_q s\right)\theta(s) \quad = M_{\delta_e}\delta_e(s) \tag{5.12}$$

$$\begin{bmatrix} \left(s - X_u - X_{T_u}\right) & -X_\alpha & g\cos\theta_1 \\ -Z_u & \left[s\left(U_1 - Z_{\dot{\alpha}}\right) - Z_\alpha\right] & \left[-\left(Z_q + U_1\right)s + g\sin\theta_1\right] \\ -\left(M_u + M_{T_u}\right) & -\left(M_{\dot{\alpha}}s + M_\alpha + M_{T_\alpha}\right) & \left(s^2 - M_q s\right) \end{bmatrix} \begin{bmatrix} \frac{u(s)}{\delta_e(s)} \\ \frac{\alpha(s)}{\delta_e(s)} \\ \frac{\theta(s)}{\delta_e(s)} \end{bmatrix} = \begin{bmatrix} X_{\delta_e} \\ Z_{\delta_e} \\ M_{\delta_e} \end{bmatrix} \tag{5.13}$$

The Transfer Function For $\frac{u(s)}{\delta_e(s)}$:

$$\frac{u(s)}{\delta_e(s)} = \frac{\begin{vmatrix} X_{\delta_e} & -X_\alpha & g\cos\theta_1 \\ Z_{\delta_e} & \left[s\left(U_1 - Z_{\dot{\alpha}}\right) - Z_\alpha\right] & \left[-\left(Z_q + U_1\right)s + g\sin\theta_1\right] \\ M_{\delta_e} & -\left(M_{\dot{\alpha}}s + M_\alpha + M_{T_\alpha}\right) & \left(s^2 - M_q s\right) \end{vmatrix}}{\begin{vmatrix} \left(s - X_u - X_{T_u}\right) & -X_\alpha & g\cos\theta_1 \\ -Z_u & \left[s\left(U_1 - Z_{\dot{\alpha}}\right) - Z_\alpha\right] & \left[-\left(Z_q + U_1\right)s + g\sin\theta_1\right] \\ -\left(M_u + M_{T_u}\right) & -\left(M_{\dot{\alpha}}s + M_\alpha + M_{T_\alpha}\right) & \left(s^2 - M_q s\right) \end{vmatrix}} = \frac{N_u}{D_1} \quad (5.14)$$

with:

$$D_1 = As^4 + Bs^3 + Cs^2 + Ds + E \quad (5.15)$$

$$N_u = A_u s^3 + B_u s^2 + C_u s + D_u \quad (5.16)$$

where:

$$A = U_1 - Z_{\dot{\alpha}}$$

$$B = -\left(U_1 - Z_{\dot{\alpha}}\right)\left(X_u + X_{T_u} + M_q\right) - Z_\alpha - M_{\dot{\alpha}}\left(U_1 + Z_q\right)$$

$$C = \left(X_u + X_{T_u}\right)\left[\begin{array}{l} M_q\left(U_1 - Z_{\dot{\alpha}}\right) + Z_\alpha + M_{\dot{\alpha}}\left(U_1 - Z_q\right) + \\ + M_q Z_\alpha - Z_u X_\alpha + M_{\dot{\alpha}} g\sin\theta_1 - \\ -\left(M_\alpha + M_{T_\alpha}\right)\left(U_1 - Z_q\right) \end{array}\right]$$

$$D = \left\{ \begin{array}{l} g\sin\theta_1\left[M_\alpha + M_{T_\alpha} - M_{\dot{\alpha}}\left(X_u + X_{T_u}\right)\right] + \\ +g\cos\theta_1\left[Z_u M_{\dot{\alpha}} + \left(M_u + M_{T_u}\right)\left(U_1 - Z_{\dot{\alpha}}\right)\right] + \\ +\left(M_u + M_{T_u}\right)\left[-X_\alpha\left(U_1 + Z_q\right)\right] + Z_u X_\alpha M_q + \\ +\left(X_u + X_{T_u}\right)\left[\left(M_\alpha + M_{T_\alpha}\right)\left(U_1 + Z_q\right) - M_q Z_\alpha\right] \end{array} \right\}$$

$$E = \left\{ \begin{array}{l} g\cos\theta_1\left[\left(M_\alpha + M_{T_\alpha}\right)Z_u - Z_\alpha\left(M_u + M_{T_u}\right)\right] + \\ +g\sin\theta_1\left[\left(M_u + M_{T_u}\right)X_\alpha - \left(X_u + X_{T_u}\right)\left(M_\alpha + M_{T_\alpha}\right)\right] \end{array} \right\}$$

$$A_u = X_{\delta_e}\left(U_1 - Z_{\dot{\alpha}}\right)$$

$$B_u = -X_{\delta_e}\left[\left(U_1 - Z_{\dot{\alpha}}\right)M_q + Z_\alpha + M_{\dot{\alpha}}\left(U_1 + Z_q\right)\right] + Z_{\delta_e} X_\alpha$$

$$C_u = \left\{ \begin{array}{l} X_{\delta_e}\left[M_q Z_\alpha - \left(M_\alpha + M_{T_\alpha}\right)\left(U_1 - Z_q\right)\right] + \\ +Z_{\delta_e}\left[-M_{\dot{\alpha}} g\sin\theta_1 - X_\alpha M_q\right] + \\ +M_{\delta_e}\left[X_\alpha\left(U_1 + Z_q\right) - \left(U_1 + Z_{\dot{\alpha}}\right)g\cos\theta_1\right] \end{array} \right\}$$

$$D_u = \left\{ \begin{array}{l} X_{\delta_e}\left(M_\alpha + M_{T_\alpha}\right)g\sin\theta_1 - Z_{\delta_e} M_\alpha g\cos\theta_1 + \\ +M_{\delta_e}\left(Z_\alpha g\cos\theta_1 - X_\alpha g\sin\theta_1\right) \end{array} \right\}$$

The Transfer Function For $\frac{\alpha(s)}{\delta_e(s)}$:

$$\frac{\alpha(s)}{\delta_e(s)} = \frac{\begin{vmatrix} \left(s - X_u - X_{T_u}\right) & X_{\delta_e} & g\cos\theta_1 \\ -Z_u & Z_{\delta_e} & \left[-\left(Z_q + U_1\right)s + g\sin\theta_1\right] \\ -\left(M_u + M_{T_u}\right) & M_{\delta_e} & \left(s^2 - M_q s\right) \end{vmatrix}}{D_1} = \frac{N_\alpha}{D_1} \quad (5.17)$$

with:

$$N_\alpha = A_\alpha s^3 + B_\alpha s^2 + C_\alpha s + D_\alpha \qquad (5.18)$$

where:

$$A_\alpha = Z_{\delta_e}$$

$$B_\alpha = X_{\delta_e} Z_u + Z_{\delta_e}\left[-M_q - \left(X_u + X_{T_u}\right)\right] + M_{\delta_e}\left(U_1 + Z_q\right)$$

$$C_u = \left\{\begin{array}{l} X_{\delta_e}\left[\left(U_1 - Z_q\right)\left(M_u + M_{T_u}\right) - M_q Z_u\right] + \\ +Z_{\delta_e} M_q\left(X_u + X_{T_u}\right) + \\ +M_{\delta_e}\left[-g\sin\theta_1 - \left(U_1 + Z_q\right)\left(X_u + X_{T_u}\right)\right] \end{array}\right\}$$

$$D_u = \left\{\begin{array}{l} -X_{\delta_e}\left(M_u + M_{T_u}\right) g\sin\theta_1 + Z_{\delta_e}\left(M_u + M_{T_u}\right) g\cos\theta_1 + \\ +M_{\delta_e}\left[\left(X_u + X_{T_u}\right) g\sin\theta_1 - Z_u g\cos\theta_1\right] \end{array}\right\}$$

The Transfer Function For $\frac{\theta(s)}{\delta_e(s)}$:

$$\frac{\theta(s)}{\delta_e(s)} = \frac{\begin{vmatrix} \left(s - X_u - X_{T_u}\right) & -X_\alpha & X_{\delta_e} \\ -Z_u & \left[s\left(U_1 - Z_{\dot{\alpha}}\right) - Z_\alpha\right] & Z_{\delta_e} \\ -\left(M_u + M_{T_u}\right) & -\left(M_{\dot{\alpha}} s + M_\alpha + M_{T_\alpha}\right) & M_{\delta_e} \end{vmatrix}}{D_1} = \frac{N_\theta}{D_1} \qquad (5.19)$$

with:

$$N_\theta = A_\theta s^2 + B_\theta s + C_\theta \qquad (5.20)$$

where:

$$A_\theta = Z_{\delta_e} M_{\dot{\alpha}} + M_{\delta_e}\left(U_1 - Z_{\dot{\alpha}}\right)$$

$$B_\theta = \left\{ \begin{array}{l} X_{\delta_e}\left[Z_u M_{\dot{\alpha}} + \left(U_1 - Z_{\dot{\alpha}} \right)\left(M_u + M_{T_u} \right) \right] + \\ + Z_{\delta_e}\left[\left(M_\alpha + M_{T_\alpha} \right) - M_{\dot{\alpha}}\left(X_u + X_{T_u} \right) \right] + \\ + M_{\delta_e}\left[-Z_\alpha - \left(U_1 - Z_{\dot{\alpha}} \right)\left(X_u + X_{T_u} \right) \right] \end{array} \right\}$$

$$C_\theta = \left\{ \begin{array}{l} X_{\delta_e}\left[\left(M_\alpha + M_{T_\alpha} \right) Z_u - Z_\alpha \left(M_u + M_{T_u} \right) \right] + \\ + Z_{\delta_e}\left[\left(M_\alpha + M_{T_\alpha} \right)\left(X_u + X_{T_u} \right) + X_\alpha \left(M_u + X_{T_u} \right) \right] + \\ + M_{\delta_e}\left[Z_\alpha \left(X_u + X_{T_u} \right) - X_\alpha Z_u \right] \end{array} \right\}$$

It was seen in Equations 5.14, 5.17, and 5.19 that the longitudinal transfer functions all have the same denominator polynomial in s:

$$D_1 = As^4 + Bs^3 + Cs^2 + Ds + E \qquad (5.21)$$

The stability behavior of the airplane depends entirely on the roots of the characteristic equation:

$$As^4 + Bs^3 + Cs^2 + Ds + E = 0 \qquad (5.22)$$

The longitudinal stability is determined by the characteristic equation. This equation is set to zero, and the roots are used to determine the longitudinal stability characteristics of the airplane. For an airplane with 2 complex pairs of roots, they are cast in the form:

$$\begin{aligned} \lambda_{1,2} &= n_{1,2} + jw_{1,2} \\ \lambda_{3,4} &= n_{3,4} + jw_{3,4} \end{aligned} \qquad (5.23)$$

where:

λ : root of a characteristic equation

The complex pair of roots with the highest frequency is referred to as the short period mode, and the lower frequency pair as the phugoid mode.

For airplanes with one pair of complex roots and 2 real roots, a mode called the 'third' oscillation results from placing the complex pair in the same form as the short period and phugoid. The real roots are cast into time constants, which are defined as follows:

$$\lambda_{1,2} = n_{1,2} + jw_{1,2}$$

$$\lambda_3,\ \lambda_4 \qquad (5.24)$$

For airplanes with 4 real roots, all are formed into time constants.

Only one of the three possible combinations will result in the output: 2 complex pairs, 1 complex pair and 2 time constants, or 4 time constants. The other output variables are left undefined.

Finally the inverses can be computed with the aid of Laplace Transform Tables. It is possible to show that the general form of this response can be written as:

$$u(t) = K_{u_0} + K_{u_1} e^{\lambda_1 t} + K_{u_2} e^{\lambda_2 t} + K_{u_3} e^{\lambda_3 t} + K_{u_4} e^{\lambda_4 t} \qquad (5.25)$$

$$\alpha(t) = K_{\alpha_0} + K_{\alpha_1} e^{\lambda_1 t} + K_{\alpha_2} e^{\lambda_2 t} + K_{\alpha_3} e^{\lambda_3 t} + K_{\alpha_4} e^{\lambda_4 t} \qquad (5.26)$$

$$\theta(t) = K_{\theta_0} + K_{\theta_1} e^{\lambda_1 t} + K_{\theta_2} e^{\lambda_2 t} + K_{\theta_3} e^{\lambda_3 t} + K_{\theta_4} e^{\lambda_4 t} \qquad (5.27)$$

The constants K_{u_i}, K_{α_i}, and K_{θ_i} (i = 0, 1, 2, 3, 4) depend on the numerator and denominator constants of Equations 5.15, 5.16, 5.18, and 5.20. The exponential terms λ_i are, the roots of the characteristics Equation 5.22.

5.1.1.2 LONGITUDINAL FLYING QUALITIES

The longitudinal characteristic equation has four roots, usually consisting of two pairs of complex roots which represent the following modes:

- Short period : Highly damped, high frequency oscillation.
- Phugoid : Slowly damped, low frequency oscillation.

The Flying Quality Levels are calculated from these complex roots. The short period frequency can be plotted against the flying quality requirements. The flying quality levels (Appendix A) are determined for each Flight Phase Category.

The Military Specification-Flying Qualities of Piloted Airplanes, MIL-F-8785C[4], requires the equivalent short period undamped natural frequency of the short period mode to be within the following limits for the three Flight Phase Categories. Common

design practice is to adopt the military requirements because the Federal Aviation Regulation (FAR) requirements do not set specific limits on the undamped natural frequency.

The short period undamped natural frequency and the steady state normal acceleration per unit of angle of attack are used to determine the flight phase level (Appendix E), based on the following requirements:

- Flight Phase Category A Requirements
- Flight Phase Category B Requirements
- Flight Phase Category C Requirements

Short Period Frequency and Damping

It is considered good design practice to use the following military requirements for civilian airplanes. The FAR requirements only require the short period oscillation to be heavily damped. The equivalent short period damping ratio must be within the limits presented in the Table 5.5.

Table 5.5 The limits of the short period damping ratio

Flying Quality	Category A and Category C		Category B	
	$\xi_{SP_{min}}$	$\xi_{SP_{max}}$	$\xi_{SP_{min}}$	$\xi_{SP_{max}}$
Level 1	0.35	1.30	0.30	2.00
Level 2	0.25	2.00	0.20	2.00
Level 3	0.15	----	0.15	----

where:

ξ : damping ratio

Phugoid

The long-period air-speed oscillations (phugoid) which occur when an airplane seeks a stabilized air-speed following a disturbance must meet the following requirements:

Table 5.6 Phugoid Damping Requirements

Flying Quality	MIL-F-8785C Requirement	FAR 23 and FAR 25 Requirement
Level 1	$\xi_{P_{long}} \geq 0.04$	No requirement
Level 2	$\xi_{P_{long}} \geq 0.00$	No requirement
Level 3	$\xi_{P_{long}} \leq \frac{-\ln(2)}{55\omega_{n_{P_{long}}}}$ *or* $T_{2_{P_{long}}} \geq 55\text{sec}$	No requirement

where:

T_2 : time to double amplitude

w_n : undamped natural frequency

5.1.2 LATERAL-DIRECTIONAL DYNAMIC STABILITY AND RESPONSE

5.1.2.1 EQUATIONS OF MOTION AND TRANSFER FUNCTIONS

The complete lateral-directional, small perturbation equations of motions are assembled as Equations 5.4, 5.5, and 5.6 in Table 5.2. For better visibility into the physical characteristics it is customary to divide both sides of equations by m, I_{xx}, and I_{zz} respectively. At the same time it is convenient to assign new symbols to the resulting expressions for aerodynamic and thrust forces and moments. These new symbols are again called 'dimensional stability derivatives' and their definitions are given in Table 5.7.

The resulting Equations 5.28-5.30 are simple algebraically and contain nothing but accelerations, linear or angular. To solve Equations 5.28-5.30 the one-sided Laplace Transform for zero initial conditions is applied and the result rearranged to form Equations 5.31-5.33. Then these equations rewrote in the matrix format (Equation 5.34).

Table 5.7 Lateral-Directional Dimensional Stability Derivatives

$$Y_\beta = \frac{\bar{q}_1 S C_{y_\beta}}{m}$$

$$Y_p = \frac{\bar{q}_1 S b C_{y_p}}{2mU_1}$$

$$Y_r = \frac{\bar{q}_1 S b C_{y_r}}{2mU_1}$$

$$Y_{\delta_a} = \frac{\bar{q}_1 S C_{y_{\delta_a}}}{m}$$

$$Y_{\delta_r} = \frac{\bar{q}_1 S C_{y_{\delta_r}}}{m}$$

$$L_\beta = \frac{\bar{q}_1 S b C_{l_\beta}}{I_{xx}}$$

$$L_p = \frac{\bar{q}_1 S b^2 C_{l_p}}{2I_{xx}U_1}$$

$$L_r = \frac{\bar{q}_1 S b^2 C_{l_r}}{2I_{xx}U_1}$$

$$L_{\delta_a} = \frac{\bar{q}_1 S b C_{l_{\delta_a}}}{I_{xx}}$$

$$L_{\delta_r} = \frac{\bar{q}_1 S b C_{l_{\delta_r}}}{I_{xx}}$$

$$N_\beta = \frac{\bar{q}_1 S b C_{n_\beta}}{I_{zz}}$$

$$N_{T\beta} = \frac{\bar{q}_1 S b C_{n_{T\beta}}}{I_{zz}}$$

$$N_p = \frac{\bar{q}_1 S b^2 C_{n_p}}{2I_{zz}U_1}$$

$$N_r = \frac{\bar{q}_1 S b^2 C_{n_r}}{2I_{zz}U_1}$$

$$N_{\delta_a} = \frac{\bar{q}_1 S b C_{n_{\delta_a}}}{I_{zz}}$$

$$N_{\delta_r} = \frac{\bar{q}_1 S b C_{n_{\delta_r}}}{I_{zz}}$$

Table 5.8 Development of the lateral-directional small perturbation equations of motion in dimensional derivatives and matrix format.

$$\dot{v} + U_1 r = g\phi\cos\theta_1 + Y_\beta\beta + Y_r r + Y_{\delta_a}\delta_a + Y_{\delta_r}\delta_r \tag{5.28}$$

$$\dot{p} - A_1\dot{r} = L_\beta\beta + L_p p + L_r r + L_{\delta_a}\delta_a + L_{\delta_r}\delta_r \tag{5.29}$$

$$\dot{r} - B_1\dot{p} = N_\beta\beta + N_{T_\alpha}\alpha + N_p p + N_r r + N_{\delta_a}\delta_a + N_{\delta_r}\delta_r \tag{5.30}$$

$$(sU_1 - Y_\beta)\beta(s) \quad -(sY_p + g\cos\theta_1)\phi(s) \quad +s(U_1 Y_r)\psi(s) = Y_\delta\delta(s) \tag{5.31}$$

$$-L_\beta\beta(s) \quad +(s^2 - L_p s)\phi(s) \quad -(s^2 A_1 + sL_r)\psi(s) = Y_\delta\delta(s) \tag{5.32}$$

$$-(N_\beta + N_{T_\beta})\beta(s) \quad -(s^2 B_1 + N_p s)\phi(s) \quad +(s^2 - N_r s)\psi(s) = N_\delta\delta(s) \tag{5.33}$$

$$\begin{bmatrix} (sU_1 - Y_\beta) & -(sY_p + g\cos\theta_1) & +s(U_1 Y_r) \\ -L_\beta & +(s^2 - L_p s) & -(s^2 A_1 + sL_r) \\ -(N_\beta + N_{T_\beta}) & -(s^2 B_1 + N_p s) & +(s^2 - N_r s) \end{bmatrix} \begin{bmatrix} \frac{\beta(s)}{\delta(s)} \\ \frac{\phi(s)}{\delta(s)} \\ \frac{\psi(s)}{\delta(s)} \end{bmatrix} = \begin{bmatrix} Y_\delta \\ L_\delta \\ N_\delta \end{bmatrix} \tag{5.34}$$

Note: $\delta = \delta_a$ for aileron response calculations
$\delta = \delta_r$ for rudder response calculations

with:

$$A_1 = \frac{I_{xz}}{I_{xx}}$$

$$B_1 = \frac{I_{xz}}{I_{zz}}$$

where:

I_{xz} : products of inertia in XZ system

Notice that the column matrix of variables has been written in terms of the ratio of the Laplace Transform of the particular motion variable to the Laplace Transform of the elevator input. The ratios $\frac{\beta(s)}{\delta(s)}$, $\frac{\phi(s)}{\delta(s)}$, and $\frac{\psi(s)}{\delta(s)}$ are called the lateral-directional airplane transfer functions. If the response due to aileron is to be studied, then $\delta = \delta_a$. If the response due to rudder is to be studied, $\delta = \delta_r$. Explicit formulas for the lateral-directional transfer functions $\frac{\beta(s)}{\delta(s)}$, $\frac{\phi(s)}{\delta(s)}$, and $\frac{\psi(s)}{\delta(s)}$ are shown in Equations 5.35, 5.38, and 5.40.

where:

ϕ : perturbed bank (roll) angle

ψ : perturbed heading angle

The Transfer Function For $\frac{\beta(s)}{\delta(s)}$:

$$\frac{\beta(s)}{\delta(s)} = \frac{\begin{vmatrix} Y_\delta & -(sY_p + g\cos\theta_1) & +s(U_1 Y_r) \\ L_\delta & +(s^2 - L_p s) & -(s^2 A_1 + sL_r) \\ N_\delta & -(s^2 B_1 + N_p s) & +(s^2 - N_r s) \end{vmatrix}}{\begin{vmatrix} (sU_1 - Y_\beta) & -(sY_p + g\cos\theta_1) & +s(U_1 Y_r) \\ -L_\beta & +(s^2 - L_p s) & -(s^2 A_1 + sL_r) \\ -(N_\beta + N_{T_\beta}) & -(s^2 B_1 + N_p s) & +(s^2 - N_r s) \end{vmatrix}} = \frac{N_\beta}{D_2} \quad (5.35)$$

with:

$$D_2 = s(As^4 + Bs^3 + Cs^2 + Ds + E) \quad (5.36)$$

$$N_\beta = s(A_\beta s^3 + B_\beta s^2 + C_\beta s + D_\beta) \quad (5.37)$$

where:

$$A = U_1(1 - A_1 B_1)$$

$$B = -Y_\beta(1 - A_1 B_1) - U_1(L_p + N_r + A_1 N_p + B_1 L_r)$$

$$C = \begin{Bmatrix} U_1\left(L_p N_r - L_r N_p\right) + Y_\beta\left(N_r + L_p + A_1 N_p + B_1 L_r\right) - \\ -Y_p\left(L_\beta + N_\beta A_1 + N_{T_\beta} A_1\right) + U_1\left(L_\beta B_1 + N_\beta + N_{T_\beta}\right) - \\ -Y_r\left(L_\beta B_1 + N_\beta + N_{T_\beta}\right) \end{Bmatrix}$$

$$D = \begin{Bmatrix} -Y_\beta\left(L_p N_r - L_r N_p\right) + Y_p\left(L_\beta N_r - N_\beta L_r - N_{T_\beta} L_r\right) - \\ -g\cos\theta_1\left(L_\beta + N_\beta A_1 + N_{T_\beta} A_1\right) + \\ +U_1\left(L_\beta N_p - N_\beta L_p - N_{T_\beta} L_p\right) - \\ -Y_r\left(L_\beta N_p - N_\beta L_p - N_{T_\beta} L_p\right) \end{Bmatrix}$$

$$E = g\cos\theta_1\left(L_\beta N_r - N_\beta L_r - N_{T_\beta} L_r\right)$$

$$A_\beta = Y_\delta\left(1 - A_1 B_1\right)$$

$$B_\beta = \begin{Bmatrix} -Y_\delta\left(L_p + N_r + A_1 N_p + B_1 L_r\right) - Y_p\left(L_\delta + N_\delta A_1\right) + \\ +Y_r\left(L_\delta B_1 + N_\delta\right) - U_1\left(L_\delta B_1 + N_\delta\right) \end{Bmatrix}$$

$$C_\beta = \begin{Bmatrix} Y_\delta\left(L_p N_r - L_r N_p\right) + Y_p\left(N_\delta L_r - L_\delta N_r\right) + \\ +g\cos\theta\left(L_\delta + N_\delta A_1\right) + Y_r\left(L_\delta N_p - L_p N_\delta\right) + \\ +U_1\left(L_\delta N_p - L_p N_\delta\right) \end{Bmatrix}$$

$$D_\beta = g\cos\theta_1\left(N_\delta L_r - L_\delta N_r\right)$$

The Transfer Function For $\frac{\phi(s)}{\delta(s)}$:

$$\frac{\phi(s)}{\delta(s)} = \frac{\begin{vmatrix} \left(sU_1 - Y_\beta\right) & Y_\delta & +s\left(U_1 Y_r\right) \\ -L_\beta & L_\delta & -\left(s^2 A_1 + sL_r\right) \\ -\left(N_\beta + N_{T_\beta}\right) & N_\delta & +\left(s^2 - N_r s\right) \end{vmatrix}}{D_2} = \frac{N_\phi}{D_2} \quad (5.38)$$

with:

$$N_\phi = s(A_\phi s^2 + B_\phi s + C_\phi) \tag{5.39}$$

where:

$$A_\phi = U_1\left(L_\delta + N_\delta A_1\right)$$

$$B_\phi = \left\{\begin{matrix} U_1\left(N_\delta L_r - L_\delta N_r\right) - Y_\beta\left(L_\delta + N_\delta A_1\right) + \\ +Y_\delta\left(L_\beta + N_\beta A_1 + N_{T_\beta} A_1\right) \end{matrix}\right\}$$

$$C_\phi = \left\{\begin{matrix} -Y_\beta\left(N_\delta L_r - L_\delta N_r\right) + Y_\delta\left(L_r N_\beta + L_r N_{T_\beta} - N_r L_\beta\right) + \\ +\left(U_1 - Y_r\right)\left(N_\beta L_\delta + N_{T_\beta} L_\delta - L_\beta N_\delta\right) \end{matrix}\right\}$$

The Transfer Function For $\frac{\psi(s)}{\delta(s)}$:

$$\frac{\psi(s)}{\delta(s)} = \frac{\begin{vmatrix} \left(sU_1 - Y_\beta\right) & -\left(sY_p + g\cos\theta_1\right) & Y_\delta \\ -L_\beta & +\left(s^2 - L_p s\right) & L_\delta \\ -\left(N_\beta + N_{T_\beta}\right) & -\left(s^2 B_1 + N_p s\right) & N_\delta \end{vmatrix}}{D_2} = \frac{N_\psi}{D_2} \tag{5.40}$$

with:

$$N_\psi = A_\psi s^3 + B_\psi s^2 + C_\psi s + D_\psi \tag{5.41}$$

where:

$$A_\psi = U_1\left(N_\delta - L_\delta B_1\right)$$

$$B_\psi = \left\{\begin{matrix} U_1\left(L_\delta - N_\delta L_p\right) - Y_\beta\left(N_\delta + B_1 L_\delta\right) + \\ +Y_\delta\left(L_\beta B_1 + N_\beta + N_{T_\beta}\right) \end{matrix}\right\}$$

$$C_\psi = \left\{\begin{matrix} -Y_\beta\left(L_\delta N_p - L_p N_\delta\right) + Y_p\left(N_\beta L_\delta + N_{T\beta} L_\delta - L_\beta N_\delta\right) + \\ +Y_\delta\left(L_\beta N_p - N_\beta L_p - N_{T_\beta} L_p\right) \end{matrix}\right\}$$

$$D_\psi = g\cos\theta_1\left(N_\beta L_\delta + N_{T_\beta} L_\delta - L_\beta N_\delta\right)$$

As seen in Equations 5.36, 5.39, and 5.41 that the longitudinal transfer functions all have the same denominator polynomial in s:

$$D_l = s(As^4 + Bs^3 + Cs^2 + Ds + E) \tag{5.42}$$

By inspection of Equations 5.35, 5.38, and 5.40, it is seen that the root s = 0 (an indication of neutral stability) is due to the fact that the airplane has no heading stability. If instead of heading angle, ψ, the rate of change of heading angle $\dot{\psi}$ (yaw rate) had been selected as variable in Equations 4.28-30, the free s in Equation 4.40 would not have occurred. For all practical purposes the characteristic equation for the lateral-directional case is thus:

$$As^4 + Bs^3 + Cs^2 + Ds + E = 0 \tag{5.43}$$

This characteristic equation has four roots, and after calculating their numerical values it is possible to determine the stability character of the airplane.

Most airplanes have one pair of complex roots and two real roots. The complex pair of roots is called the dutch-roll mode of the aircraft. The two time constants are the roll time constant and the spiral time constant. The real root closest to the origin (in the s-plane) is called the spiral root, and the other is the roll root.

In an airplane where there are two pairs of complex roots, this second pair is called the lateral phugoid. In the case where there are four real roots, the aircraft is determined to have four time constants, with none being specified as the roll or spiral mode time constant.

Only one of the three possible combinations will result in the output: a dutch-roll mode with a lateral phugoid for 2 pairs of complex roots, a dutch-roll mode with a spiral and roll time constant for 1 complex pair and 2 time constants, or 4 lateral time constants. The other output variables are left undefined.

Finally the inverses can be computed with the aid of Laplace Transform Tables. It is possible to show that the general form of this response can be written as:

$$\beta(t) = K_{\beta_0} + K_{\beta_1} e^{\lambda_1 t} + K_{\beta_2} e^{\lambda_2 t} + K_{\beta_3} e^{\lambda_3 t} + K_{\beta_4} e^{\lambda_4 t} \tag{5.44}$$

$$\phi(t) = K_{\phi_0} + K_{\phi_1} e^{\lambda_1 t} + K_{\phi_2} e^{\lambda_2 t} + K_{\phi_3} e^{\lambda_3 t} + K_{\phi_4} e^{\lambda_4 t} \tag{5.45}$$

$$\psi(t) = K_{\psi_0} + K_{\psi_1} e^{\lambda_1 t} + K_{\psi_2} e^{\lambda_2 t} + K_{\psi_3} e^{\lambda_3 t} + K_{\psi_4} e^{\lambda_4 t} \qquad (5.46)$$

5.1.2.2 LATERAL-DIRECTIONAL FLYING QUALITIES

The lateral-directional characteristic equation has four roots, generally consisting of a pair of complex roots and two real roots which represent the following modes:

- Dutch roll mode: Slowly damped, moderately low frequency oscillation.
- Rolling mode : Highly unstable.
- Spiral mode : Unstable or marginally stable.

Dutch Roll Mode

The minimum Dutch roll frequency and damping characteristics are specified in Table 5.9.

Table 5.9 Minimum Dutch Roll Undamped Natural Frequency and Damping Ratio Requirements

Level	Flight Phase Category	Airplane Class	$Min.\xi_D$ *	$Min.\xi_D\omega_{n_D}$ * (rad/sec)	$Min.\omega_{n_D}$ (rad/sec)
1	A - combat & ground attack	IV	0.4	---	1.0
	A - other	I and IV	0.19	0.35	1.0
		II and III	0.19	0.35	0.4**
	B	All	0.08	0.15	0.4**
	C	I, II-C, and IV	0.08	0.15	1.0
		II-L and III	0.08	0.10	0.4**
2	All	All	0.02	0.05	0.4**
3	All	All	0		0.4**

* : The governing requirements is that which yields the largest damping ratio value.

** : Class III airplanes may be excepted from these requirements

Roll Performance

The airplane roll mode time constant is a measure of rapidity of roll response. A small roll time constant signifies a rapid build up of roll rate following a lateral control input by the pilot.

The roll mode time constant (T_R) shall be no greater than the appropriate value shown in Table 5.10.

Table 5.10 Maximum roll mode time constant requirements

Class	Flight Phase Category	$T_{R_{max}}$ (seconds)		
		Level 1	Level 2	Level 3
I and IV	A	1.0	1.4	10
II and III	A	1.4	3.0	10
All	B	1.4	3.0	10
I, II-C*, IV	C	1.0	1.4	10
II-L*, III	C	1.4	3.0	10

Spiral Mode

The time to double the amplitude in the spiral mode may be calculated from:

$$T_{2_s} = \frac{\ln 2}{\frac{1}{TC_{spiral}}} \qquad (5.47)$$

$TC_{spiral} < 0$ Spiral is not damped. T_{2_s} is the time to double the amplitude in the spiral mode.

$TC_{spiral} > 0$ Spiral is damped. T_{2_s} changes to $T_{1/2_s}$.

where:

$T_{1/2}$: time to half amplitude

Note: There are no specific requirements for spiral stability in any airplane. However, the military requirements place limits on the allowable divergence of the spiral mode.

Following a disturbance in a bank of up to 20 degrees, the time for the bank angle to double is greater than the values shown in the Table 5.11. This requirement shall be met with the airplane trimmed for wings-level, zero-yaw rate flight with the cockpit controls free:

Table 5.11 Spiral mode requirements

Flight Phase Category	T_{2_s} (second)		
	Level 1	Level 2	Level 3
A	12	8	4
B	20	8	4
C	12	8	4

5.2 *CALCULATIONS OF DYNAMIC STABILITY AND RESPONSE CHARACTERISTICS* FOR THE TEST AIRCRAFT

The software AAA was used for all of the calculations. This software is based on the method of Dr. Jan Roskam[1,11]. The results which are obtained with using AAA are presented in Chapter 5.3. Because of obtaining some real design values of the aircraft is impossible, moment of inertia values are obtained from the Figures 5.3, 5.4, and 5.5 of Reference 11.

I_{xx} = 125000 slug-ft^2

I_{yy} = 97000 slug-ft^2

I_{zz} = 250000 slug-ft^2

Using AAA the transfer functions which are in s-domain are obtained. For obtaining dynamic response of the airplane, the software Matlab[15] is used. In Simulink part of this software first the transfer function is defined in s-domain, next input signal is connected to the transfer function, and finally output signal is get in time-domain. An example page is put in Appendix B.

Two different input signals are used. First one is step input (Figure 5.1). Control deflection angle is one degree for one second. Other one is variable input (Figure 5.2). First 0.8 degree

for three seconds, next -1.2 degree for two seconds, then 1.1 degree for one second, and last -1.1 degree for one second.

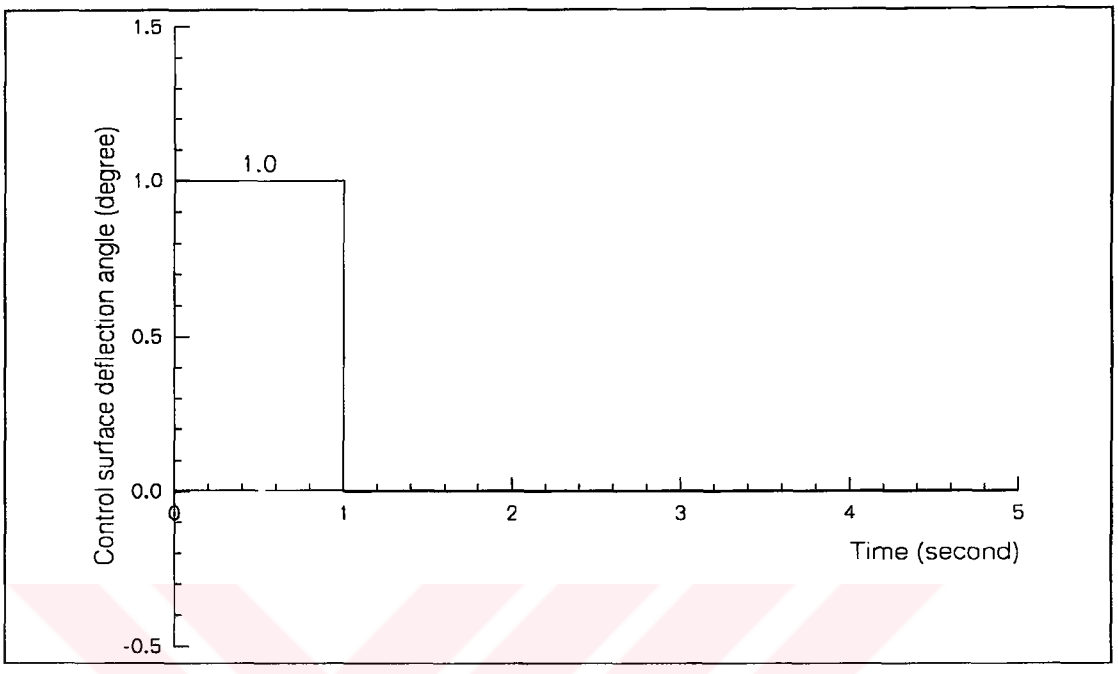

Figure 5.1 Step input for transfer functions

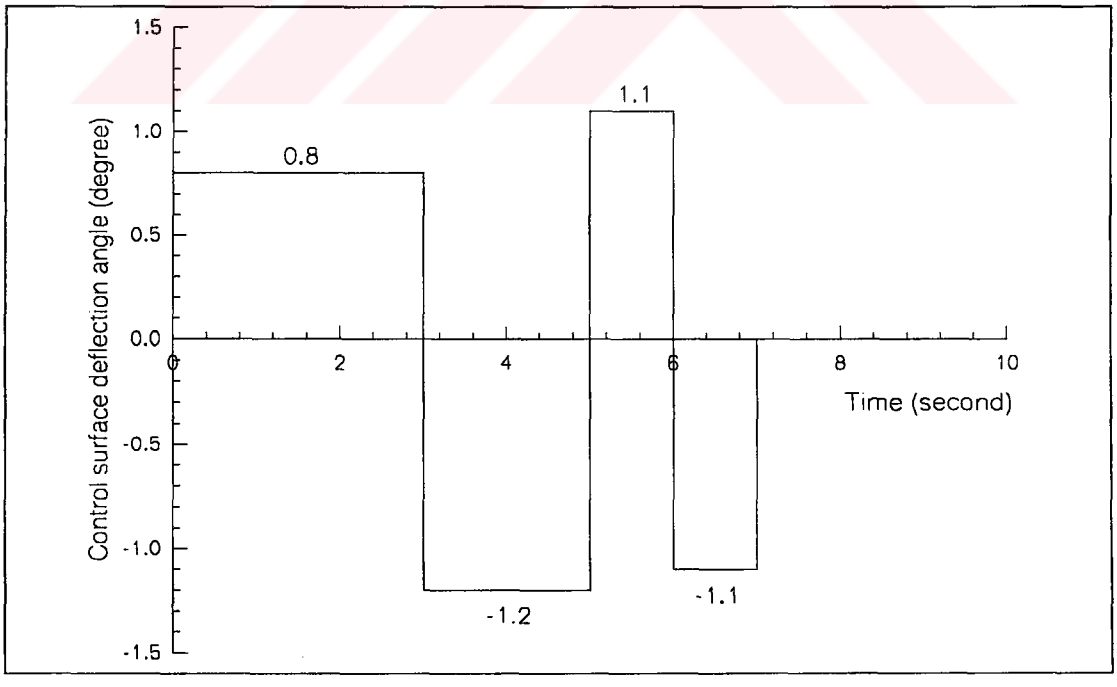

Figure 5.2 Variable input for transfer functions

5.3 RESULTS

5.3.1 RESULTS RELATED TO FLYING QUALITY LEVELS

The results about the flying quality levels are tabulated in Table 5.12. All of the parameters for two different center of gravity locations are inside the Level 1 except time to double the amplitude in the spiral mode, T_{2_s}. It is inside the Level 2.

Table 5.12 Parameters for flying quality levels

	Front cg	Aft cg	Minimum limit	Maximum limit
SP damping frequency, ω_{nSP} (rad/s)	4.5152	3.7493		
SP damping ratio, ξ_{SP}	0.6610	0.7488	Level 1: 0.30 Level 2: 0.20 Level 3: 0.15	Level 1: 2.00 Level 2: 2.00 Level 3: -----
Phugoid damping frequency, ω_{nP} (rad/s)	0.1110	0.1099		
Phugoid damping ratio, ξ_P	0.0674	0.0674	Level 1: 0.04 Level 2: 0.00 Level 3:	
Dutch roll Undamped natural frequency, ω_{nD} (rad/s)	1.1383	0.9889	Level 1: 0.08 Level 2: 0.02 Level 3: 0	
Dutch roll Undamped damping ratio, ξ_D	0.1705	0.1711	Level 1: 0.4 Level 2: 0.4 Level 3: 0.4	
Roll mode time constant, T_R (s)	0.4480	0.4470		Level 1: 1.4 Level 2: 3.0 Level 3: 10
Time to double the amplitude in the spiral mode, T_{2_s} (s)	15.7370	11.3840	Level 1: 20 Level 2: 8 Level 3: 4	

5.3.2 RESULTS FOR DYNAMIC STABILITY AND RESPONSE

Using the software AAA the coefficients of the transfer functions which are given in Chapter 5.2 are obtained and they are presented in the following parts.

5.3.2.1 RESULTS FOR LONGITUDINAL DYNAMIC STABILITY AND RESPONSE

5.3.2.1.1 TRANSFER FUNCTIONS FOR ELEVATOR DEFLECTION

The derivatives $\frac{u(s)}{\delta_e(s)}$, $\frac{\alpha(s)}{\delta_e(s)}$, and $\frac{\theta(s)}{\delta_e(s)}$ are obtained by using the software AAA and presented in Equations 5.48 to 5.53.

Transfer Functions For $\bar{x}_{cg}$ Is At 0.16 $\bar{c}$

$$\frac{u(s)}{\delta_e(s)} = \frac{-582.0585s^3 - 4260.3606s^2 + 87404.4007s + 224476.6065}{415.7551s^4 + 2488.0686s^3 + 8518.4547s^2 + 157.4818s + 104.4982} \quad (5.48)$$

$$\frac{\alpha(s)}{\delta_e(s)} = \frac{-45.7807s^3 - 6589.5383s^2 - 103.7139s - 88.4665}{415.7551s^4 + 2488.0686s^3 + 8518.4547s^2 + 157.4818s + 104.4982} \quad (5.49)$$

$$\frac{\theta u(s)}{\delta_e(s)} = \frac{-6635.3882s^2 - 7186.2411s - 167.9512}{415.7551s^4 + 2488.0686s^3 + 8518.4547s^2 + 157.4818s + 104.4982} \quad (5.50)$$

Transfer Functions For $\bar{x}_{cg}$ Is At 0.30 $\bar{c}$

$$\frac{u(s)}{\delta_e(s)} = \frac{-581.8662s^3 - 4052.7088s^2 + 87204.3634s + 224432.0673}{415.6177s^4 + 2339.7469s^3 + 5881.9977s^2 + 114.6664s + 70.5527} \quad (5.51)$$

$$\frac{\alpha(s)}{\delta_e(s)} = \frac{-45.7807s^3 - 6371.9443s^2 - 100.4067s - 85.3592}{415.6177s^4 + 2339.7469s^3 + 5881.9977s^2 + 114.6664s + 70.5527} \quad (5.52)$$

$$\frac{\theta(s)}{\delta_e(s)} = \frac{-6397.2302s^2 - 7189.6198s - 164.9651}{415.6177s^4 + 2339.7469s^3 + 5881.9977s^2 + 114.6664s + 70.5527} \quad (5.53)$$

5.3.2.1.2 LONGITUDINAL DYNAMIC RESPONSE FOR ELEVATOR DEFLECTION

Using transfer functions and input elevator deflections, Figures 5.3 to 5.8 are obtained.

Positive elevator deflection creates negative pitching moment with creating negative angle of attack and pitch angle. The nose of the aircraft goes down. After only one second, angle of attack reaches its minimum value, around -1.1 degree for aft cg. Then it increases up to its maximum value, 0.04 degree. Finally it begins to decrease and reaches zero after only three seconds.

But damping process for forward velocity and pitch angle takes too much time. First forward velocity begins to increase. While forward velocity increasing, pitch angle reaches the minimum peak value, it is nearly -2 degree for aft cg. After negative peak value, pitch angle increases. When pitch angle crosses zero degree, forward velocity reaches the maximum peak value, 6 m/s for aft cg. Then forward velocity decreases while pitch angle is increasing. When pitch angle reaches the maximum value, it is nearly one degree, forward velocity crosses zero. After that point pitch angle begins to decrease while forward velocity is decreasing. Next pitch angle again crosses zero degree. But this time forward velocity reaches the minimum peak value, it is nearly -5 m/s.

This process continues while pitch angle and forward velocity are damping. Peak values decrease at every cycle. After 750 seconds, they nearly become zero and aircraft reaches the steady state condition.

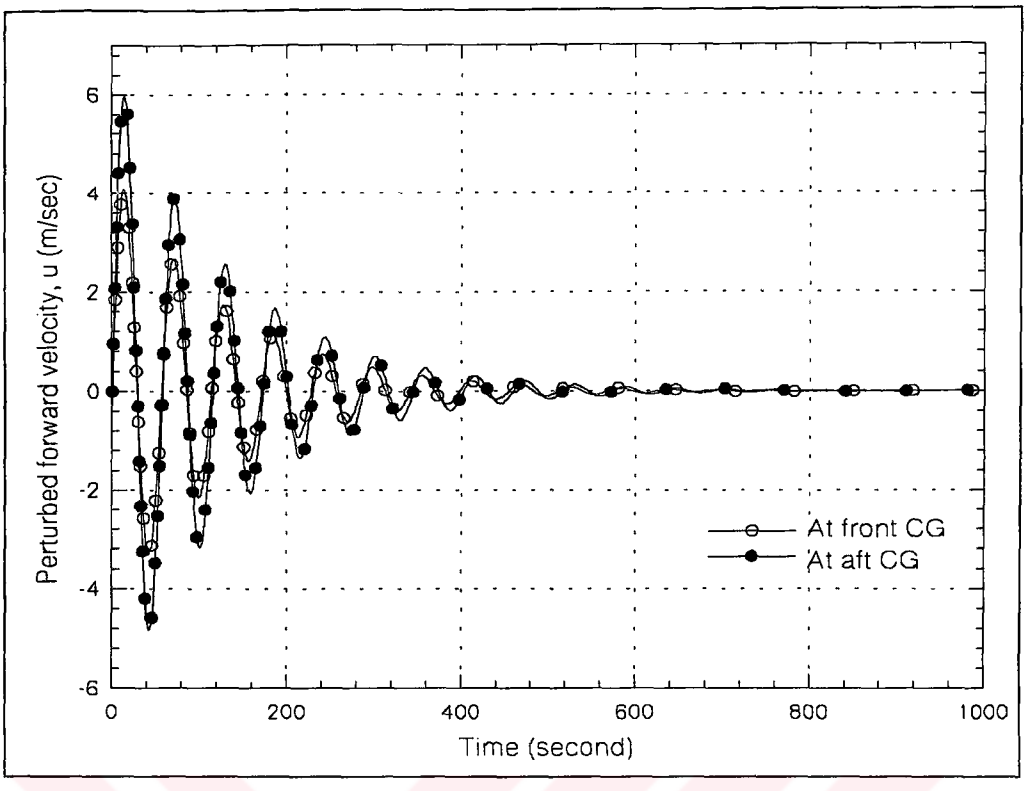

Figure 5.3 Dynamic response of u for step input.

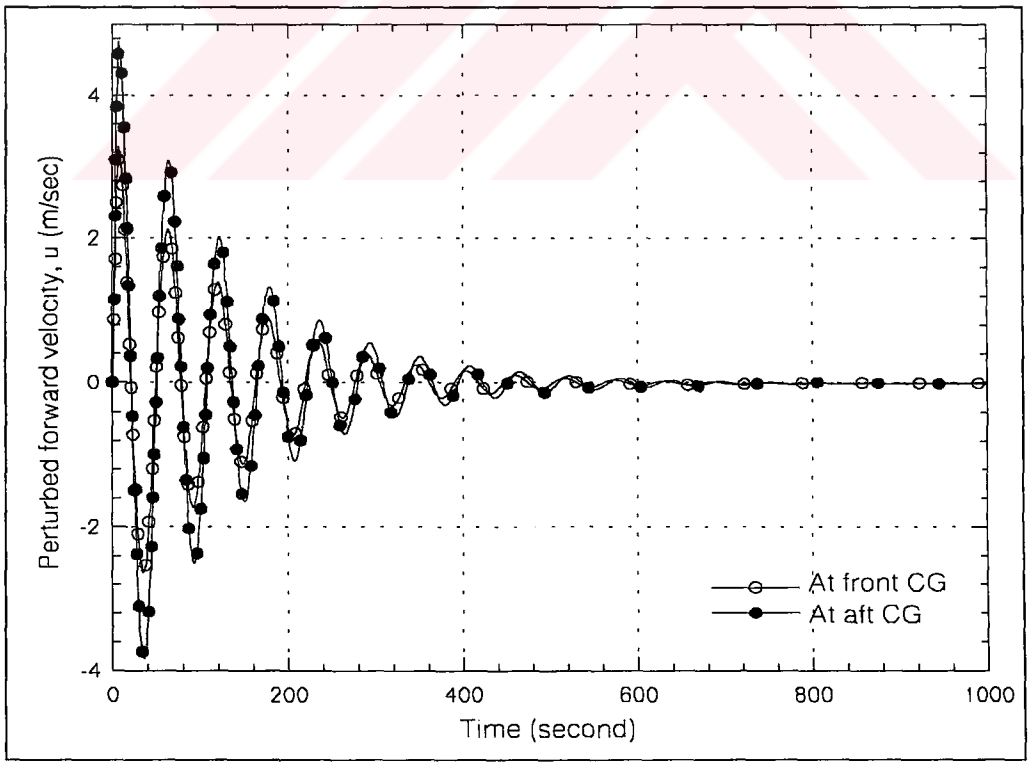

Figure 5.4 Dynamic response of u for variable input.

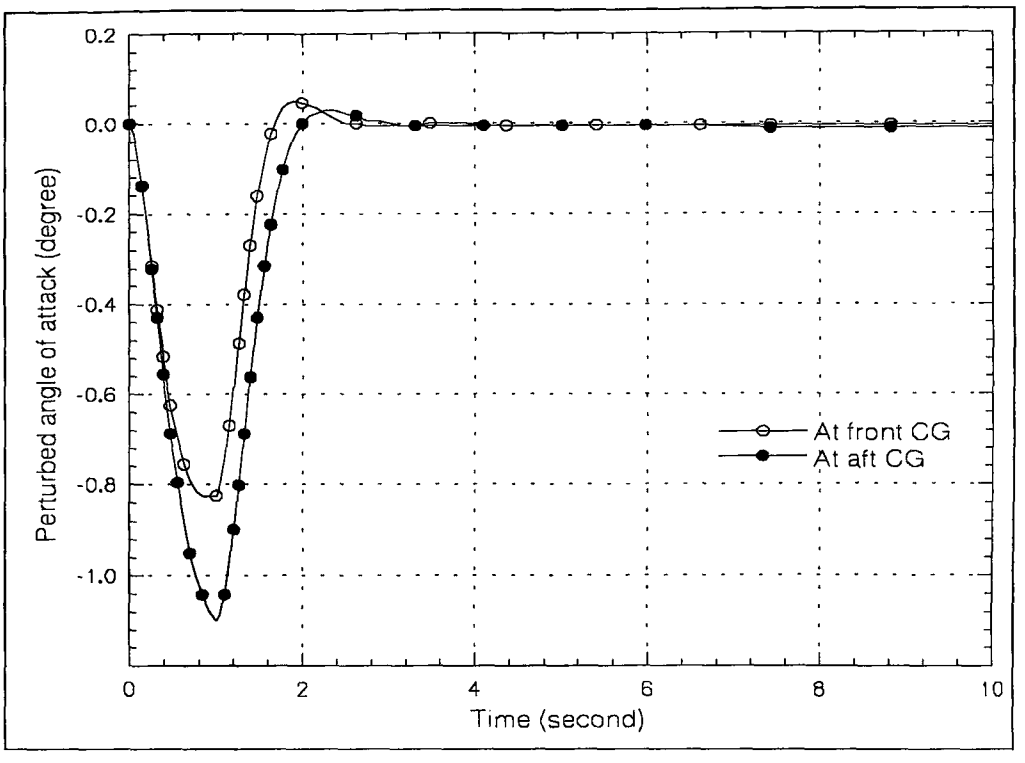

Figure 5.5 Dynamic response of angle of attack for step input.

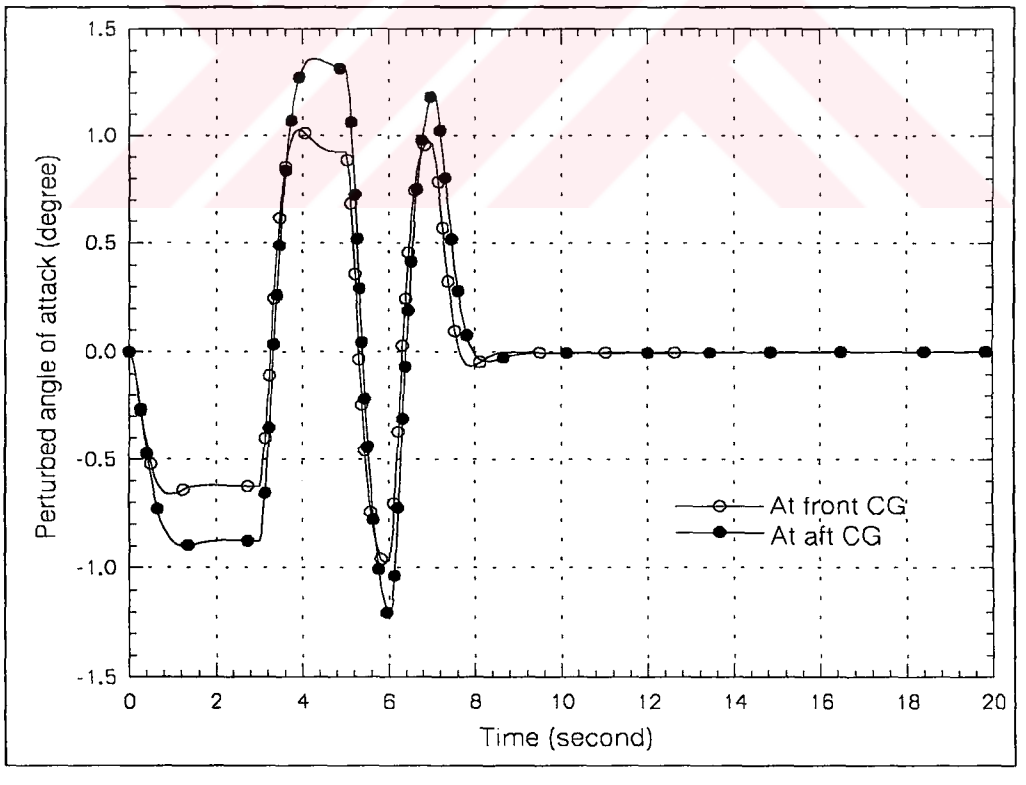

Figure 5.6 Dynamic response of angle of attack for variable input.

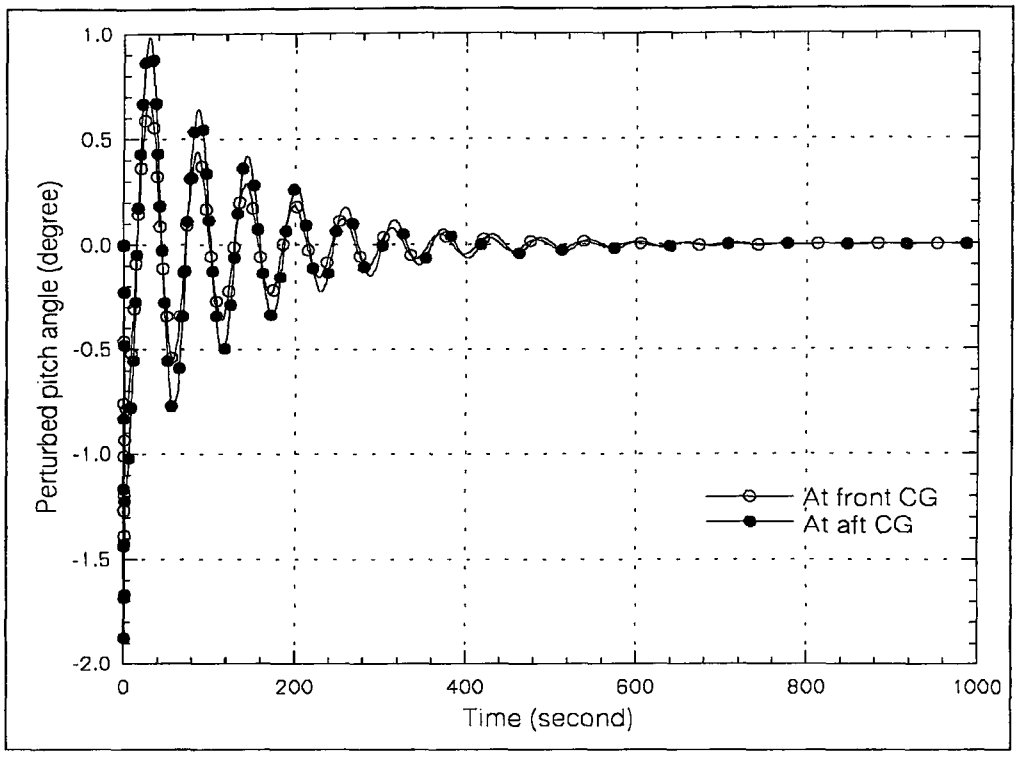

Figure 5.7 Dynamic response of pitch angle for step input.

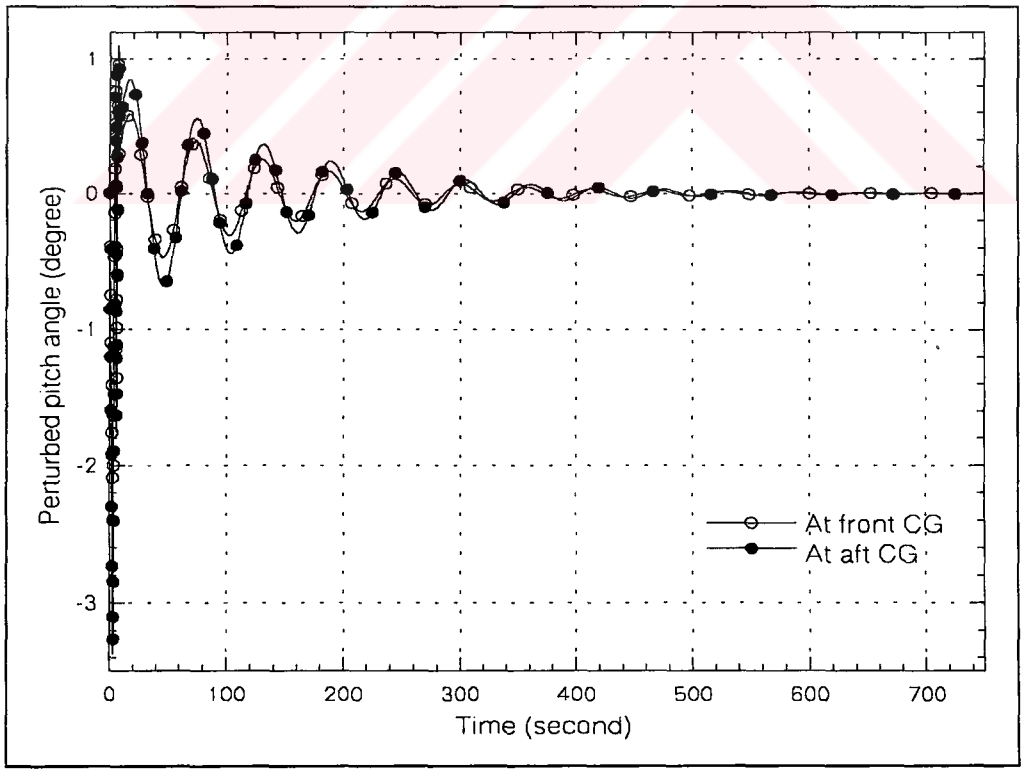

Figure 5.8 Dynamic response of pitch angle for variable input.

5.3.2.2 RESULTS FOR LATERAL-DIRECTIONAL DYNAMIC STABILITY AND RESPONSE

5.3.2.2.1 TRANSFER FUNCTIONS FOR RUDDER DEFLECTION

The derivatives $\frac{\beta(s)}{\delta_r(s)}$, $\frac{\phi(s)}{\delta_r(s)}$, and $\frac{\psi(s)}{\delta_r(s)}$ are obtained by using the software AAA and presented in Equations 5.54 to 5.59.

Transfer Functions For $\bar{x}_{cg}$ Is At 0.16 $\bar{c}$

$$\frac{\beta(s)}{\delta_r(s)} = \frac{21.3144s^4 + 1300.0118s^3 + 2625.1716s^2 - 48.4079s}{411.9165s^5 + 1097.0554s^4 + 938.9465s^3 + 1232.0580s^2 + 52.4488s} \quad (5.54)$$

$$\frac{\phi(s)}{\delta_r(s)} = \frac{404.5083s^3 - 637.9364s^2 - 7117.6475s}{411.9165s^5 + 1097.0554s^4 + 938.9465s^3 + 1232.0580s^2 + 52.4488s} \quad (5.55)$$

$$\frac{\psi(s)}{\delta_r(s)} = \frac{-1257.0185s^3 - 2910.7914s^2 - 638.1991s - 540.9151}{411.9165s^5 + 1097.0554s^4 + 938.9465s^3 + 1232.0580s^2 + 52.4488s} \quad (5.56)$$

Transfer Functions For $\bar{x}_{cg}$ Is At 0.30 $\bar{c}$

$$\frac{\beta(s)}{\delta_r(s)} = \frac{21.3145s^4 + 1257.0451s^3 + 2536.1717s^2 - 45.1204s}{411.9166s^5 + 1086.9086s^4 + 779.667s^3 + 945.6915s^2 + 54.9286s} \quad (5.57)$$

$$\frac{\phi(s)}{\delta_r(s)} = \frac{404.8708s^3 - 596.1072s^2 - 7027.8690s}{411.9166s^5 + 1086.9086s^4 + 779.667s^3 + 945.6915s^2 + 54.9286s} \quad (5.58)$$

$$\frac{\psi(s)}{\delta_r(s)} = \frac{-1214.0613s^3 - 2817.5522s^2 - 629.4698s - 534.5297}{411.9166s^5 + 1086.9086s^4 + 779.667s^3 + 945.6915s^2 + 54.9286s} \quad (5.59)$$

5.3.2.2.2 LATERAL-DIRECTIONAL DYNAMIC RESPONSE FOR RUDDER DEFLECTION

Using transfer functions and input rudder deflections, Figures 5.9 to 5.14 are obtained. Dynamic responses for step and variable inputs are nearly same except the magnitudes of peak values. The peak values for variable input is greater than the step input values.

A positive rudder deflection towards to left wing creates a negative yawing moment and positive sideslip angle. After two seconds maximum peak value is obtained, 2 degree for step input and aft cg (Figure 5.9). Then sideslip angle decreases and reaches its minimum peak value, -1.4 degree. This oscillation continues while sideslip angle is damping. After 40 seconds it reaches zero degree and the aircraft turns the steady state condition.

Dynamic response of rolling angle for rudder deflection shows an interesting behavior. At the very beginning of the process, positive rudder deflection creates positive rolling moment, on the mean time it also creates positive sideslip angle. This sideslip angle causes a negative rolling moment. The change in rolling moment caused by a variation in sideslip angle, C_{l_β} is nearly 6 times greater than the change in rolling moment coefficient with variation in rudder deflection, $C_{l_{\delta_r}}$. Because of this, after a positive rolling angle for a very short time, aircraft begins to roll towards left. Then rolling angle oscillates and damps and finally reaches zero degree after 100 seconds.

Dynamic responses of heading angle are different for step input and variable input. It is stabilized at a negative value for step input, but it reaches zero degree for variable input. Because of negative yawing angle, the aircraft begins to turn to left for step input. After oscillations, heading angle damps and the aircraft turns to left for around 10 degree.

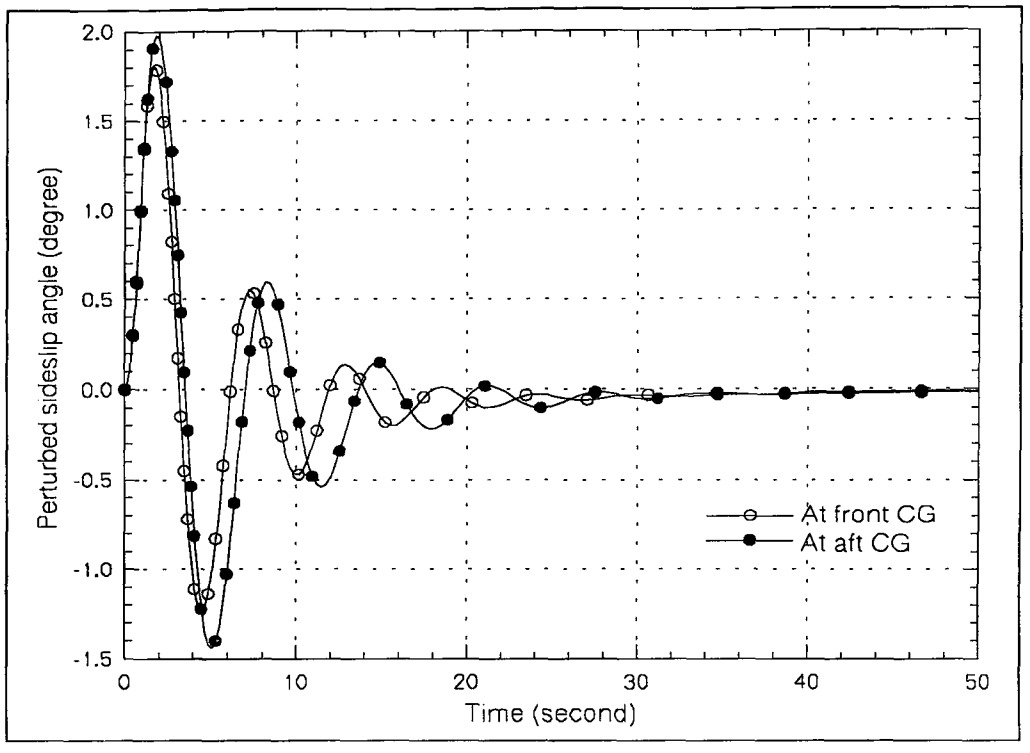

Figure 5.9 Dynamic response of sideslip angle for step input.

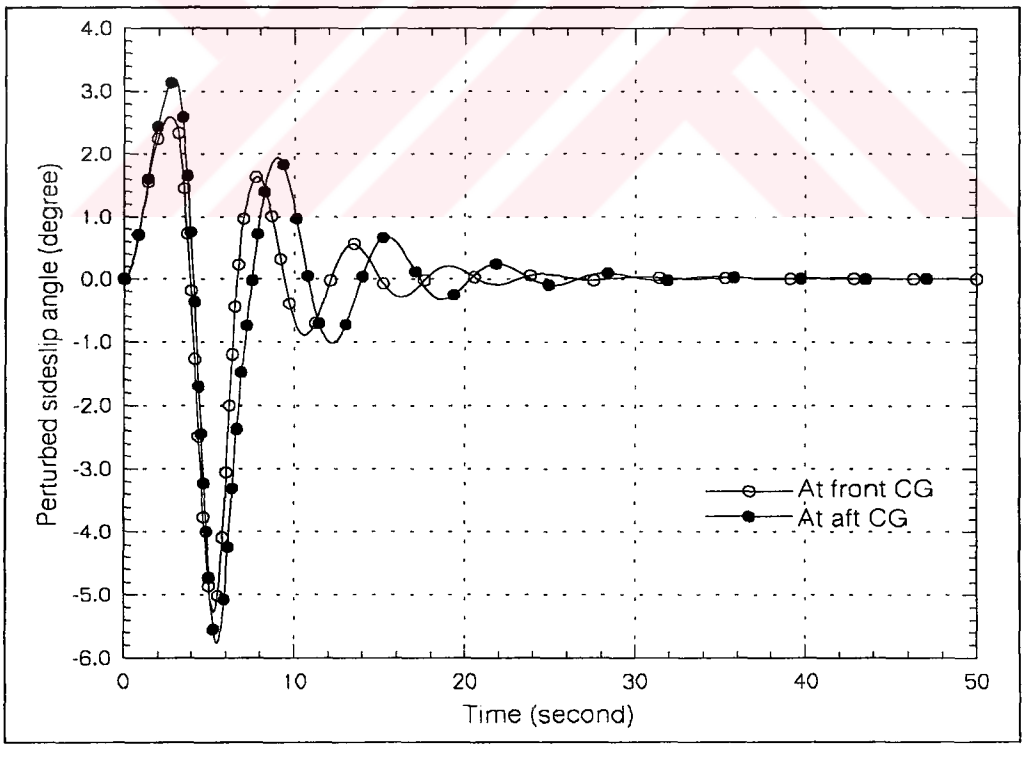

Figure 5.10 Dynamic response of sideslip angle for variable input.

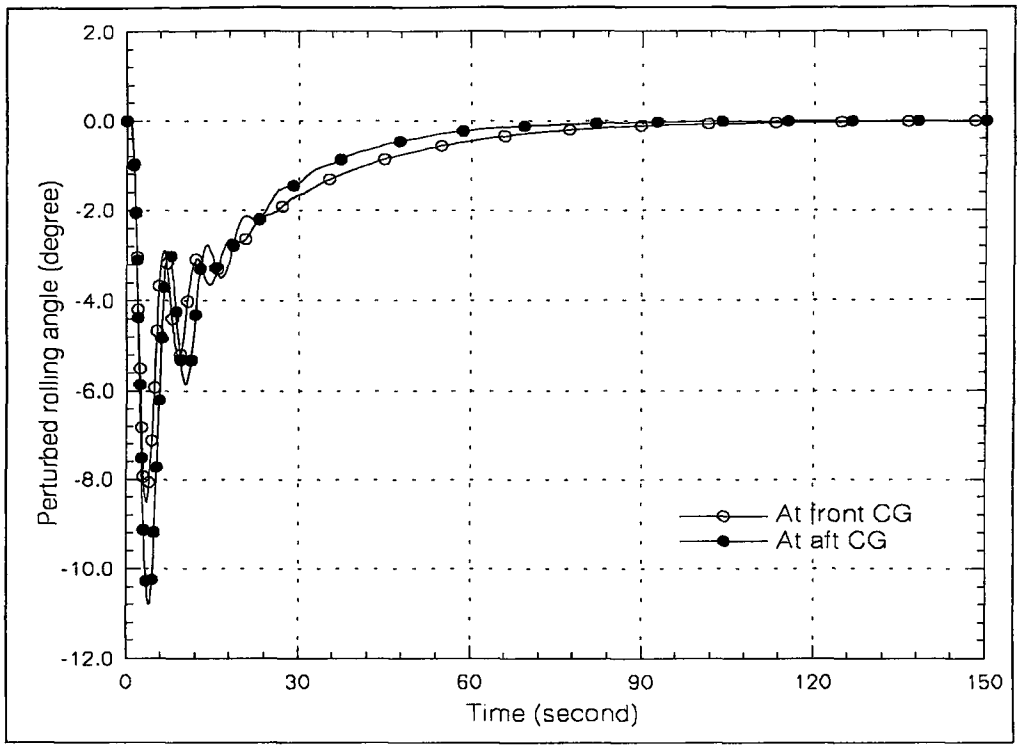

Figure 5.11 Dynamic response of rolling angle for step input.

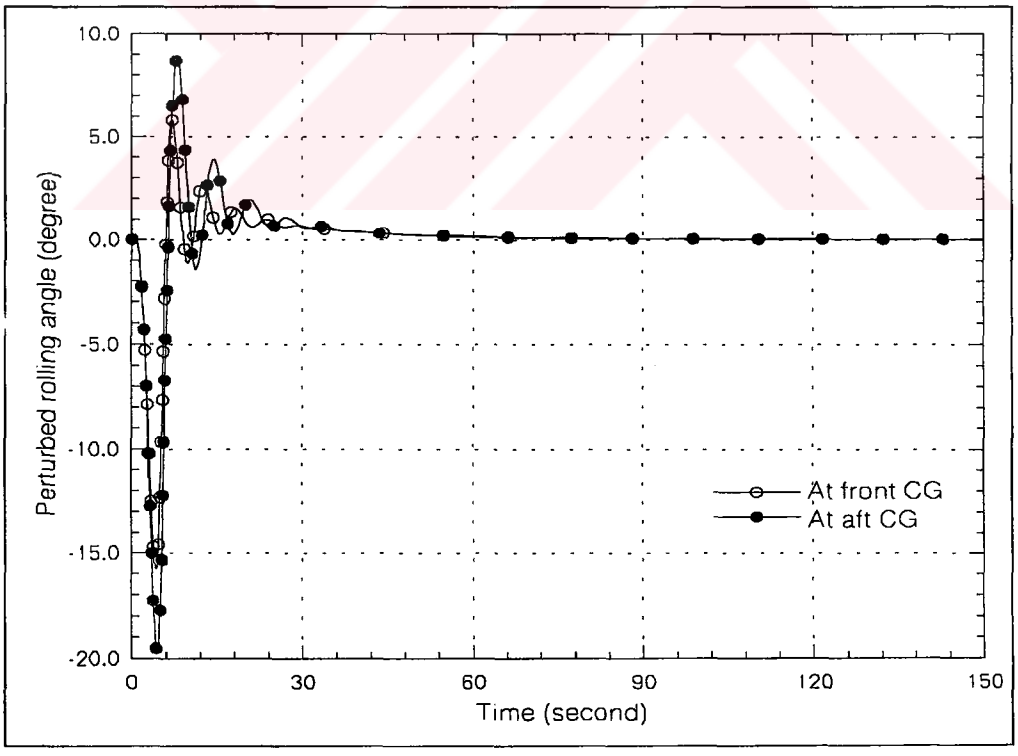

Figure 5.12 Dynamic response of rolling angle for variable input.

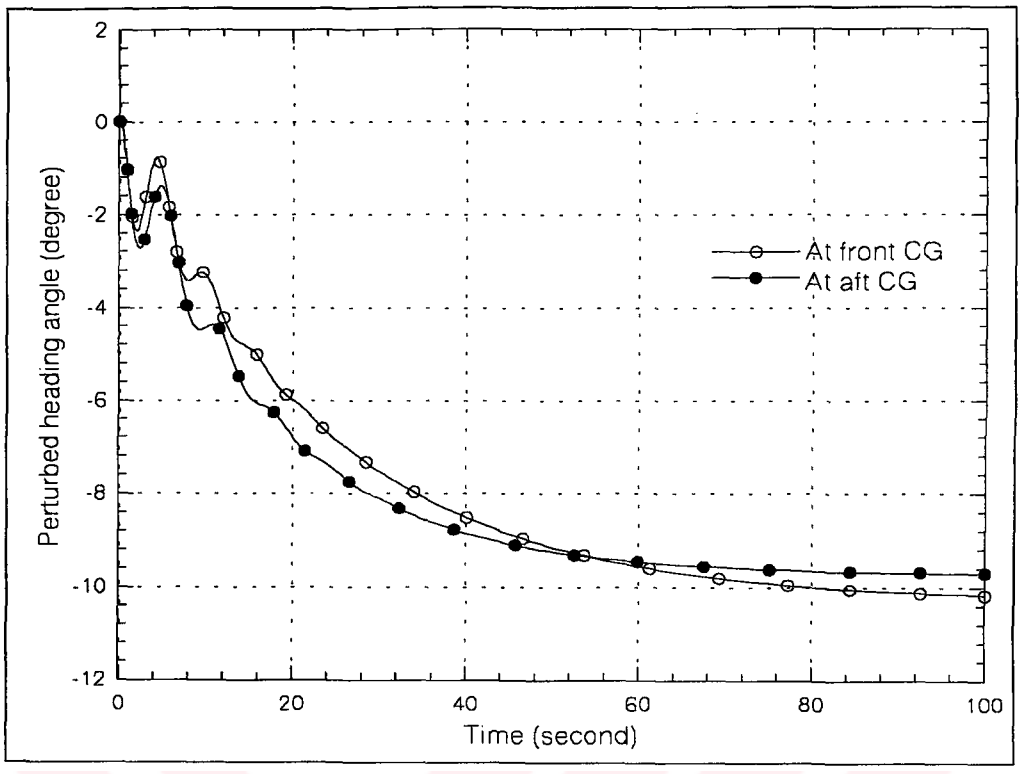

Figure 5.13 Dynamic response of heading angle for step input.

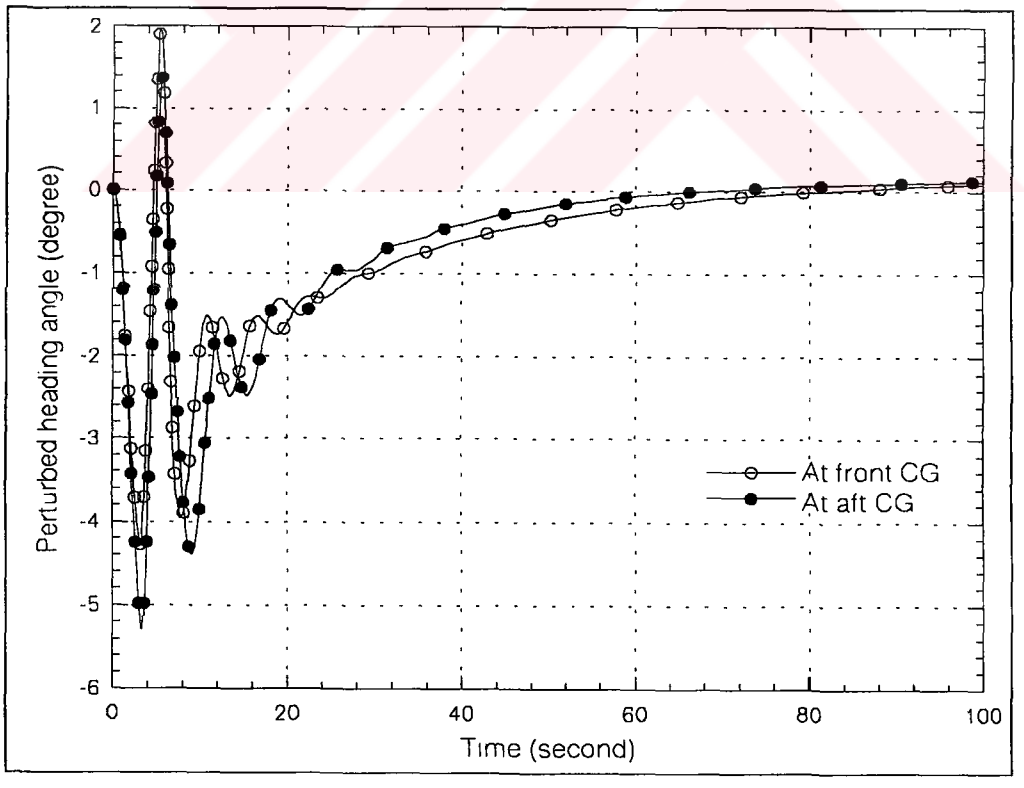

Figure 5.14 Dynamic response of heading angle for variable input.

5.3.2.3 TRANSFER FUNCTIONS FOR AILERON DEFLECTION

The derivatives $\frac{\beta(s)}{\delta_a(s)}$, $\frac{\phi(s)}{\delta_a(s)}$, and $\frac{\psi(s)}{\delta_a(s)}$ are obtained by using the software AAA and presented in Equations 5.60 to 5.65.

Transfer Functions For $\bar{x}_{cg}$ Is At $0.16\bar{c}$

$$\frac{\beta(s)}{\delta_a(s)} = \frac{89.9267s^3 + 777.0079s^2 + 84.5954s}{411.9165s^5 + 1097.0554s^4 + 938.9465s^3 + 1232.0580s^2 + 52.4488s} \quad (5.60)$$

$$\frac{\phi(s)}{\delta_a(s)} = \frac{3097.3301s^3 + 1919.0450s^2 + 2296.6503s}{411.9165s^5 + 1097.0554s^4 + 938.9465s^3 + 1232.0580s^2 + 52.4488s} \quad (5.61)$$

$$\frac{\psi(s)}{\delta_a(s)} = \frac{-93.4978s^3 - 565.6593s^2 - 146.9588s + 156.7997}{411.9165s^5 + 1097.0554s^4 + 938.9465s^3 + 1232.0580s^2 + 52.4488s} \quad (5.62)$$

Transfer Functions For $\bar{x}_{cg}$ Is At $0.30\bar{c}$

$$\frac{\beta(s)}{\delta_a(s)} = \frac{87.0635s^3 + 756.1270s^2 + 78.9496s}{411.9166s^5 + 1086.9086s^4 + 779.667s^3 + 945.6915s^2 + 54.9286s} \quad (5.63)$$

$$\frac{\phi(s)}{\delta_a(s)} = \frac{3097.3089s^3 + 1846.4122s^2 + 1293.0162s}{411.9166s^5 + 1086.9086s^4 + 779.667s^3 + 945.6915s^2 + 54.9286s} \quad (5.64)$$

$$\frac{\psi(s)}{\delta_a(s)} = \frac{-90.6028s^3 - 543.6971s^2 - 140.3179s + 79.8082}{411.9166s^5 + 1086.9086s^4 + 779.667s^3 + 945.6915s^2 + 54.9286s} \quad (5.65)$$

5.3.2.3.1 LATERAL-DIRECTIONAL DYNAMIC RESPONSE FOR AILERON DEFLECTION

Using transfer functions and input aileron deflections, Figures 5.15 to 5.20 are obtained.

Left aileron down is defined as positive, a positive deflection produces a rolling moment to the right which is also positive. Down aileron increases lift and produces more drag on the left wing. But up aileron decreases the lift and drag on the right wing. Because of the difference between drag on the up and down ailerons, a negative yawing moment is created.

Negative yawing moment creates a positive sideslip angle. After approximately 2.5 seconds, maximum peak value is obtained, 0.6 degree for step input and aft cg (Figure 5.15). Then sideslip angle decreases and reaches its minimum peak value, -0.3 degree. This oscillation continues while sideslip angle is damping. After 40 seconds it reaches zero degree and the aircraft turns the steady state condition.

Left aileron down and right aileron up produces positive rolling moment and the aircraft begins to bank to right. First bank angle reaches maximum peak value, 2.8 degree for step input and aft cg (Figure 5.17). Then it begins to oscillate and damp. Finally after 100 seconds, it is stabilized at zero degree. For variable input, it oscillates around zero degree and finally after 50 seconds it reaches zero degree.

Dynamic responses of heading angle are different for step input and variable input. It is stabilized at a positive value for step input, but it reaches zero degree for variable input.

Because of negative yawing angle, the aircraft first begins to turn to left for step input. But after a certain time it begins to turn to right. This behavior of the aircraft is called Adverse Yaw. After oscillations, heading angle damps and the aircraft turns to right for around 1.5 degree for aft cg.

For variable input, first the aircraft turns to left. Then it begins to turn right. After oscillations at positive heading angles, it stabilizes around zero degree.

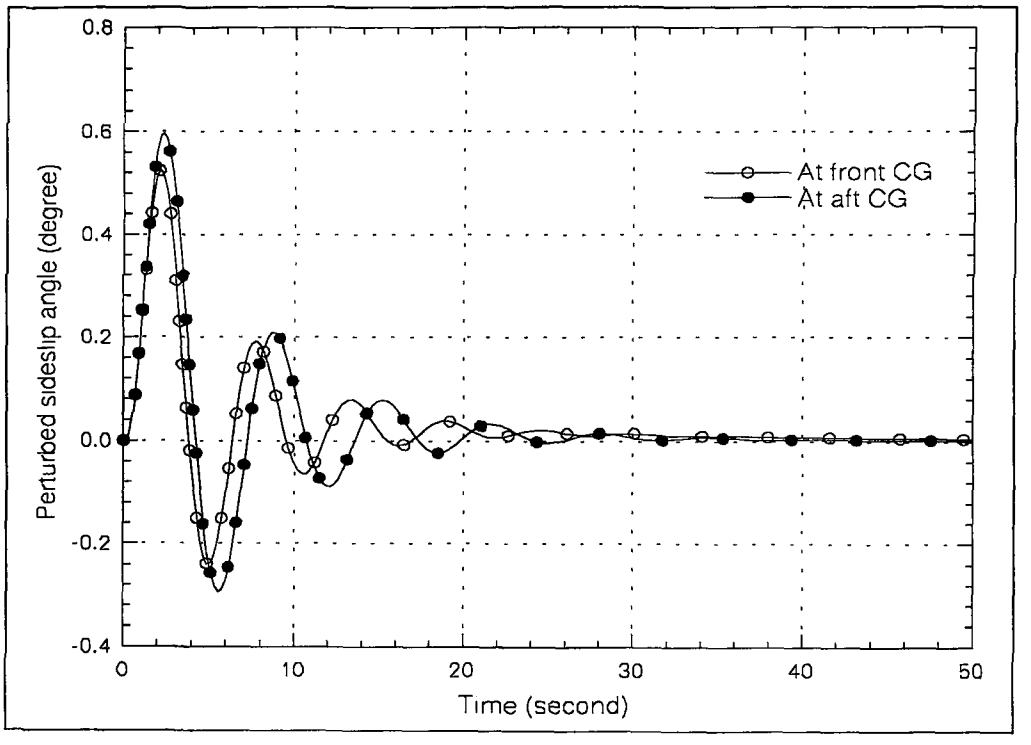

Figure 5.15 Dynamic response of sideslip angle for step input.

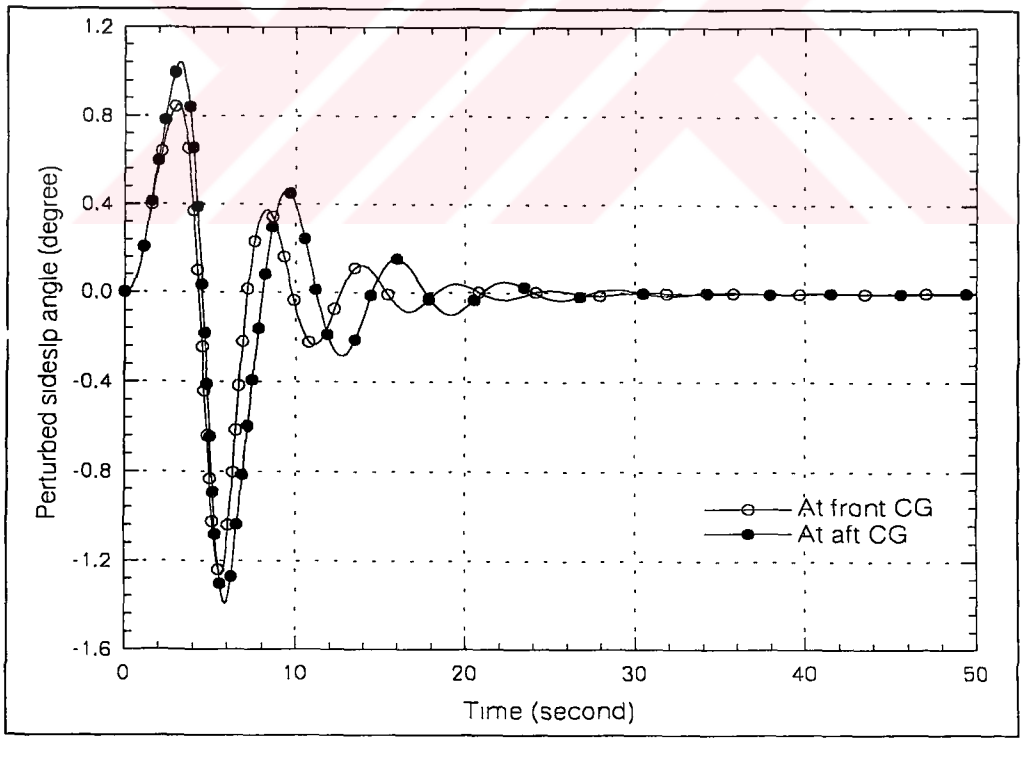

Figure 5.16 Dynamic response of sideslip angle for variable input.

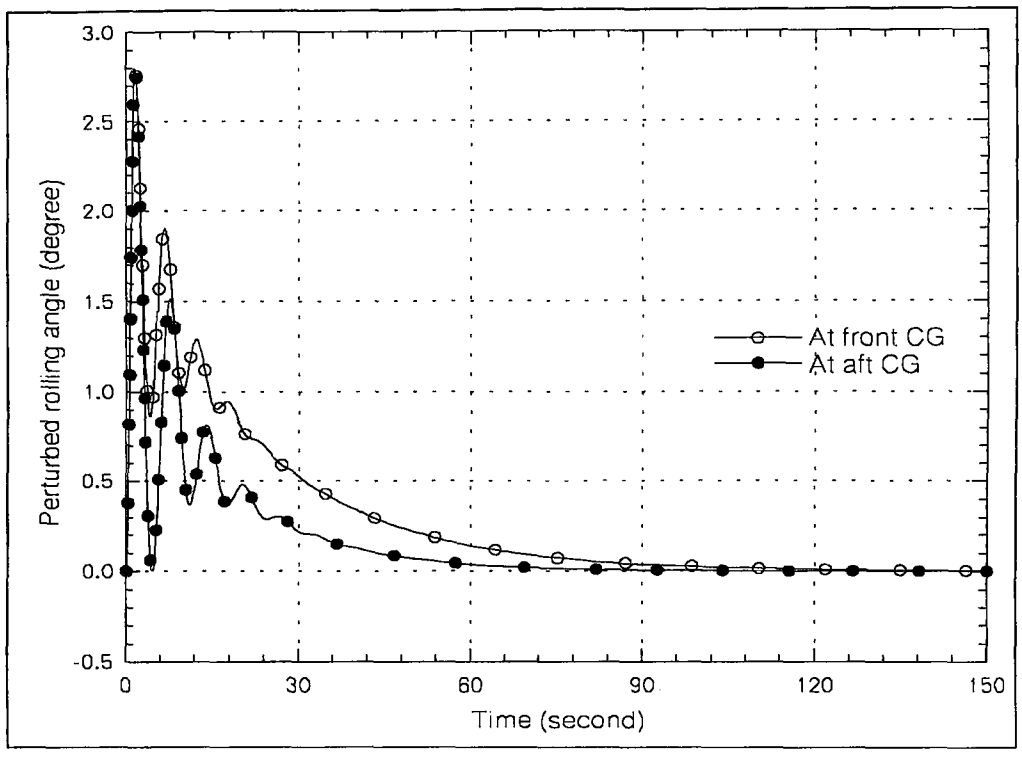

Figure 5.17 Dynamic response of rolling angle step input.

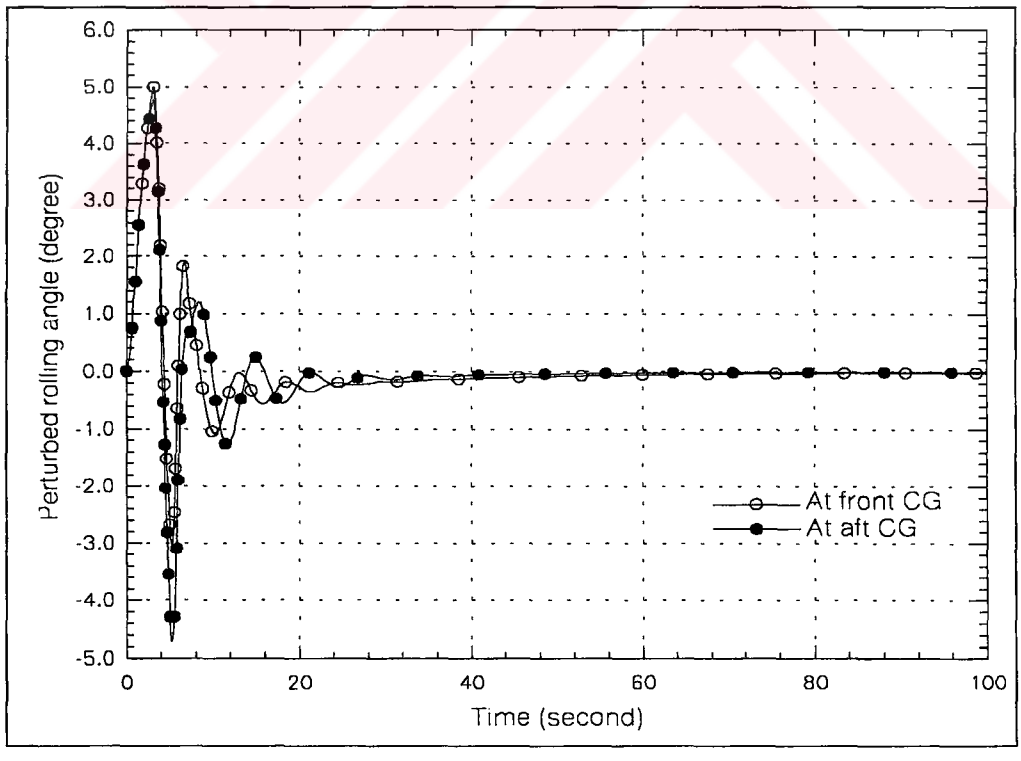

Figure 5.18 Dynamic response of rolling angle for variable input.

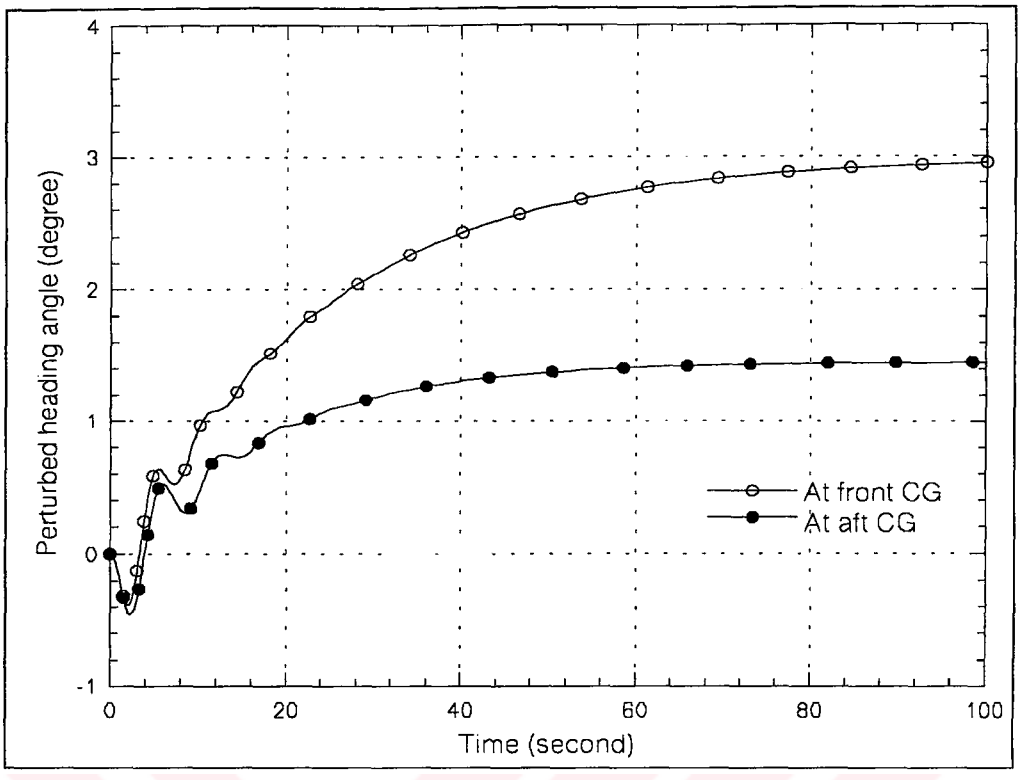

Figure 5.19 Dynamic response of heading angle for step input.

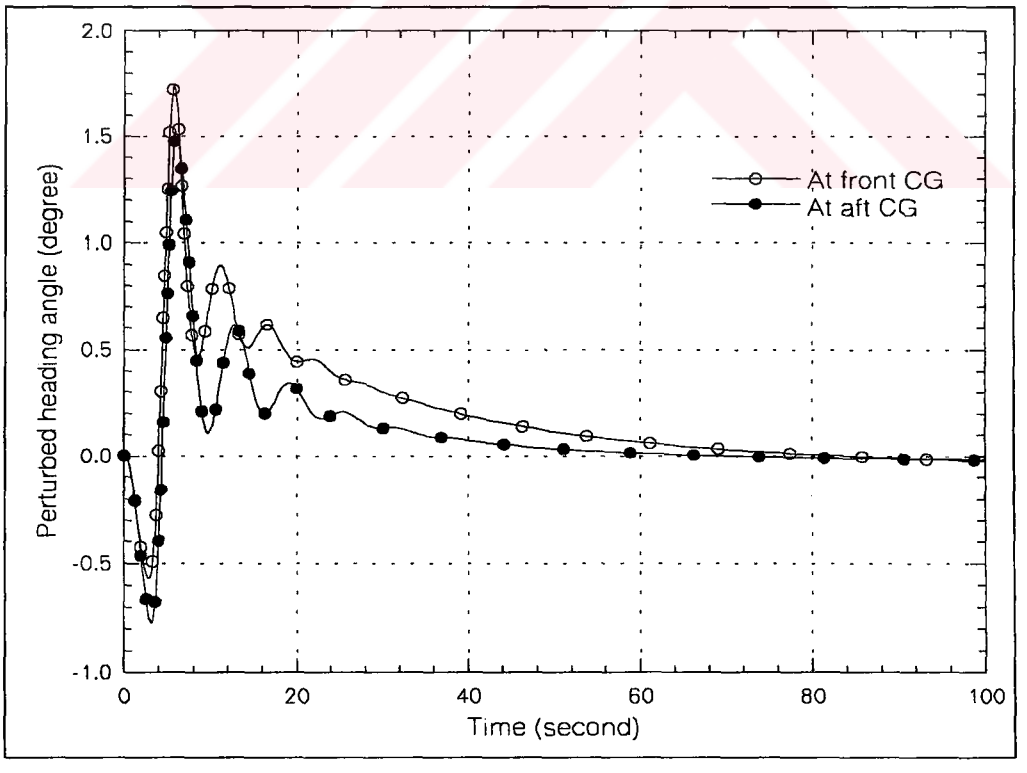

Figure 5.20 Dynamic response of heading angle for variable input.

CHAPTER 6

6. PERFORMANCE CALCULATIONS

In this chapter, the performance calculations are made.

6.1 THEORY OF PERFORMANCE CALCULATIONS

The theory which is used in this chapter is based on Reference 2, 13, and 14. The purpose of this chapter is to present the methods for the calculation of performance parameters.

6.1.1 STALL SPEED

Stall speed is the lowest possible speed of the aircraft. It occurs when the lift coefficient is a maximum value.

$$V_s = \sqrt{\frac{2W}{\rho C_{L_{\max}} S}} \tag{6.1}$$

6.1.2 TAKEOFF GROUND ROLL

Takeoff ground roll is the distance from beginning of the takeoff roll to the point where the airplane is liftoff. Because of military specifications, the aircraft must reach the liftoff speed at the end of the ground roll:

$$V_{LOF} \approx 1.1 V_{S_{TO}} \tag{6.2}$$

where:

V_{LOF} : liftoff speed
$V_{S_{TO}}$: stall speed at takeoff configuration.

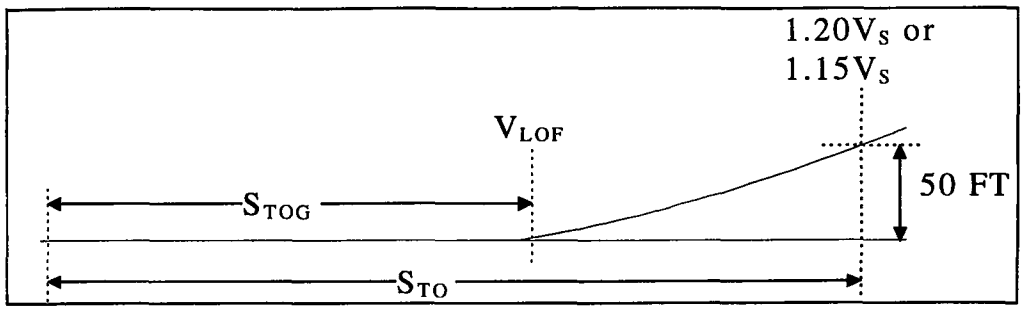

Figure 6.1 Definition of military takeoff distance

Takeoff ground roll:

$$S_{TOG} = \frac{V_{LOF}^2}{2g\left[\left(\frac{\bar{T}}{W}\right)_{TO} - \mu'\right]} \tag{6.3}$$

with:

$$\mu' = \mu_g + 0.72\frac{C_{D_0}}{C_{L_{\max TO}}} \tag{6.4}$$

where:

$\left(\frac{\bar{T}}{W}\right)_{TO}$: the mean thrust to weight ratio taken at a speed of $0.707V_{LOF}$

μ_g : the friction coefficient as determined from page 40 of Reference 13.

6.1.3 RANGE

The range of an aircraft is its velocity multiplied by the amount of time it can remain in the air. Time in the air equals the amount of fuel carried divided by the rate at which the fuel is burned. This in turn is the required thrust multiplied by the specific fuel consumption. For propeller aircraft, range can be maximized by flying at the speed and lift coefficient for maximum L/D.

$$R = \frac{550\eta_p}{C_{bhp}} \frac{L}{D} \ln\left(\frac{W_{initial}}{W_{end}}\right) \tag{6.5}$$

where:

C_{bhp} : specific fuel consumption

6.1.4 ENDURANCE

The amount of time an aircraft can remain in the air is simply its fuel capacity divided by the rate of fuel consumption (thrust multiplied by specific fuel consumption). During endurance for a propeller aircraft, the aircraft flies at a velocity which is 76% of the velocity for best L/D and the L/D when flying at the minimum power velocity is 86.6% of the best L/D.

$$E = \frac{L}{D} \frac{550\eta_p}{C_{bhp} V} \ln\left(\frac{W_{initial}}{W_{end}}\right) \tag{6.6}$$

6.1.5 LANDING GROUND ROLL

Landing ground roll is the distance from touchdown to end of landing roll.

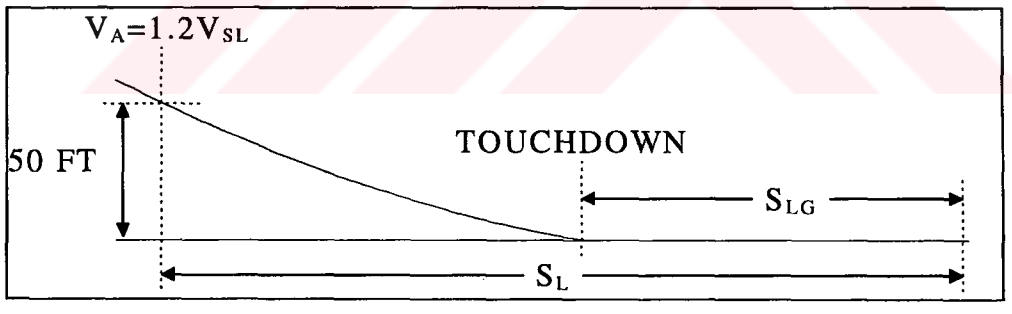

Figure 6.2 Definition of military landing distance

$$S_{LG} = \frac{V_{TD}^2}{2\bar{a}} \tag{6.7}$$

with:

$$V_{TD} = V_A \sqrt{1 - \frac{\left(\bar{\gamma}\right)^2}{\Delta n}} \tag{6.8}$$

$$V_A = 1.2 V_{S_L} \tag{6.9}$$

$$\bar{\gamma} = \left(\frac{D-T}{W}\right)_{average} \tag{6.10}$$

where:

$\frac{\bar{a}}{g}$ = 0.35 to 0.45 for turboprops without use of reversible propellers.

Δn = 0.1 as a reasonable average: this quantity depends on pilot technique and on airplane handling qualities.

V_{S_L} : The stall speed for landing configuration.

6.2 CALCULATION OF PERFORMANCE PARAMETERS

Because of obtaining some input values for performance calculations is impossible, instead of real values, assumed logical values are used.

6.2.1 CALCULATION OF STALL SPEED

Stall speed depends on the current weight of the aircraft, air density, maximum lift coefficient, and wing area.

6.2.1.1 Stall speed at flaps up position

W = 15100 kg
ρ = 1.225 kg/m^3
S = 59.1 m^2
$C_{L_{max}}$ =1.501

$$V_s = \sqrt{\frac{2W}{\rho C_{L_{max}} S}} = \sqrt{\frac{2(148131)}{(1.225)(1.501)(59.1)}} = 52.21 \text{ m/s} = 187.97 \text{ km/h}$$

The stall speed at flaps up position in Jane's[3] is 186 km/h. The calculated value is 1.06% bigger than the value in Jane's.

6.2.1.2 Stall speed at flaps down position

W = 15100 kg
ρ = 1.225 kg/m^3
S = 59.1 m^2
$C_{L_{max}}$ =1.905

$$V_S = \sqrt{\frac{2W}{\rho C_{L_{max}} S}} = \sqrt{\frac{2(148131)}{(1.225)(1.905)(59.1)}} = 46.35 \text{ m/s} = 166.85 \text{ km/h}$$

The stall speed at flaps down position in Jane's[3] is 156 km/h. The calculated value is 6.96% bigger than the value in Jane's.

6.2.2 CALCULATION OF TAKEOFF GROUND ROLL

$V_{S_{TO}}$ = 49.24 m/s from Chapter 3.2.1.

$$V_{LOF} \approx 1.1 V_{S_{TO}} = 54.16 \text{ m/s}$$

η_p = 0.8 as assumed value.

$\frac{W}{hp}$ = 5.78 kg/kW from Jane's.

Assume mean velocity during takeoff ground is 35 m/s.

$$\frac{\bar{T}}{W} = \frac{550\eta_p}{V}\frac{hp}{W} = 0.3007$$

μ_g = 0.02 for concrete or asphalt from Reference 13.
C_{D_0} = 0.0370 from Chapter 3.3.2.
$C_{L_{max_{TO}}}$ = 1.688 from Chapter 3.3.1.

$$\mu' = \mu_g + 0.72\frac{C_{D_0}}{C_{L_{max_{TO}}}} = 0.0358$$

$$S_{TOG} = \frac{V_{LOF}^2}{2g\left[\left(\frac{\bar{T}}{W}\right)_{TO} - \mu'\right]} = 564.37 \text{ m}$$

Takeoff ground roll in Jane's[3] is 554 m. The calculated value is 1.87% bigger than the value in Jane's.

6.2.3 CALCULATION OF RANGE

Mission profile of the aircraft can be divided into 5 segments for range calculation: Warmup and takeoff, climb, cruise, loiter and landing. Due to information of Jane's[3], range altitude is 5485 meter and range segment also consists of 45 minute hold (loiter). Maximum fuel is 4230 kg and maximum takeoff weight is 15100 kg

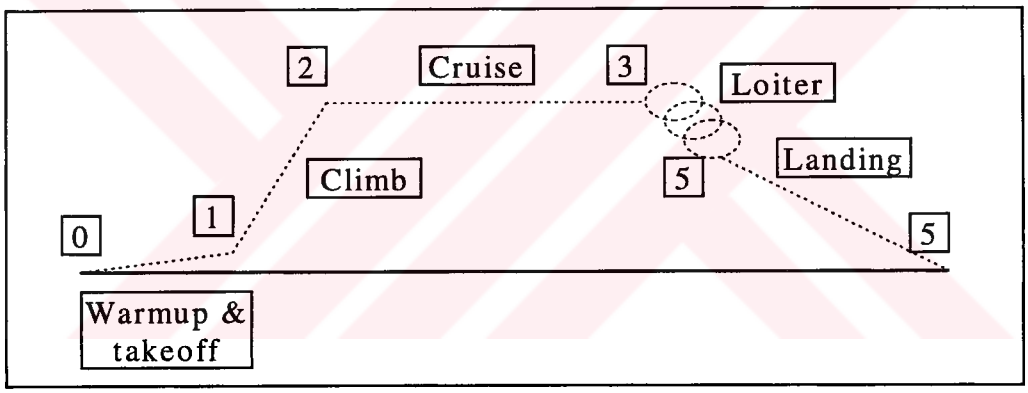

Figure 6.3 Mission profile for range calculation

W_0 = 15100 kg
W_f = 4230 kg
E_L = 45 min

where:

W_0 : Maximum takeoff weight
W_f : Maximum fuel weight
E_L : Loiter time

From Table 3.2 of Reference 2:

$$\frac{W_1}{W_0} = 0.97$$

$$\frac{W_2}{W_1} = 0.985$$

$$\frac{W_5}{W_4} = 0.995$$

From drag polar curves in Figure 3.14, maximum L/D ratio can be obtained.

$$\left.\frac{L}{D}\right)_{max} = 18.13$$

$$C_L)\left.\frac{L}{D}\right)_{max} = 0.774$$

C_{bhp} = 0.470 lb/h/shp from Jane's[3]

ρ = 0.6982 kg/m^3 at 18000 feet.

Assume mean weight of loiter segment is 12000 kg.

$$V)\left.\frac{L}{D}\right)_{max} = \sqrt{\frac{2W}{\rho C_L)\left.\frac{L}{D}\right)_{max} S}} = 85.86 \text{ m/s}$$

During endurance for a propeller aircraft, the aircraft flies at a velocity which is 76% of the velocity for best L/D and the L/D when flying at the minimum power velocity is 86.6% of the best L/D.

$$E_L = (0.76)\frac{L}{D}\frac{550\eta_p}{C_{bhp}(0.866)V}\ln\left(\frac{W_3}{W_4}\right)$$

$$\Rightarrow \quad \frac{W_4}{W_3} = 0.986$$

The useable fuel can be calculated by using Equation 6.7 of Reference 2.

$$W_{f_{useable}} = \frac{W_f}{1.06} = 3990.57 \text{ kg}$$

$$W_5 = W_0 - W_{f_{useable}} = 11347.86 \text{ kg}$$

$$\frac{W_5}{W_0} = 0.7515$$

$$\frac{W_5}{W_0} = \frac{W_5}{W_4}\frac{W_4}{W_3}\frac{W_3}{W_2}\frac{W_2}{W_1}\frac{W_1}{W_0}$$

$$\Rightarrow \quad \frac{W_3}{W_2} = 0.8017$$

$$R = \frac{550\eta_p}{C_{bhp}}\frac{L}{D}\ln\left(\frac{W_2}{W_3}\right) = 4116 \text{ km}$$

Range in Jane's[3] is 3910 km. The calculated value is 5.27% bigger than the value in Jane's.

6.2.4 CALCULATION OF ENDURANCE

Mission profile of the aircraft can be divided into 4 segments for endurance calculation: Warmup and takeoff, climb, loiter and landing.

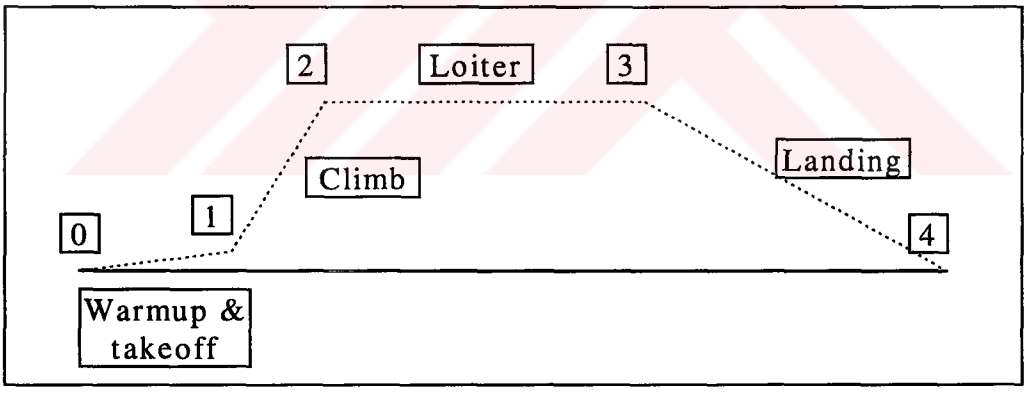

Figure 6.3 Mission profile for endurance calculation

From drag polar curves in Figure 3.14, maximum L/D ratio can be obtained.

$$\left(\frac{L}{D}\right)_{max} = 18.13$$

$$C_L)\frac{L}{D}\Big)_{max} = 0.774$$

C_{bhp} = 0.470 lb/h/shp from Jane's[3]

ρ = 0.6982 kg/m^3 at 18000 feet.

From Table 3.2 of Reference 2:

$$\frac{W_1}{W_0} = 0.97$$

$$\frac{W_2}{W_1} = 0.985$$

$$\frac{W_5}{W_4} = 0.995$$

From Chapter 6.2.3:

W_0 = 15100 kg

$$\frac{W_4}{W_0} = 0.7515$$

$$\frac{W_4}{W_0} = \frac{W_4}{W_3}\frac{W_3}{W_2}\frac{W_2}{W_1}\frac{W_1}{W_0}$$

$$\Rightarrow \quad \frac{W_3}{W_2} = 0.7905$$

$$W_2 = \frac{W_2}{W_1}\frac{W_1}{W_0}W_0 = 14427.30 \text{ kg}$$

$$W_3 = \frac{W_3}{W_2}\frac{W_2}{W_1}\frac{W_1}{W_0}W_0 = 11404.78 \text{ kg}$$

Mean weight for endurance:

$$W = \frac{W_2 + W_3}{2} = 12916.04 \text{ kg}$$

$$V)\frac{L}{D}\Big)_{max} = \sqrt{\frac{2W}{\rho C_L)\frac{L}{D}\Big)_{max} S}} = 89.08 \text{ m/s}$$

During endurance for a propeller aircraft, the aircraft flies at a velocity which is 76% of the velocity for best L/D and the L/D

when flying at the minimum power velocity is 86.6% of the best L/D.

$$E = (0.76)\frac{L}{D}\frac{550\eta_p}{C_{bhp}(0.866)V}\ln\left(\frac{W_2}{W_3}\right)$$

$\Rightarrow$ E = 11 hours 58 minutes

6.2.5 CALCULATION OF LANDING GROUND ROLL

V_{S_L} = 46.27 m/s from Chapter 3.2.1.

$$V_A = 1.2V_{S_L} = 55.52 \text{ m/s}$$

C_{D_1} = 0.0973 from Chapter 3.3.2.

q = 1890.42 N/m^2 from Chapter 3.2.2.

$$D = C_{D_{old}}qS = 10870.73 \text{ N}$$

Thrust, T can be assumed 0 during landing.

W = 147640.5 N

$$\bar{\gamma} = \left(\frac{D-T}{W}\right)_{average} = 0.0736$$

Δn = 0.1 as a reasonable average: this quantity depends on pilot technique and on airplane handling qualities.

$$V_{TD} = V_A\sqrt{1-\frac{\left(\bar{\gamma}\right)^2}{\Delta n}} = 54.0 \text{ m/s}$$

Assume $\frac{\bar{a}}{g}$ is 0.4.

$$\bar{a} = \frac{\bar{a}}{g}g = (0.4)(9.81) = 3.924 m/s^2$$

$$S_{LG} = \frac{V_{TD}^2}{2\bar{a}} = \frac{54.0^2}{2(3.924)} = 371.56 \text{ m.}$$

6.3 SUMMARY OF RESULTS

In this chapter, the performance parameters are calculated. Results are listed in Table 6.1. Stall speed at flaps up position is 187.67 km/h. The calculated value is 1.06% bigger than the value in Jane's. The stall speed at flaps down position is 166.85 km/h. The calculated value is 6.96% bigger than the value in Jane's.

Takeoff ground roll is 564.37 meters. The calculated value is 1.87% bigger than the value in Jane's.

Range is 4116 km. The calculated value is 5.27% bigger than the value in Jane's.

Endurance is 11 hours and 58 minutes. Landing ground roll is 371.56 meters.

Table 6.1 % Difference in performance parameters

Performance Parameter	Calculated value	The value in Jane's	% Difference
Stall Speed at flaps up position (km/h)	187.97	186	1.06
Stall Speed at flaps down position (km/h)	166.85	156	6.96
Takeoff Ground Roll (meter)	564.37	554	1.87
Range (km)	4116	3910	5.27
Endurance	11h58min		
Landing Ground Roll (meter)	371.56		

CHAPTER 7

7. DISCUSSION AND CONCLUSION

In this report, aerodynamics, flight mechanics and performance predictions for a medium range cargo aircraft are made. Because of center of gravity (cg) restriction of the test aircraft due to its Flight Manuel, the calculations are made for two cg locations. First one is the front cg limit at 16% of the mean geometric chord (mgc) of the wing and the other one is the aft cg limit is at 30% of mgc.

Many different software and computer programs are used during calculations. The software named Advanced Aircraft Analysis (AAA)[8] is used for nearly all parts of the calculations. The software Matlab[15] is used to visualize the dynamic response of the aircraft for input control surface deflections. A computer program[7] for the incompressible aerodynamics analysis of airfoils is used to calculate the transition points of the wing, horizontal tail and vertical tail airfoils.

Because of obtaining some real design or production values of the aircraft is impossible, proper values are obtained from different references or assumed values are used.

The calculations are divided into 4 parts: aerodynamics, static stability and control, dynamic stability and response characteristics, and performance.

Aerodynamic calculations are made for three flight conditions: cruise, takeoff and landing. Results of this chapter can be divided into three parts: results related to lift coefficient versus angle of attack (AOA) curves, drag polar curves and pitching moment versus AOA curves.

Center of gravity position does not affect C_L-α curves. Effects of using of single slotted flaps :

- Zero lift angle of attack angle is decreased.
- Aircraft lift curve slope is decreased.
- Aircraft maximum lift coefficient is increased

For cruise condition, zero lift drag coefficient and minimum drag coefficient have the same value because of flap deflection angle is zero. But for the other two flight conditions, zero lift drag coefficient and minimum drag coefficient don't have the same values. Because the flap deflection angles are different from zero.

Zero lift pitching moment coefficients are affected from horizontal tail downwash angle for zero wing body angle of attack and cg location.

Total airplane pitching moment coefficient vs. AOA slopes are changed due to lift curve slope and cg location.

Using different elevator deflection angle does not change the total airplane pitching moment coefficient vs. AOA slope. But pitch moment for same angle of attack changes. It decreases if elevator deflection angle increases and it increases if elevator deflection angle decreases.

Static stability and control derivatives are calculated for two cg locations. All of the calculated static stability and control derivatives have proper values to the theoretical values.

The analysis of dynamic stability and response characteristics is made for cruise flight condition with zero flap deflection and landing gears in up position. Results of this chapter can be divided into two parts: results related to flying quality levels and dynamic stability and response.

All of the flying quality parameters are inside the Level 1, the best flying quality level, except time to double the amplitude in the spiral mode, T_{2_s}. It is inside the Level 2.

The analysis of dynamic stability and response is made for input elevator, rudder, and aileron deflections. Two different input control surface deflections are used. These are step and variable inputs.

Dynamic responses of the aircraft for control surface deflections are proper to theoretical characteristics. The effect of cg location on dynamic response is only in terms of magnitudes. It changed the peak values of responses.

Performance calculations are made for 5 parameters: stall speed, takeoff ground roll, range, endurance, and landing ground roll. Results are listed in Table 7.1.

Stall speed at flaps up position is 187.67 km/h. The calculated value is 1.06% bigger than the value in Jane's. The stall speed at flaps down position is 166.85 km/h. The calculated value is 6.96% bigger than the value in Jane's.

Takeoff ground roll is 564.37 meters. The calculated value is 1.87% bigger than the value in Jane's. Range is 4116 km. The calculated value is 5.27% bigger than the value in Jane's.

Endurance is 12 hours and 25 minutes. Landing ground roll is 371.56 meters.

In this analysis, basic methods are used. Because of this, the parameters which are calculated in this thesis may not have exact values. For obtaining more accurate values, the Computational Fluid Dynamics (CFD) codes and wind tunnel tests must be used.

REFERENCES

1. Roskam, J., Airplane Design, part 6, Roskam Aviation and Engineering Corporation, Rt 4, Box 274, Ottowa, Kansas, 66067 USA.

2. Raymer, D. P., Aircraft Design : A Conceptual Approach, AIAA Education Series, 1992, ISBN : 0-930403-51-7.

3. Jane's All the World's Aircraft, Jane's Information Group, Sentinel House, 163 Brighton Road, Coulsdon, Surrey CR5 2NH, UK, ISBN for 1991-1992 issue : 0 7106 0965 5.

4. MIL-F-8785C, Military specification, Flying Qualities of Piloted Airplanes.

5. Fox, R. W. and McDonald, A. T., Introduction to Fluid Mechanics, John Wiley & Sons.

6. CASA CN-235 Maintenance Manual.

7. Kavsaoglu, M. S., Airfoil : A computer program for aerodynamic analysis of airfoils, Middle East Technical University, November 1994.

8. DARcorporation, Advanced Aircraft Analysis Version 2.0, 120 East Street, Suite 2, Lawrence, Kansas 66044 USA.

9. Schetz, J. A., Boundary Layer Analysis, Prentice Hall, Eaglewood Cliffs, New Jersey 07632, 1993.

10. Gaudet L., and Winter K.G., Measurements of the drag of some characteristic aircraft excrescences immersed in turbulent boundary layers, AGARD Conference Proceedings No.124, Aerodynamic Drag, 1973

11. Roskam, J., Airplane Flight Dynamics and Automatic Flight Controls, Part I, Roskam Aviation and Engineering Corporation, Rt 4, Box 274, Ottowa, Kansas, 66067 USA

12. Smetena, Frederick O., Computer Assisted Analysis of Aircraft Performance Stability and Control, McGraw-Hill Book Company.

13. Roskam, J., Airplane Design, part 7, Roskam Aviation and Engineering Corporation, Rt 4, Box 274, Ottowa, Kansas, 66067 USA.

14. John D. Anderson, Jr., Fundamentals of Aerodynamics, McGraw-Hill, Inc.

15. Matlab with SIMULINK, The MathWorks, Inc.

APPENDIX A

FLYING QUALITY LEVELS

The Flying Quality Levels are defined in MIL-F-8785C, "Military Specification - Flying Qualities of Piloted Airplanes." Although the FAR requirements do not set specific flying quality levels, common design practice is to adopt the military definitions. Airplanes must be designed to satisfy the Level 1 flying quality requirements with all systems in their normal operating state.

Level 1: Flying qualities are clearly adequate for the mission Flight Phase.

Level 2: Flying qualities are adequate to accomplish the mission Flight Phase, but some increase in pilot workload or degradation in mission effectiveness, or both, exists.

Level 3: Flying qualities such that the airplane can be controlled safely, but the pilot workload is excessive or mission effectiveness is inadequate, or both. Category A Flight Phases can be terminated safely, and Category B and C Flight Phases can be completed.

The required levels of flying qualities are tied into the probability with which certain system failures can occur. For example, it is desired to have:

- at least Level 1 for airplane normal (no failure) state,
- at least Level 2 after failures that occur less than once per 100 flights,
- at least Level 3 after failures that occur less than once per 10,000 flights.

Flying quality levels below Level 3 are not allowed except in special circumstances.

APPENDIX B

SAMPLE MATLAB-SIMULINK FILE

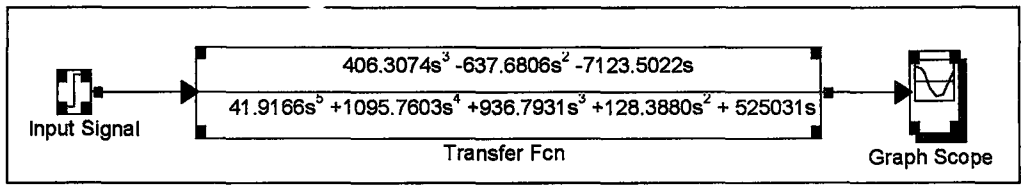

APPENDIX C

FIGURES

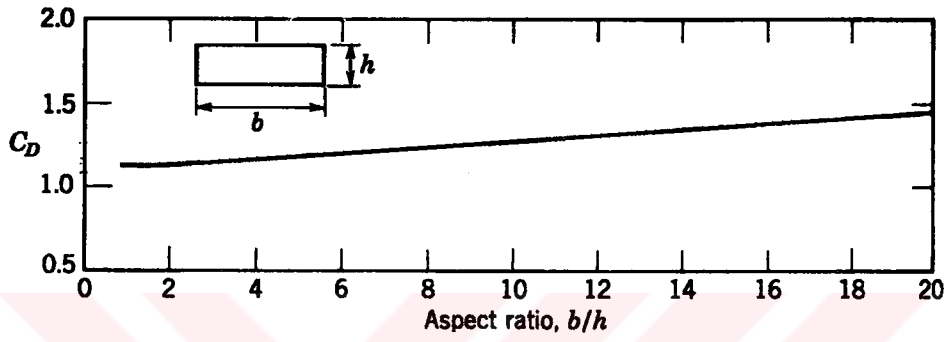

Fig. 9.10 Variation of drag coefficient with aspect ratio for a flat plate of finite width normal to the flow with $Re_h > 1000$ [14].

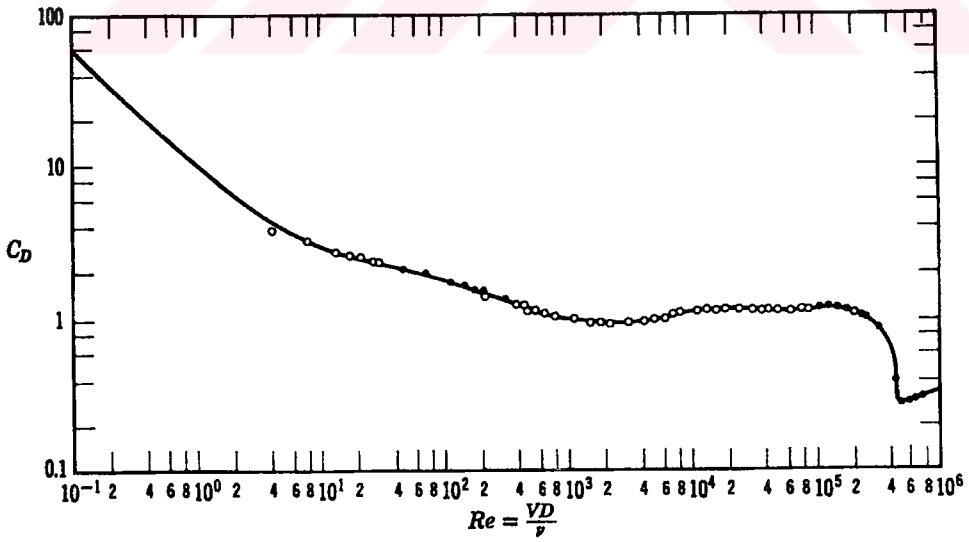

Fig. 9.13 Drag coefficient for circular cylinders as a function of Reynolds number [3].

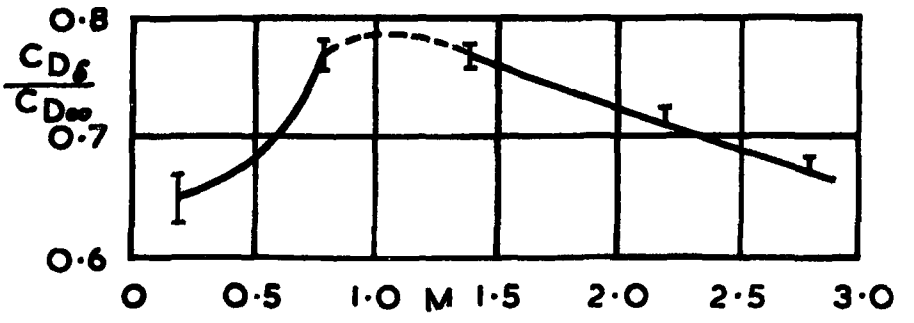

Fig. 19 Circular cylinders - drag ratio for $s = \delta_{99}$

APPENDIX D

THE INFORMATION ABOUT CASA CN-235 AIRCRAFT IN JANE'S

AIRTECH

AIRCRAFT TECHNOLOGY INDUSTRIES

PRESIDENT: Prof Dr-Ing B. J. Habibie (IPTN)
VICE-PRESIDENT: Javier Alvarez Vara (CASA)
PARTICIPATING COMPANIES:

Construcciones Aeronauticas SA, Rey Francisco 4, Apartado 193, 28008 Madrid, Spain
Telephone: (91) 247 2500
Telex: 27418 CASA E

IPTN (Industri Pesawat Terbang Nusantara), PO Box 563, Jalan Pajajaran 154, Bandung, Indonesia
Telephone: (022) 611081/2
Telex: 28295 IPTN BD

Airtech is a joint company formed by CASA and IPTN to develop a twin-turboprop transport known as the CN-235. Design and production work is shared 50-50 between the two companies.

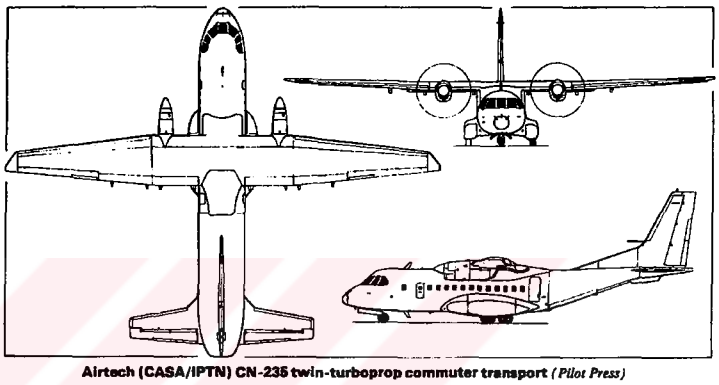

Airtech (CASA/IPTN) CN-235 twin-turboprop commuter transport *(Pilot Press)*

AIRTECH (CASA/IPTN) CN-235 SERIES 100

Preliminary design of the CN-235 was initiated in January 1980, and prototype construction in May 1981. Two prototypes were built, one in each country (ECT-100 and PK-XNC), plus static and fatigue test airframes. Simultaneous rollouts were made on 10 September 1983, and first flights took place on 11 November (CASA) and 30 December 1983 (IPTN).

The first production CN-235 made its initial flight on 19 August 1986. Spanish and Indonesian certification was received on 20 June 1986, and FAA type approval to FAR Pts 25 and 121 on 3 December that year. First delivery, of an IPTN aircraft to Merpati Nusantara Airlines, was made on 15 December 1986; the first two CN-235s from the CASA assembly line, equipped as VIP transports for the Royal Saudi Air Force, were handed over on 4 February 1987, with two more (in **CN-235 M** military transport configuration) following in April 1987. Commercial operation, by the first Merpati aircraft, began on 1 March 1988.

Firm orders for the CN-235 totalled 133 by May 1989 (59 civil and 74 military). Twenty-two of these are for Spanish customers including two for the Air Force, equipped as VIP transports, and four for Binter Canarias. Four others are for Saudi Arabia, eight for the French Armée de l'Air, one each for the Ecuadorian Army and Navy, two for the Botswana Defence Force, one for the Panamanian National Guard, seven for the Moroccan Air Force and two for the US National Safety Council. The other 85 are for Indonesian customers (Deraya 11, Merpati 14, Pelita 10, Indonesian Air Force 32, and Indonesian Navy 18, including six in ASW/maritime patrol configuration). The Chilean Air Force has decided in principle to order six CN-235 Ms. CASA markets the aircraft in the Americas and Europe, IPTN in Asia, with other markets shared as appropriate.

CASA builds the wing centre-section, inboard flaps, forward and centre fuselage and engine nacelles; the outer wings, outboard flaps, ailerons, rear fuselage and tail unit are built by IPTN. Numerical control machinery is used extensively in the CN-235's manufacture. Design has been optimised for short-haul operations, enabling the CN-235 to fly four 100 nm (185 km; 115 mile) stage lengths, with reserves, before needing to refuel, and to operate from either paved runways or unprepared strips.

Initial production CN-235s have General Electric CT7-7A engines, as described in previous editions of *Jane's*, and are designated **Series 10**. The following description applies to the **Series 100** version, with CT7-9C engines in new composites nacelles, which replaced it in 1988 from the 31st (and 16th Spanish) production aircraft:

TYPE: Twin-turboprop commuter and utility transport.

WINGS: Cantilever high-wing monoplane. NACA 65_3-218 wing section. Constant chord centre-section, without dihedral; 3° dihedral on tapered outer panels. Incidence 3°. Sweepback 3° 51′ 36″ at quarter-chord on outer panels. Three main assemblies each consist of a machined fail-safe box structure of aluminium/copper alloy, with main spars at 15 and 55 per cent chord, plus leading- and trailing-edge structures. Inboard flaps on centre-section, outboard flap segments and ailerons on outer panels. Fail-safe attachment of centre-section to top of fuselage; large wing/fuselage fairing, made of composites. Chemically milled skins. Leading-edges each made up of a false spar, ribs and skin panels. Flap segments each have a machined aluminium spar, two sheet metal ribs of aluminium/zinc alloy, and leading/trailing-edges of glassfibre laminates with honeycomb core. Inboard and outboard pairs are interchangeable port/starboard. Flaps are single-slotted and actuated hydraulically by Dowty Rotol irreversible jacks. Ailerons, of similar construction to flaps, are statically and dynamically balanced and have duplicated flight controls. Mechanically operated servo tab and electrically actuated trim tab in each aileron. Raked wingtips are of glassfibre. Pneumatic boot anti-icing of outer leading-edges.

FUSELAGE: Conventional fail-safe pressurised semi-monocoque structure (including baggage compartment), built mainly of aluminium/copper and aluminium/zinc alloy longerons, frames, stringers and skin panels. Flattened circular cross-section, upswept at rear. Glassfibre nose radome, reinforced with glassfibre/Nomex honeycomb/glassfibre sandwich, forward of front pressure bulkhead. Forward pressurised section includes flight deck and bulkhead at front of passenger cabin. Central (passenger cabin) section is 19 frames long, at 508 mm (20 in) pitch. Rear fuselage, 15 frames long, includes rear cargo ramp and door, baggage compartment, and the tailcone, which incorporates the rear pressure bulkhead. Composite fairings on fuselage sides house some equipment and systems, in addition to retracted main landing gear.

TAIL UNIT: Sweptback fin and statically and dynamically balanced rudder, large dorsal fin, two small honeycomb ventral fins, and non-swept fixed incidence tailplane with statically and dynamically balanced elevators. Main fin and tailplane boxes are two-spar aluminium/copper alloy structures, with detachable leading-edges and glassfibre tips. Rudder and elevators have glassfibre skin, Nomex honeycomb core, and leading-edge vortex generators. Rudder and elevators actuated mechanically. Mechanically operated servo tab and electrically actuated trim tab in rudder and starboard elevator; trim tab only in port elevator. Pneumatic boot anti-icing of fin and tailplane leading-edges.

LANDING GEAR: Messier-Hispano-Bugatti retractable tricycle type with levered suspension, suitable for operation from semi-prepared runways. Electrically controlled hydraulic extension/retraction, with mechanical backup for emergency extension. Oleo-pneumatic shock absorber in each unit. Each main unit comprises two wheels in tandem, retracting rearward into fairing on side of fuselage. Mainwheels semi-exposed when retracted. Single steerable nosewheel (±48°) retracts forward into unpressurised bay under flight deck. Dunlop 28 × 9.00-12 (12 ply rating) tubeless mainwheel tyres standard, pressure 5.17 bars (75 lb/sq in) on civil version, 5.58 bars (81 lb/sq in) on military version; low pressure mainwheel tyres optional, size 11.00-12/10, pressure 3.45 bars (50 lb/sq in). Dunlop 24 × 7.7 (10/12 ply rating) tubeless nosewheel tyre, pressure 5.65 bars (82 lb/sq in) on civil version, 6.07 bars (88 lb/sq in) on military version. Dunlop hydraulic differential disc brakes; Dunlop anti-skid units on main gear.

POWER PLANT: Two General Electric CT7-9C turboprops, each flat rated at 1,305 kW (1,750 shp) (S/L, to 41°C) for take-off and 1,394.5 kW (1,870 shp) up to 31°C with automatic power reserve. Hamilton Standard 14-RF21 four-blade constant-speed propellers, with full feathering and reverse-pitch capability. Blades are of glassfibre, with metal spar and urethane foam core. Lightweight low-drag composites nacelles. Fuel in two 1,042 litre (275 US gallon; 229 Imp gallon) integral main tanks in wing

centre-section and two 1,592 litre (421 US gallon; 350 Imp gallon) integral outer-wing auxiliary tanks; total fuel capacity 5,268 litres (1,392 US gallons; 1,158 Imp gallons), of which 5,128 litres (1,355 US gallons; 1,128 Imp gallons) are usable. Single pressure refuelling point in starboard main landing gear fairing; gravity filling point in top of each tank. Propeller braking permits engine to be used as an on-ground APU. Oil capacity 13.97 litres (3.69 US gallons; 3.07 Imp gallons).

ACCOMMODATION: Crew of two on flight deck, plus cabin attendant (civil version) or third crew member (military version). Accommodation in commuter version for up to 45 passengers in four-abreast seating, at 76 cm (30 in) pitch, with 22 seats each side of central aisle. Toilet, galley and overhead luggage bins standard. Pressurised baggage compartment at rear of cabin, aft of movable bulkhead; additional stowage in rear ramp area and in overhead lockers. Can also be equipped as mixed passenger/cargo combi (eg, 19 passengers and two LD3 containers), or for all-cargo operation, with roller loading system, carrying four standard LD3 containers, five LD2s, or two 2.24 × 3.18 m (88 × 125 in) and one 2.24 × 2.03 m (88 × 80 in) pallets; or for military duties, carrying up to 48 troops or 46 paratroops. Other options include layouts for aeromedical (24 stretchers and four medical attendants), ASW/maritime patrol (with 360° search radar and Exocet missiles or Mk 46 torpedoes), electronic warfare, geophysical survey or aerial photographic duties. Main passenger door, outward and forward opening with integral stairs, aft of wing on port side, serving also as a Type I emergency exit. Type III emergency exit facing this door on starboard side. Crew/service downward opening door (forward, starboard) has built-in stairs, and serves also as a Type I emergency exit, or as passenger door in combi version; a second Type III exit is provided, opposite this door, on the port side. Wide ventral door/cargo ramp in underside of upswept rear fuselage, for loading of bulky cargo. Accommodation fully air-conditioned and pressurised.

SYSTEMS: Hamilton Standard air-conditioning system, using engine compressor bleed air. AiResearch electropneumatic pressurisation system (max differential 0.25 bars; 3.6 lb/sq in) giving cabin environment of 2,440 m (8,000 ft) up to operating altitude of 5,485 m (18,000 ft). Hydraulic system, operating at nominal pressure of 207 bars (3,000 lb/sq in), comprises two engine driven, variable displacement axial electric pumps, a self pressurising standby mechanical pump, and a modular unit incorporating connectors, filters and valves; system is employed for actuation of wing flaps, landing gear extension/retraction, wheel brakes, emergency and parking brakes, nosewheel steering, cargo ramp and door, and propeller braking. Accumulator for backup braking system. No pneumatic system. 28V DC primary electrical system powered by two 400A Auxilec engine driven starter/generators, with two 24V 37Ah nickel-cadmium batteries for engine starting and 30 min (minimum) emergency power for essential services. Constant frequency single-phase AC power (115/26V) provided at 400Hz by three 600VA static inverters (two for normal operation plus one standby); two three-phase engine driven alternators for 115/200V variable frequency AC power. Fixed oxygen installation for crew of three (single cylinder at 124 bars; 1,800 lb/sq in pressure); three portable units and individual masks for passengers. Pneumatic boot anti-icing of wing (outboard of engine nacelles), fin and tailplane leading-edges. Electric anti-icing of propellers, engine air intakes, flight deck windscreen, pitot tubes and angle of attack indicators. No APU: starboard engine, with propeller braking, can be used to fulfil this function. Hand type fire extinguishers on flight deck (one) and in passenger cabin (two); smoke detector in baggage compartment. Engine fire detection and extinguishing system.

AVIONICS AND EQUIPMENT: Standard avionics include two Collins VHF-22B com radios, one Avtech DADS crew interphone, one Collins TDR-90 ATC transponder, two Collins VIR-32 VOR/ILS/marker beacon receivers, one Collins DME-42, one Collins ADF-60A, one Collins WXR-300 weather radar, two Collins 332D-11T vertical gyros, two Collins MCS-65 directional gyros, two Collins ADI-85A, two Collins HSI-85, two Collins RMI-36, one Collins APS-65 autopilot/flight director, one Collins ALT-55B radio altimeter, one Fairchild/Teledyne flight data recorder, one Fairchild A-100A cockpit voice recorder, one Avtech PACIS PA system, two Collins 345A-7 rate of turn sensors, one Sfena H-301 APM standby attitude director indicator, one Dorne & Margolin ELT 8-1 emergency locator transmitter, and one Sundstrand Mk II GPWS. Collins EFIS-85 five-tube CRT system optional. Other options include Collins EFIS-85B; second TDR-90, DME-42 and ADF-60A; plus Collins HF-230 com radio, Collins RNS-325 radar nav, Litton LTN-72R inertial nav or Global GNS-500A Omega navigation system. Navigation lights, anti-collision strobe lights, 600W landing light in front end of each main landing gear fairing, taxi lights, ice inspection lights, emergency door lights, flight deck and flight deck emergency lights, cabin and baggage compartment lights, individual passenger reading lights, and instrument panel white lighting, are all standard.

ARMAMENT (military version): Three attachment points under each wing. Indonesian Navy ASW version can be fitted with two AM39 Exocet anti-shipping missiles.

DIMENSIONS, EXTERNAL:

Wing span	25.81 m (84 ft 8 in)
Wing chord: at root	3.00 m (9 ft 10 in)
at tip	1.20 m (3 ft 11¼ in)
Wing aspect ratio	11.3
Length overall	21.353 m (70 ft 0¾ in)
Length of fuselage	20.90 m (68 ft 7 in)
Fuselage: Max width	2.90 m (9 ft 6 in)
Max depth	2.615 m (8 ft 7 in)
Height overall	8.177 m (26 ft 10 in)
Tailplane span	11.00 m (36 ft 1 in)
Wheel track (c/l of mainwheels)	3.90 m (12 ft 9½ in)
Wheelbase	6.919 m (22 ft 8½ in)
Propeller diameter	3.35 m (11 ft 0 in)
Propeller ground clearance	1.66 m (5 ft 5¼ in)
Distance between propeller centres	7.00 m (22 ft 11½ in)
Passenger door (port, rear), paratroop door (stbd, rear) and service door (stbd, fwd): Height	1.70 m (5 ft 7 in)
Width	0.73 m (2 ft 4¾ in)
Height to sill	1.22 m (4 ft 0 in)
Ventral upper door (rear): Length	2.366 m (7 ft 9¼ in)
Width	2.349 m (7 ft 8½ in)
Height to sill	1.22 m (4 ft 0 in)
Ventral ramp/door (rear): Length	3.042 m (9 ft 11¾ in)
Width	2.349 m (7 ft 8½ in)
Height to sill	1.22 m (4 ft 0 in)
Type III emergency exits (port, fwd, and stbd, rear):	
Height	0.91 m (3 ft 0 in)
Width	0.51 m (1 ft 8 in)

DIMENSIONS, INTERNAL:

Cabin, excl flight deck: Length	9.65 m (31 ft 8 in)
Max width	2.70 m (8 ft 10½ in)
Width at floor	2.366 m (7 ft 9 in)
Max height	1.88 m (6 ft 2 in)
Floor area	22.822 m² (245.65 sq ft)
Volume	43.24 m³ (1,527.0 cu ft)
Baggage compartment volume:	
ramp	5.30 m³ (187.2 cu ft)
overhead bins	1.68 m³ (59.3 cu ft)

AREAS:

Wings, gross	59.10 m² (636.1 sq ft)
Ailerons (total, incl tabs)	3.07 m² (33.06 sq ft)
Trailing-edge flaps (total)	10.87 m² (117.0 sq ft)
Fin, incl dorsal fin	11.38 m² (122.49 sq ft)
Rudder, incl tabs	3.32 m² (35.74 sq ft)
Tailplane	21.20 m² (228.2 sq ft)
Elevators (total, incl tabs)	6.17 m² (66.41 sq ft)

WEIGHTS AND LOADINGS:

Operating weight empty:	
passenger version	9,400 kg (20,725 lb)
cargo and military versions	8,600 kg (18,960 lb)
Max fuel	4,230 kg (9,325 lb)
Max payload: passenger version	4,200 kg (9,260 lb)
cargo and military versions	5,000 kg (11,025 lb)
Max weapon load (CN-235 M)	3,500 kg (7,716 lb)
Max T-O weight	15,100 kg (33,290 lb)
Max landing weight	15,050 kg (33,180 lb)
Max zero-fuel weight	13,600 kg (29,980 lb)
Cabin floor loading:	
cargo and military versions	1,504 kg/m² (308.0 lb/sq ft)
Max wing loading	255.5 kg/m² (52.36 lb/sq ft)
Max power loading without APR	5.78 kg/kW (9.51 lb/shp)

PERFORMANCE (civil versions at max T-O weight, ISA, except where indicated):

Max operating speed at S/L	240 knots (445 km/h; 276 mph) IAS
Max cruising speed at 4,575 m (15,000 ft)	244 knots (452 km/h; 280 mph)
Stalling speed at S/L:	
flaps up	100 knots (186 km/h; 116 mph) IAS
flaps down	84 knots (156 km/h; 97 mph) IAS
Max rate of climb at S/L	465 m (1,527 ft)/min
Rate of climb at S/L, one engine out	128 m (420 ft)/min
Service ceiling	8,110 m (26,600 ft)
Service ceiling, one engine out	4,550 m (14,925 ft)
T-O run	554 m (1,818 ft)
T-O to 10.7 m (35 ft) at S/L	687 m (2,254 ft)
Landing from 15 m (50 ft) at S/L	585 m (1,920 ft)
Min ground turning radius	18.98 m (62 ft 3¼ in)
Range at 5,485 m (18,000 ft), reserves for 87 nm (161 km; 100 mile) diversion and 45 min hold:	
with max payload	208 nm (385 km; 239 miles)
with max fuel	2,110 nm (3,910 km; 2,429 miles)

OPERATIONAL NOISE LEVELS (civil versions):

T-O	84.0 EPNdB
Approach	87.0 EPNdB
Sideline	86.0 EPNdB

PERFORMANCE (CN-235 M at max T-O weight, ISA, except where indicated):

As for civil versions except:	
Max rate of climb at S/L	579 m (1,900 ft)/min
Rate of climb at S/L, one engine out	156 m (512 ft)/min
Service ceiling	7,620 m (25,000 ft)
Service ceiling, one engine out	4,665 m (15,300 ft)
Min ground turning radius:	
nosewheel	9.50 m (31 ft 2 in)
wingtip	18.98 m (62 ft 3¼ in)
T-O to 15 m (50 ft)	732 m (2,400 ft)
Landing from 15 m (50 ft)	772 m (2,530 ft)
Landing run, with propeller reversal	286 m (939 ft)
Range at 6,100 m (20,000 ft), long-range cruising speed, reserves for 45 min hold:	
with max payload	669 nm (1,240 km; 770 miles)
with 2,400 kg (5,291 lb) payload	2,304 nm (4,270 km; 2,653 miles)

APPENDIX E

FLIGHT PHASE CATEGORIES

Definition of Flight Phase Category A:

Those non-terminal flight phases that require rapid maneuvering, precision tracking or precise flight path control. Included in this category are:

MIL-F-8785C Suggested Civilian Equivalent:VLA, FAR 23, and FAR 25

Air-to-air combat	None
Ground attack	None
Weapon delivery/launch	None
Aerial recovery	None
Reconnaissance, Observation, Pipeline spotting and monitoring	
In-flight refueling (receiver)	None as yet
Terrain following	None
Anti-submarine search	Fish spotting
Close formation flying	Air-show demonstrations

Definition of Flight Phase Category B:

Those non-terminal flight phases that are normally accomplished using gradual maneuvers and without precision tracking, although accurate flight-path control may be required. Included in this category are:

MIL-F-8785C Suggested Civilian Equivalent:VLA, FAR 23, and FAR 25

Climb	Various climb segments
Cruise	Various cruise segments
Loiter	Flight in holding pattern